Modeling Coupled THMC Processes and Brine Migration in Salt at High Temperatures

Fuel Cycle Research & Development

Prepared for

U.S. Department of Energy
Used Fuel Disposition

Jonny Rutqvist
Laura Blanco Martín
Sumit Mukhopadhyay
Jim Houseworth
Jens Birkholzer
Lawrence Berkeley National Laboratory

August, 2014

FCRD-UFD-2014-000341

DISCLAIMER

This information was prepared as an account of work sponsored by an agency of the U.S. Government. While this document is believed to contain correct information, Neither the U.S. Government nor any agency thereof, nor the Regents of the University of California, nor any of their employees, makes any warranty, expressed or implied, or assumes any legal liability or responsibility for the accuracy, completeness, or usefulness, of any information, apparatus, product, or process disclosed, or represents that its use would not infringe privately owned rights. References herein to any specific commercial product, process, or service by trade name, trade mark, manufacturer, or otherwise, does not necessarily constitute or imply its endorsement, recommendation, or favoring by the U.S. Government or any agency thereof, or the Regents of the University of California. The views and opinions of authors expressed herein do not necessarily state or reflect those of the U.S. Government or any agency thereof or the Regents of the University of California.

Revision 2
12/20/2012

APPENDIX E

FCT DOCUMENT COVER SHEET [1]

Name/Title of Deliverable/Milestone/Revision No.	Modeling Coupled THMC Processes and Brine Migration in Salt at High Temperatures
Work Package Title and Number	DR Salt R&D – LBNL FT-14LB081804
Work Package WBS Number	1.02.08.18
Responsible Work Package Manager	Jens Birkholzer (signature on file) (Name/Signature)

Date Submitted 08/15/2014

Quality Rigor Level for Deliverable/Milestone[2]	☐ QRL-3	☐ QRL-2	☐ QRL-1 ☐ Nuclear Data	☒ Lab/Participant QA Program (no additional FCT QA requirements)

This deliverable was prepared in accordance with Lawrence Berkeley National Laboratory
(Participant/National Laboratory Name)

QA program which meets the requirements of
☒ DOE Order 414.1 ☐ NQA-1-2000 ☐ Other

This Deliverable was subjected to:

☐ Technical Review ☐ Peer Review

Technical Review (TR)

Review Documentation Provided

☐ Signed TR Report or,
☐ Signed TR Concurrence Sheet or,
☐ Signature of TR Reviewer(s) below

Peer Review (PR)

Review Documentation Provided

☐ Signed PR Report or,
☐ Signed PR Concurrence Sheet or,
☐ Signature of PR Reviewer(s) below

Name and Signature of Reviewers

NOTE 1: *Appendix E should be filled out and submitted with the deliverable. Or, if the PICS:NE system permits, completely enter all applicable information in the PICS:NE Deliverable Form. The requirement is to ensure that all applicable information is entered either in the PICS:NE system or by using the FCT Document Cover Sheet.*

NOTE 2: *In some cases there may be a milestone where an item is being fabricated, maintenance is being performed on a facility, or a document is being issued through a formal document control process where it specifically calls out a formal review of the document. In these cases, documentation (e.g., inspection report, maintenance request, work planning package documentation or the documented review of the issued document through the document control process) of the completion of the activity along with the Document Cover Sheet is sufficient to demonstrate achieving the milestone. If QRL 1, 2, or 3 is not assigned, then the Lab/Participant QA Program (no additional FCT QA requirements box must be checked, and the work is understood to be performed, and any deliverable developed, in conformance with the respective National Laboratory/Participant, DOE- or NNSA-approved QA Program.*

This page is intentionally blank.

CONTENTS

1. INTRODUCTION 1

2. UPDATED TOOLS TO MODEL THM PROCESSES IN SALINIFEROUS MATERIALS 3
   2.1 Updated TOUGH-FLAC simulator for large strain and creep 3
   2.2 Pore pressure definitions in geomechanics 7
   2.3 Improvements in the modeling of THM processes in natural salt 8
   2.4 Improvements on the modeling of THM processes in crushed salt 10

3. MODELING OF THM PROCESSES IN THE LONG TERM FOR A GENERIC SALT-BASED REPOSITORY 11
   3.1 Model description 11
   3.2 THM base-case scenario 15
   3.3 Comparison of TH and THM results 19
   3.4 Importance of capillary forces 21
   3.5 Sensitivity of the THM predictions to the initial saturation of the host rock 22

4. INTERNATIONAL BENCHMARK EXERCISES 23
   4.1 First benchmark exercise: 2D model of emplacement drift for HLW, backfilled with crushed salt 25
      4.1.1 Benchmark description 25
      4.1.2 Comparison and analysis of the results 27
   4.2 Second benchmark exercise: 3D modeling of the TSDE experiment and recalculation of model parameters 33

5. CONSTITUTIVE RELATIONSHIPS FOR BRINE MIGRATION 35
   5.1 Background 35
   5.2 Recent Observations and Advances 37
   5.3 Modeling Approach 38
   5.4 Governing Equations 39
   5.5 Fluxes and Inter-Continuum Exchange Terms 42
   5.6 Numerical Formulation 46

6. CONCLUSIONS 47

ACKNOWLEDGMENT 49

REFERENCES 49

FIGURES

Figure 2-1. Explicit sequential THM analysis scheme (adapted from (Rutqvist et al., 2002)). The highlighted zones correspond to the time step between time t^n and t^{n+1}. 5

Figure 2-2. Mesh update in large strain mode. Example of initial and deformed discretizations in the (left) flow sub-problem and (right) geomechanics sub-problem. 7

Figure 3-1. Geometry of the generic salt repository studied, with enlarged view of the drift area. 12

Figure 3-2. Heat load per meter of drift for a waste package containing 10 PWR assemblies, assuming underground emplacement 20 years after reactors shut-down (after Carter et al., 2011). 13

Figure 3-3. THM base case scenario: evolution of temperature at several locations in the repository..... 16

Figure 3-4. THM base case scenario: evolution of porosity within the crushed salt during the first 20 years. 17

Figure 3-5. THM base case scenario: extension of EDZ at three different moments. For t=0 s, k=10^{-20} m^2; t=4 years, k=10^{-18} m^2 and t=7 years, k=10^{-22} m^2. 18

Figure 3-6. THM base case scenario: evolution of (left) equivalent pore pressure and (right) liquid saturation at several locations in the repository. 19

Figure 3-7. TH-only scenario: evolution of temperature at the locations displayed in Figure 3-3. 20

Figure 3-8. TH-only scenario: evolution of (left) pressure (maximum pore pressure) and (right) liquid saturation at the five locations displayed in Figure 3-6. 20

Figure 3-9. THM predictions without capillary pressure. Evolution of (left) equivalent pore pressure and (right) liquid saturation at the locations shown in Figure 3-6 (the crushed salt element right above the waste package has been added to the saturation plot). 22

Figure 3-10. THM predictions with 50 % initial saturation in the host rock. Evolution of (left) equivalent pore pressure and (right) liquid saturation at the locations shown in Figure 3-6. 23

Figure 4-1. Geometry of the generic salt repository studied in the first benchmark exercise, with enlarged view of the drift area. 26

Figure 4-2. First benchmark exercise: evolution of temperature. Solid lines correspond to TOUGH-FLAC; lines with points correspond to FLAC-TOUGH. 28

Figure 4-3. First benchmark exercise: evolution of dilatancy at the drift contour during the first years of post-closure phase, as obtained by TOUGH-FLAC (top) and FLAC-TOUGH (bottom). 29

Figure 4-4. First benchmark exercise: evolution of porosity within the backfill during the first 20 years of post-closure phase. Solid lines correspond to TOUGH-FLAC; lines with points correspond to FLAC-TOUGH. 30

Figure 4-5. First benchmark exercise: evolution of (left) pore pressure and (right) liquid saturation. Solid lines correspond to TOUGH-FLAC; lines with points correspond to FLAC-TOUGH. 31

Figure 4-6. First benchmark exercise: evolution of $\Delta P_{Fl}=\sigma_3+P$ predicted by TOUGH-FLAC (top) and FLAC-TOUGH (bottom). 32

Figure 4-7. Schematic view of the two drift tests used in the TSDE experiment (800 m level of the Asse salt mine). From (Bechthold et al., 1999). 33

Figure 4-8. Views of the 3D mesh used in the modeling of the TSDE experiment (flow and geomechanics discretization). 34

Figure 5-1. Schematic diagram showing the interconnected pore space and the intracystalline inclusions within an representative elementary volume (REV) in a dual-continuum conceptualization of salt formations. Figure also shows the various fluxes and inter-continuum exchanges 39

Figure 5-2. Space discretization and flow-term evaluation in the integral finite difference approach. 46

TABLES

Table 3.1. Mechanical and flow properties of the crushed salt, natural salt and sandstone layers. 14

Table 3.2. Initial flow parameters of the crushed salt, natural salt and sandstone layers. 15

Table 4.1. Initial flow parameters of the crushed salt, natural salt and confining sandstone layers considered in the first benchmark exercise. 27

ACRONYMS

DOE	Department of Energy
EBS	Engineered Barrier System
EDZ	Excavation Damaged Zone
FLAC	Fast Lagrangian Analysis of Continua
GSR	Generic Salt Repository
HLW	High-level Nuclear Waste
LBNL	Lawrence Berkeley National Laboratory
PWR	Pressurized Water Reactor
TH	thermal-hydrological
THM	thermal-hydrological-mechanical
THMC	thermal-hydrological-mechanical-chemical
TM	thermal-mechanical
TSDE	Thermal Simulation for Drift Emplacement
TOUGH	Transport of Unsaturated Groundwater and Heat
TUC	Clausthal University of Technology (TU Clausthal)
UFD	Used Fuel Disposition

1. INTRODUCTION

In this report, we present FY2014 progress by Lawrence Berkeley National Laboratory (LBNL) related to modeling of coupled thermal-hydrological-mechanical-chemical (THMC) processes in salt and their effect on brine migration at high temperatures. LBNL's work on the modeling of coupled THMC processes in salt was initiated in FY2012, focusing on exploring and demonstrating the capabilities of an existing LBNL modeling tool (TOUGH-FLAC) for simulating temperature-driven coupled flow and geomechanical processes in salt. This work includes development related to, and implementation of, essential capabilities, as well as testing the model against relevant information and published experimental data related to the fate and transport of water. An important component in this work is LBNL's collaboration with a research group led by Professor Lux at Clausthal University of Technology (TUC) in Germany, a world-leading research institution in salt geomechanics. The DOE UFD campaign and LBNL greatly benefit from TUC's experience in salt geomechanics and modeling of salt thermal-mechanical (TM) processes using FLAC3D. Conversely, TUC benefits from LBNL's expertise in modeling multiphase and heat transport processes at high temperature with TOUGH2 as well as LBNL's experience with the TOUGH-FLAC simulator for the modeling coupled THM processes in nuclear waste isolation. By leveraging on existing complementary capabilities of the LBNL and TUC, we have within a few years been able to develop and validate an advanced numerical simulation tool for modeling of coupled THM processes in salt and have demonstrated its applicability to nuclear waste isolation.

In FY2013, we implemented an advanced geomechanical constitutive model for rock salt (the Lux/Wolters model), a model that can handle creep, damage, sealing, and healing of the salt as a function of stress, temperature, and pore pressure. Moreover, we used the TOUGH-FLAC code with this newly implemented model together with other constitutive models for crushed salt backfill, and successfully completed model simulations of a generic salt-based repository over 100,000 years of simulation time. Finally, we developed and tested alternative ways for modeling hydraulic and mechanical coupling under large strain, including compaction of crushed salt from 30% porosity to a state equivalent to the solid host rock.

In FY2014, LBNL's work has been focused on continued testing, application, and improvement of the computational models and tools to simulate high temperature coupled processes and its effect on brine accessibility and migration. This includes improvements to the TOUGH-FLAC simulator related to implemented constitutive models for both solid rock salt and crushed salt, as well as related to the use of a Voronoi discretization for improved accuracy in the flow subproblem. The Voronoi discretization is implemented to handle mesh deformation over time due to creep and the large strains associated with the mechanical behavior of the system. Based on these model improvements, we have updated and completed our study of long-term THM behavior of a generic repository, and this has been summarized and submitted for publication in a journal (Blanco Martin 2014d).

In FY2014, we have also conducted benchmarking in collaboration with the TUC research team, focusing on comparison of the different approaches for sequential coupling of TOUGH2 and FLAC3D. Another benchmark calculation has been initiated involving modeling of the TSDE (*Thermal Simulation for Drift Emplacement*) test conducted in the Asse Mine, Germany. The TSDE analysis will be a major modeling effort that will provide the opportunity to validate the TOUGH-FLAC simulator for drift closure and backfill compaction at a large 3D field setting.

Finally, in FY2014 LBNL has initiated studies of constitutive relationships for brine migration, including a review of existing formulations for the various mechanisms that cause brine mobilization and migration in rock salt, as well as the development of a conceptual model for simulating the flow and transport of brine in salt formations. In particular, we are developing a dual-continuum approach that accounts for brine migration through both interconnected intergranular (i.e., intercrystalline) pore spaces and isolated fluid inclusions (i.e., intracrystalline brine inclusions), considering both pressure and temperature gradients. The plan is to implement such an advanced brine-migration dual-continuum model into the TOUGH2 and TOUGH-FLAC simulators, and then validate the brine-migration model and its implementation against experimental data.

Within the Natural Barrier System (NBS) group of the Used Fuel Disposition (UFD) Campaign at DOE's Office of Nuclear Energy, LBNL's research activities have focused on understanding and modeling coupled processes and impacts of the EDZ and high-temperature on parameters and processes relevant to performance of a salt repository. This report documents results from some of these activities. These activities address key Features, Events and Processes (FEPs), which have been ranked in importance from medium to high, as listed in Table 7 of the *Used Fuel Disposition Campaign Disposal Research and Development Roadmap* (FCR&D-USED-2011-000065 REV0) (Nutt, 2011). Specifically, they address FEP 2.2.01, Excavation Disturbed Zone, for salt, by investigating how coupled processes affect EDZ evolution; FEP 2.2.05, Flow and Transport Pathways; and FEP 2.2.08, Hydrologic Processes, and FEP 2.2.07, Mechanical Processes by studying near-field coupled THM processes in salt repositories. The activities documented in this report also address a number of research topics identified in *Research & Development (R&D) Plan for Used Fuel Disposition Campaign (UFDC) Natural System Evaluation and Tool Development* (Wang, 2011), including Topics S3, Disposal system modeling – Natural system; P14, Technical basis for thermal loading limits; and P15 Modeling of disturbed rock zone (DRZ) evolution (salt repository).

In the following sections of this report, we provide more details on the FY2014 work, first presenting updated tools and improvements made to the TOUGH-FLAC simulator, and the use of this updated tool in a new model simulation of long-term THM behavior within a generic repository in a salt formation (Section 2). This is followed by the description of current benchmarking and validations efforts, including the TSDE experiment (Section 3). We then present the current status in the development of constitutive relationships and the dual-continuum model for brine migration (Section 4). We conclude with an outlook for FY2015, which will be much focused on model validation against field experiments and on the use of the model for the design studies related to a proposed heater experiment.

2. UPDATED TOOLS TO MODEL THM PROCESSES IN SALINIFEROUS MATERIALS

A modified version of the TOUGH-FLAC simulator (Rutqvist and Tsang, 2003; Rutqvist, 2011) was developed during FY2013 (Rutqvist et al. 2013) to accommodate some aspects related to the modeling of THM processes in saliniferous formations. This version included an algorithm to update geometrical data in the flow simulator (due to the use of the large-strain mode in the geomechanics problem) and a porosity evolution function that takes into account the effect of both the different flow phases present and the geomechanical response. It also included dedicated constitutive models for natural salt and crushed salt, and material-specific coupling functions from mechanics to flow.

During FY2014, we have continued working on this updated version of TOUGH-FLAC, and we now have an improved version. In this section, we explain the main improvements that we have made during this year. In addition, in FY2014 we have continued our beneficial collaboration with TUC, and we have included, in the constitutive model (referred to as *Lux/Wolters*) some recent improvements developed by Prof. Lux's team. In parallel to this, we have developed an improved version of the constitutive model available in FLAC^{3D} for crushed salt. All these improvements are detailed here.

2.1 Updated TOUGH-FLAC simulator for large strain and creep

The TOUGH-FLAC simulator, developed at LBNL (Rutqvist and Tsang 2003), is based on an explicit sequential method for coupling flow and geomechanics. The multiphase fluid and heat flows are computed by TOUGH2 (Pruess et al., 2011), and the geomechanical response of the system is calculated using FLAC^{3D} (Itasca, 2011). The main advantages of sequential methods include the use of existing robust and well-established simulators for each subproblem, the resolution of smaller systems of equations, the use of different time-stepping algorithms, and the possibility to study different domains in each subproblem (Dean et al., 2006; Felippa and Park, 1980; Thomas et al., 2003; Vijalapura et al., 2005).

The coupling scheme between TOUGH2 and FLAC^{3D} is based on the fixed stress-split method (Kim et al. 2011). In this method, the flow problem is solved first (with an explicit evaluation of the volumetric total stress), and the pore pressure and temperature are prescribed during the geomechanical calculation, which therefore requires drained rock-mechanical properties.

In order to accommodate the large strains and time-dependent processes associated with saliniferous materials (creep, mesh distortions, crushed salt reconsolidation, etc.), TOUGH-FLAC has required some updates. Indeed, FLAC^{3D} has the capability to deal with large strains, but TOUGH2 does not. In FY2013, we developed an algorithm to update the mesh in the flow subproblem as the geomechanics mesh deforms (Rutqvist et al., 2013), and we implemented a recent formulation of coupled geomechanics and multiphase fluid and heat flows developed by Kim et al. (2012). This analytical formulation is an extension of the classic thermodynamic approach implemented in TOUGH2 and includes a porosity correction term that accounts for the geomechanical effect (via the volumetric component of the total stress tensor).

In FY2014, we have reformulated the balance equations solved in TOUGH2 to account for geometrical changes and ensure mass conservation. This way, after every FLAC^{3D} call, mass is conserved, but density is not. The geometrical update is made at the first iteration of the TOUGH2 Newton-Raphson process (Pruess et al., 2011). In this iteration, the primary variables

(pore pressure, temperature, and saturation) and porosity remain equal to those at the end of the previous time step (only geometrical data are different), and we check whether the system continues to be in thermodynamic equilibrium for a new time increment and new geometry. If the maximum residual exceeds a preset convergence tolerance, an iterative process is carried out. In this process, the geometry is kept unchanged (i.e., the geometry is updated in TOUGH2 after every FLAC^{3D} call, but is constant during each TOUGH2 run) and consistency in the balance equations is ensured through the porosity-variation formulation, adapted from (Kim et al., 2012). The balance equations for a grid block *n* read:

$$\frac{d\left(M_n^\kappa V_n\right)}{dt} = \sum_m A_{nm} F_{nm}^\kappa + q_n^\kappa \rightarrow \frac{dM_n^\kappa}{dt} + M_n^\kappa \frac{dV_n}{Vdt} = \frac{1}{V_n}\left(\sum_m A_{nm} F_{nm}^\kappa + q_n^\kappa\right) \tag{2.1}$$

for κ=1, *NK* (*NK* is the total number of fluid components [air, water, etc.]). In Equation (2.1), M_n^κ is the accumulation term, V_n is the volume of the grid block (new volume after FLAC^{3D} call), q_n^κ represents the sink/sources, and F_{nm}^κ is the flow of component κ across surface A_{nm} (new value after FLAC^{3D} call). We note that for second and further iterations, the term $M_n^\kappa \frac{dV_n}{Vdt}$ is not computed. The accumulation terms read

$$M_n^\kappa = \phi \sum_\beta S_\beta \rho_\beta \chi_\beta^\kappa \tag{2.2}$$

where ϕ is porosity, S_β is the phase saturation, ρ_β is the density of phase β, and χ_β^κ is the mass fraction of component κ in phase β. Porosity changes during a time step (for second and further iterations) are calculated adding a porosity variation $d\phi$, which includes a correction term, $\Delta\phi$, from geomechanics (therefore, it includes volume changes). This term is constant for a given time step. This way, the geometrical data used during the iterations of a time step are consistent, and mass conservation is ensured. The porosity variation has the form

$$d\phi = A(\alpha, \phi, K)dP + B(\alpha_{th})dT + \Delta\phi \tag{2.3}$$

where α [-] is the Biot coefficient, α_{th} [K^{-1}] is the linear thermal expansion coefficient, K [MPa] is the drained bulk modulus, and $\Delta\phi$ is the porosity correction from geomechanics. A detailed explanation of this formulation can be found in Kim et al. (2012). The Biot coefficient is defined as the ratio of the fluid-volume variation in a material element to the volume change of that element. It gives an indication of the grain compressibility with respect to the bulk compressibility, and of the coupling strength. It can take the values $\alpha \in [0,1]$; a Biot coefficient close to 1 describes a high poromechanical effect (the grains are not compressible, so the pores take an important role), whereas a low value indicates that the poromechanical effect is low (the response of the grains and the bulk material is similar, so the coupling strength is low).

Currently, the modeling sequence is as follows. TOUGH2 moves the simulation forward and FLAC^{3D} is executed once within a TOUGH2 time step, just before the Newton-Raphson iteration process to solve the residual nonlinear equations. A schematic view of the coupled THM modeling sequence is displayed in Figure 2-1. The pressure, P^n, temperature, T^n, liquid saturation, S_l^n, and porosity, ϕ^n, of each grid block computed at the end of the previous time step

(from t^{n-1} to t^n) are transferred to FLAC^{3D}. Note that the pressure transferred depends on the definition of pore pressure (Coussy 2004; Kim et al. 2013); more details will be given in Subsection 2.1.1.

From flow to geomechanics, the pore-pressure change, $\Delta P = P^n - P^{n-1}$, and the temperature change, $\Delta T = T^n - T^{n-1}$, corresponding to two successive TOUGH2 time steps are accounted for as a correction to the total stress tensor, σ_{ij} (direct coupling). These changes are computed internally in FLAC^{3D} once the new values P^n and T^n are transferred. The corrected total stress tensor, σ_{ij}^c, has the form

$$\sigma_{ij}^c = \sigma_{ij} - \alpha \Delta P \delta_{ij} - 3\alpha_{th} K \Delta T \delta_{ij} \tag{2.4}$$

where δ_{ij} [-] is the Kronecker delta. Compressive stresses are defined negative here. From Equation (2.4), it can be inferred that the coupling from flow to geomechanics (TOUGH2 to FLAC^{3D}) affects only the volumetric component of the stress tensor. Porosity and liquid saturation are used to update the body forces in the quasi-static governing equations of the geomechanical analysis (Kim et al. 2012). Note that these equations account for the thermal strains that result from the temperature change ΔT.

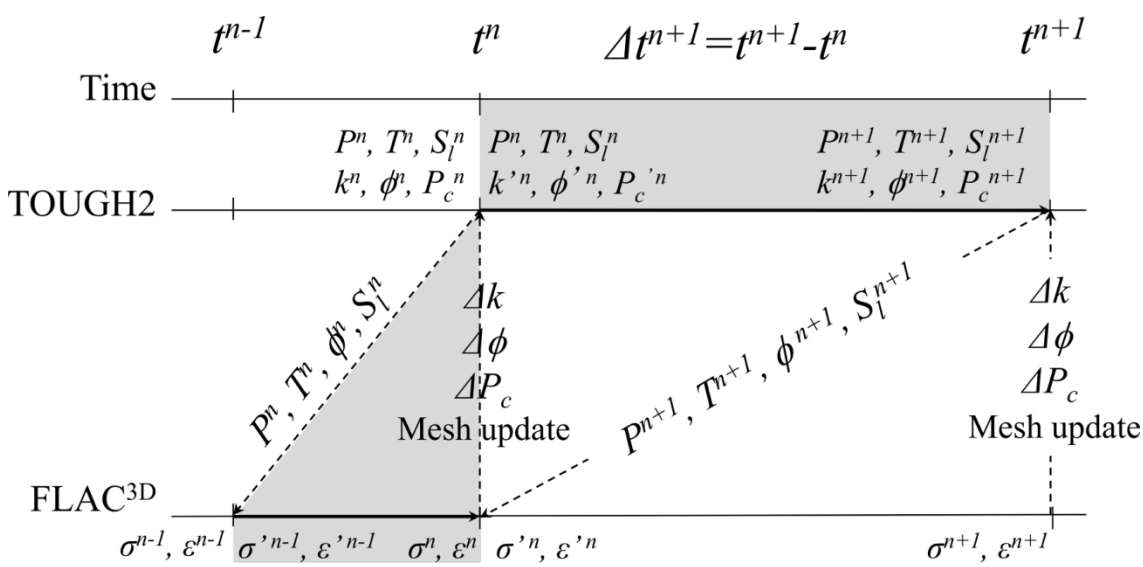

Figure 2-1. Explicit sequential THM analysis scheme (adapted from (Rutqvist et al., 2002)). The highlighted zones correspond to the time step between time t^n and t^{n+1}.

Once all the updates are made, FLAC^{3D} runs in creep and large strain modes from time t^{n-1} to time t^n. A new equilibrium mechanical state is obtained at time t^n (stresses σ^n and strains ε^n in Figure 2-1). Recall that during the mechanical calculation, the flow data (P^n, T^n, S_l^n, and ϕ^n) remain constant. In FLAC^{3D} the new static equilibrium is established internally through a dynamic-solution approach, solving the equation of motion in which the inertial terms are used as numerical means to reach the equilibrium state of the system under consideration. The established new static equilibrium brings about a new strain tensor and a new effective stress tensor (i.e., a new mechanical state).

From geomechanics to flow, geometrical changes are first accounted for. The geometrical data updated in TOUGH2 are: volume of the elements, distances of the centroids of two connected elements to their common interface, common interface area, and cosine of the angle between the gravitational acceleration vector and the line between the centroids of two connected elements. Also, as explained before, in the first Newton-Raphson iteration, the accumulation terms in the balance equations are updated to account for possible volume changes.

Additionally, the new mechanical state obtained at t^n is used through several coupling functions to compute mechanically induced changes in permeability and capillary pressure (Δk and ΔP_c in Figure 2-1). The coupling functions depend on each material (and the phenomena it goes through) and should be based on specific laboratory and theoretical results; they have been presented previously for the natural salt and the crushed salt (Rutqvist et al. 2013), and only the improvements will be discussed here. The mechanically modified flow properties (k'^n, ϕ'^n and $P_c'^n$ in Figure 2-1) are used to solve the residual equations of the flow problem. Within a time step, the Newton-Raphson iteration process is continued until the residuals are reduced below a preset convergence tolerance. At the end of the current time step (time t^{n+1} in Figure 2-1), a new set of primary thermodynamic variables (P^{n+1}, T^{n+1} and S_l^{n+1} in Figure 2-1) and new flow properties (k^{n+1}, ϕ^{n+1} and P_c^{n+1} in the figure) are obtained.

Another improvement incorporated into TOUGH-FLAC during FY2014 consists in the use of a Voronoi discretization in the flow subproblem, even when the mesh deforms over time due to the creep and the large strains associated with the mechanical behavior of saliniferous materials. Since the resolution method used in TOUGH2 is based on the Voronoi partition (Pruess et al. 2011), more accurate solutions will be obtained when the discretization of the flow subproblem conforms to this technique. If the domain under study deforms over time, the partition used in the flow subproblem should still comply with the resolution method of the code. Bearing this in mind, we use the software library Voro++ (Rycroft, 2009) to ensure that the mesh used in TOUGH2 conforms to the principles of the Voronoi tessellation. This is an innovation with respect to previous studies using TOUGH-FLAC.

As the mesh deforms in the geomechanics subproblem, Voro++ is executed to compute the corresponding Voronoi tessellation. This operation is performed every time the mesh deforms with respect to strains a preset value, typically 2–5 % (Benz 2007). In the current approach, the centroids of the deformed geomechanical mesh are transferred to Voro++, which computes the corresponding Voronoi discretization. Geometrical data of the new Voronoi mesh (volumes, common interface area between two adjacent grid blocks, etc.) are then transferred to TOUGH2.

Figure 2-2 shows a detail of two grids (flow and geomechanics) used in some of the THM simulations performed during FY2013 (initial mesh and deformed mesh after 20 years). As can be seen, the flow subproblem uses Voronoi cells, both in the initial and the deformed configurations. In addition, it can be seen in the figure that the grid blocks at the boundary between two different domains (waste package, backfill, and host rock) are slim and have the same thickness. This way, Voro++ will conserve the volume of each domain even when the mesh deforms (the generators of the Voronoi mesh are the centroids of the mesh used in FLAC^{3D}).

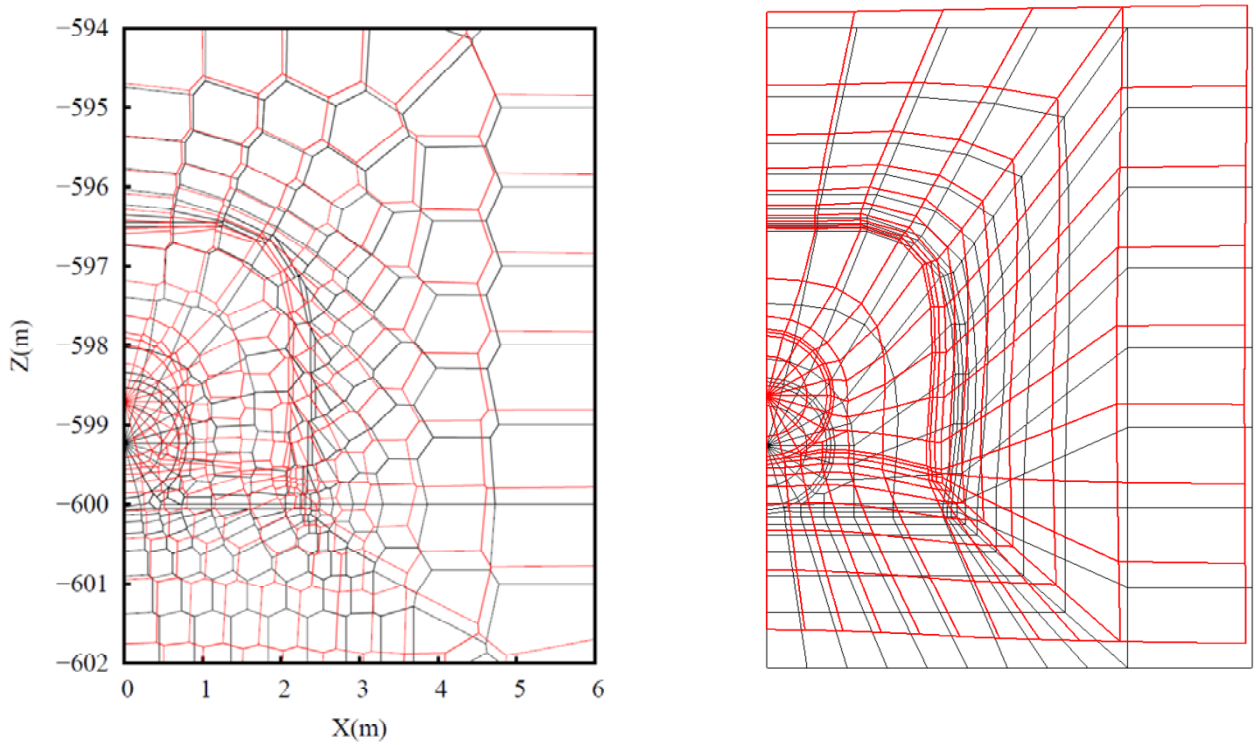

Figure 2-2. Mesh update in large strain mode. Example of initial and deformed discretizations in the (left) flow sub-problem and (right) geomechanics sub-problem.

Finally, in order to reduce the simulation times (a 2D THM simulation of one backfilled drift, run to 100,000 years, takes between 3–5 weeks on a PC [mesh discretized into about 1000 grid blocks]), it was decided to perform the coupling between TOUGH2 and FLAC^{3D} every two time steps after 10,000 years. Indeed, the most relevant coupled processes take place within the first 1000 years, as will be shown in Section 3. Performing the coupling less often when relevant processes are attenuated lets us decrease the time needed to compute one simulation and conduct more simulations to explore the effect of different parameters on the long-term predictions. We recall that FLAC^{3D} only runs on Windows-based OS, and that only two FLAC^{3D} simulations are allowed simultaneously on a PC for license reasons.

2.2 Pore pressure definitions in geomechanics

Different pore pressure concepts are available to use in geomechanics when several fluid phases occupy the pores:

- Maximum pore pressure (gas pressure in TOUGH2);
- Saturation-weighted average fluid pressure, and
- Equivalent pore pressure (Coussy, 2004). The equivalent pore pressure is defined as

$$P_{eq} = \sum_{i=1}^{NPH} P_i S_i + U \tag{2.5}$$

where P_i is phase pressure, S_i is phase saturation, U is the interfacial energy per unit of pore volume, and NPH is the number of phases present (Coussy 2004). Neglecting the temperature dependence of capillary forces, the interfacial energy can be determined from the capillary curve according to

$$U(S_w) = \int_{S_w}^{1} P_{cap}(S)dS \tag{2.6}$$

where $P_{cap}<0$ is the capillary pressure. According to Coussy (2004), the equivalent pore pressure should be used in multiphase flow problems when capillary forces are non-negligible, which is the case with natural salt and the reconsolidated crushed salt, due to their very low porosity (ϕ<1-2 %). In addition, this pressure is the proper definition of multiphase pore pressure, because it renders a formulation that is dissipative (Kim et al. 2013).

In order to investigate the sensitivity of the THM predictions to the pore pressure used in geomechanics, we have conducted simulations using the three different concepts, but we have retained the equivalent pore pressure as our reference pore pressure (i.e., this is the pore pressure used in the base-case scenario presented in Section 3). The main differences between the three concepts arise when capillary effects are important, i.e., when liquid saturation and porosity are low. In the generic salt repository considered in this research, the host rock adjacent to the drift contour will be the most sensitive zone to the pore pressure used, particularly during the first years, when liquid saturation drops in this area. The backfill THM evolution may also be sensitive to the pore-pressure concept if the saturation is low by the end of the reconsolidation process; nonetheless, our simulation results show that saturation in the backfill approaches 1 when porosity approaches the characteristic porosity of the natural salt (see Section 3 for a description of the results).

Overall, the higher the pore pressure used in geomechanics, the higher the damage to the barriers, which leads to a higher porosity increase, higher permeability increase, and also an increase in coupling effects (through the Biot coefficient, which is damage-dependent, as will be explained below). Since salt damage is reversible, once the pore pressure drops, all these effects are reversed. However, in other situations, damage may not be reversed, and hence the choice of the pore pressure used in geomechanics may have a significant impact on the numerical predictions. We note that our results show that the use of the maximum pore pressure in geomechanics leads to the most conservative predictions.

2.3 Improvements in the modeling of THM processes in natural salt

Currently, we model the behavior of the natural salt using the *Lux/Wolters* constitutive model, developed at Clausthal University of Technology (TUC). This model has been under development and improvement since the 1980s (Hou 2003; Hou and Lux 2000, 1999, 1998; Hou

1. INTRODUCTION

In this report, we present FY2014 progress by Lawrence Berkeley National Laboratory (LBNL) related to modeling of coupled thermal-hydrological-mechanical-chemical (THMC) processes in salt and their effect on brine migration at high temperatures. LBNL's work on the modeling of coupled THMC processes in salt was initiated in FY2012, focusing on exploring and demonstrating the capabilities of an existing LBNL modeling tool (TOUGH-FLAC) for simulating temperature-driven coupled flow and geomechanical processes in salt. This work includes development related to, and implementation of, essential capabilities, as well as testing the model against relevant information and published experimental data related to the fate and transport of water. An important component in this work is LBNL's collaboration with a research group led by Professor Lux at Clausthal University of Technology (TUC) in Germany, a world-leading research institution in salt geomechanics. The DOE UFD campaign and LBNL greatly benefit from TUC's experience in salt geomechanics and modeling of salt thermal-mechanical (TM) processes using FLAC3D. Conversely, TUC benefits from LBNL's expertise in modeling multiphase and heat transport processes at high temperature with TOUGH2 as well as LBNL's experience with the TOUGH-FLAC simulator for the modeling coupled THM processes in nuclear waste isolation. By leveraging on existing complementary capabilities of the LBNL and TUC, we have within a few years been able to develop and validate an advanced numerical simulation tool for modeling of coupled THM processes in salt and have demonstrated its applicability to nuclear waste isolation.

In FY2013, we implemented an advanced geomechanical constitutive model for rock salt (the Lux/Wolters model), a model that can handle creep, damage, sealing, and healing of the salt as a function of stress, temperature, and pore pressure. Moreover, we used the TOUGH-FLAC code with this newly implemented model together with other constitutive models for crushed salt backfill, and successfully completed model simulations of a generic salt-based repository over 100,000 years of simulation time. Finally, we developed and tested alternative ways for modeling hydraulic and mechanical coupling under large strain, including compaction of crushed salt from 30% porosity to a state equivalent to the solid host rock.

In FY2014, LBNL's work has been focused on continued testing, application, and improvement of the computational models and tools to simulate high temperature coupled processes and its effect on brine accessibility and migration. This includes improvements to the TOUGH-FLAC simulator related to implemented constitutive models for both solid rock salt and crushed salt, as well as related to the use of a Voronoi discretization for improved accuracy in the flow subproblem. The Voronoi discretization is implemented to handle mesh deformation over time due to creep and the large strains associated with the mechanical behavior of the system. Based on these model improvements, we have updated and completed our study of long-term THM behavior of a generic repository, and this has been summarized and submitted for publication in a journal (Blanco Martin 2014d).

In FY2014, we have also conducted benchmarking in collaboration with the TUC research team, focusing on comparison of the different approaches for sequential coupling of TOUGH2 and FLAC3D. Another benchmark calculation has been initiated involving modeling of the TSDE (*Thermal Simulation for Drift Emplacement*) test conducted in the Asse Mine, Germany. The TSDE analysis will be a major modeling effort that will provide the opportunity to validate the TOUGH-FLAC simulator for drift closure and backfill compaction at a large 3D field setting.

Finally, in FY2014 LBNL has initiated studies of constitutive relationships for brine migration, including a review of existing formulations for the various mechanisms that cause brine mobilization and migration in rock salt, as well as the development of a conceptual model for simulating the flow and transport of brine in salt formations. In particular, we are developing a dual-continuum approach that accounts for brine migration through both interconnected intergranular (i.e., intercrystalline) pore spaces and isolated fluid inclusions (i.e., intracrystalline brine inclusions), considering both pressure and temperature gradients. The plan is to implement such an advanced brine-migration dual-continuum model into the TOUGH2 and TOUGH-FLAC simulators, and then validate the brine-migration model and its implementation against experimental data.

Within the Natural Barrier System (NBS) group of the Used Fuel Disposition (UFD) Campaign at DOE's Office of Nuclear Energy, LBNL's research activities have focused on understanding and modeling coupled processes and impacts of the EDZ and high-temperature on parameters and processes relevant to performance of a salt repository. This report documents results from some of these activities. These activities address key Features, Events and Processes (FEPs), which have been ranked in importance from medium to high, as listed in Table 7 of the *Used Fuel Disposition Campaign Disposal Research and Development Roadmap* (FCR&D-USED-2011-000065 REV0) (Nutt, 2011). Specifically, they address FEP 2.2.01, Excavation Disturbed Zone, for salt, by investigating how coupled processes affect EDZ evolution; FEP 2.2.05, Flow and Transport Pathways; and FEP 2.2.08, Hydrologic Processes, and FEP 2.2.07, Mechanical Processes by studying near-field coupled THM processes in salt repositories. The activities documented in this report also address a number of research topics identified in *Research & Development (R&D) Plan for Used Fuel Disposition Campaign (UFDC) Natural System Evaluation and Tool Development* (Wang, 2011), including Topics S3, Disposal system modeling – Natural system; P14, Technical basis for thermal loading limits; and P15 Modeling of disturbed rock zone (DRZ) evolution (salt repository).

In the following sections of this report, we provide more details on the FY2014 work, first presenting updated tools and improvements made to the TOUGH-FLAC simulator, and the use of this updated tool in a new model simulation of long-term THM behavior within a generic repository in a salt formation (Section 2). This is followed by the description of current benchmarking and validations efforts, including the TSDE experiment (Section 3). We then present the current status in the development of constitutive relationships and the dual-continuum model for brine migration (Section 4). We conclude with an outlook for FY2015, which will be much focused on model validation against field experiments and on the use of the model for the design studies related to a proposed heater experiment.

2. UPDATED TOOLS TO MODEL THM PROCESSES IN SALINIFEROUS MATERIALS

A modified version of the TOUGH-FLAC simulator (Rutqvist and Tsang, 2003; Rutqvist, 2011) was developed during FY2013 (Rutqvist et al. 2013) to accommodate some aspects related to the modeling of THM processes in saliniferous formations. This version included an algorithm to update geometrical data in the flow simulator (due to the use of the large-strain mode in the geomechanics problem) and a porosity evolution function that takes into account the effect of both the different flow phases present and the geomechanical response. It also included dedicated constitutive models for natural salt and crushed salt, and material-specific coupling functions from mechanics to flow.

During FY2014, we have continued working on this updated version of TOUGH-FLAC, and we now have an improved version. In this section, we explain the main improvements that we have made during this year. In addition, in FY2014 we have continued our beneficial collaboration with TUC, and we have included, in the constitutive model (referred to as *Lux/Wolters*) some recent improvements developed by Prof. Lux's team. In parallel to this, we have developed an improved version of the constitutive model available in FLAC^{3D} for crushed salt. All these improvements are detailed here.

2.1 Updated TOUGH-FLAC simulator for large strain and creep

The TOUGH-FLAC simulator, developed at LBNL (Rutqvist and Tsang 2003), is based on an explicit sequential method for coupling flow and geomechanics. The multiphase fluid and heat flows are computed by TOUGH2 (Pruess et al., 2011), and the geomechanical response of the system is calculated using FLAC^{3D} (Itasca, 2011). The main advantages of sequential methods include the use of existing robust and well-established simulators for each subproblem, the resolution of smaller systems of equations, the use of different time-stepping algorithms, and the possibility to study different domains in each subproblem (Dean et al., 2006; Felippa and Park, 1980; Thomas et al., 2003; Vijalapura et al., 2005).

The coupling scheme between TOUGH2 and FLAC^{3D} is based on the fixed stress-split method (Kim et al. 2011). In this method, the flow problem is solved first (with an explicit evaluation of the volumetric total stress), and the pore pressure and temperature are prescribed during the geomechanical calculation, which therefore requires drained rock-mechanical properties.

In order to accommodate the large strains and time-dependent processes associated with saliniferous materials (creep, mesh distortions, crushed salt reconsolidation, etc.), TOUGH-FLAC has required some updates. Indeed, FLAC^{3D} has the capability to deal with large strains, but TOUGH2 does not. In FY2013, we developed an algorithm to update the mesh in the flow subproblem as the geomechanics mesh deforms (Rutqvist et al., 2013), and we implemented a recent formulation of coupled geomechanics and multiphase fluid and heat flows developed by Kim et al. (2012). This analytical formulation is an extension of the classic thermodynamic approach implemented in TOUGH2 and includes a porosity correction term that accounts for the geomechanical effect (via the volumetric component of the total stress tensor).

In FY2014, we have reformulated the balance equations solved in TOUGH2 to account for geometrical changes and ensure mass conservation. This way, after every FLAC^{3D} call, mass is conserved, but density is not. The geometrical update is made at the first iteration of the TOUGH2 Newton-Raphson process (Pruess et al., 2011). In this iteration, the primary variables

(pore pressure, temperature, and saturation) and porosity remain equal to those at the end of the previous time step (only geometrical data are different), and we check whether the system continues to be in thermodynamic equilibrium for a new time increment and new geometry. If the maximum residual exceeds a preset convergence tolerance, an iterative process is carried out. In this process, the geometry is kept unchanged (i.e., the geometry is updated in TOUGH2 after every FLAC^{3D} call, but is constant during each TOUGH2 run) and consistency in the balance equations is ensured through the porosity-variation formulation, adapted from (Kim et al., 2012). The balance equations for a grid block *n* read:

$$\frac{d\left(M_n^\kappa V_n\right)}{dt} = \sum_m A_{nm} F_{nm}^\kappa + q_n^\kappa \rightarrow \frac{dM_n^\kappa}{dt} + M_n^\kappa \frac{dV_n}{Vdt} = \frac{1}{V_n}\left(\sum_m A_{nm} F_{nm}^\kappa + q_n^\kappa\right) \tag{2.1}$$

for κ=1, *NK* (*NK* is the total number of fluid components [air, water, etc.]). In Equation (2.1), M_n^κ is the accumulation term, V_n is the volume of the grid block (new volume after FLAC^{3D} call), q_n^κ represents the sink/sources, and F_{nm}^κ is the flow of component κ across surface A_{nm} (new value after FLAC^{3D} call). We note that for second and further iterations, the term $M_n^\kappa \frac{dV_n}{Vdt}$ is not computed. The accumulation terms read

$$M_n^\kappa = \phi \sum_\beta S_\beta \rho_\beta \chi_\beta^\kappa \tag{2.2}$$

where ϕ is porosity, S_β is the phase saturation, ρ_β is the density of phase β, and χ_β^κ is the mass fraction of component κ in phase β. Porosity changes during a time step (for second and further iterations) are calculated adding a porosity variation $d\phi$, which includes a correction term, $\Delta\phi$, from geomechanics (therefore, it includes volume changes). This term is constant for a given time step. This way, the geometrical data used during the iterations of a time step are consistent, and mass conservation is ensured. The porosity variation has the form

$$d\phi = A(\alpha, \phi, K)dP + B(\alpha_{th})dT + \Delta\phi \tag{2.3}$$

where α [-] is the Biot coefficient, α_{th} [K^{-1}] is the linear thermal expansion coefficient, K [MPa] is the drained bulk modulus, and $\Delta\phi$ is the porosity correction from geomechanics. A detailed explanation of this formulation can be found in Kim et al. (2012). The Biot coefficient is defined as the ratio of the fluid-volume variation in a material element to the volume change of that element. It gives an indication of the grain compressibility with respect to the bulk compressibility, and of the coupling strength. It can take the values $\alpha \in [0,1]$; a Biot coefficient close to 1 describes a high poromechanical effect (the grains are not compressible, so the pores take an important role), whereas a low value indicates that the poromechanical effect is low (the response of the grains and the bulk material is similar, so the coupling strength is low).

Currently, the modeling sequence is as follows. TOUGH2 moves the simulation forward and FLAC^{3D} is executed once within a TOUGH2 time step, just before the Newton-Raphson iteration process to solve the residual nonlinear equations. A schematic view of the coupled THM modeling sequence is displayed in Figure 2-1. The pressure, P^n, temperature, T^n, liquid saturation, S_l^n, and porosity, ϕ^n, of each grid block computed at the end of the previous time step

(from t^{n-1} to t^n) are transferred to FLAC^{3D}. Note that the pressure transferred depends on the definition of pore pressure (Coussy 2004; Kim et al. 2013); more details will be given in Subsection 2.1.1.

From flow to geomechanics, the pore-pressure change, $\Delta P = P^n - P^{n-1}$, and the temperature change, $\Delta T = T^n - T^{n-1}$, corresponding to two successive TOUGH2 time steps are accounted for as a correction to the total stress tensor, σ_{ij} (direct coupling). These changes are computed internally in FLAC^{3D} once the new values P^n and T^n are transferred. The corrected total stress tensor, σ_{ij}^c, has the form

$$\sigma_{ij}^c = \sigma_{ij} - \alpha \Delta P \delta_{ij} - 3\alpha_{th} K \Delta T \delta_{ij} \tag{2.4}$$

where δ_{ij} [-] is the Kronecker delta. Compressive stresses are defined negative here. From Equation (2.4), it can be inferred that the coupling from flow to geomechanics (TOUGH2 to FLAC^{3D}) affects only the volumetric component of the stress tensor. Porosity and liquid saturation are used to update the body forces in the quasi-static governing equations of the geomechanical analysis (Kim et al. 2012). Note that these equations account for the thermal strains that result from the temperature change ΔT.

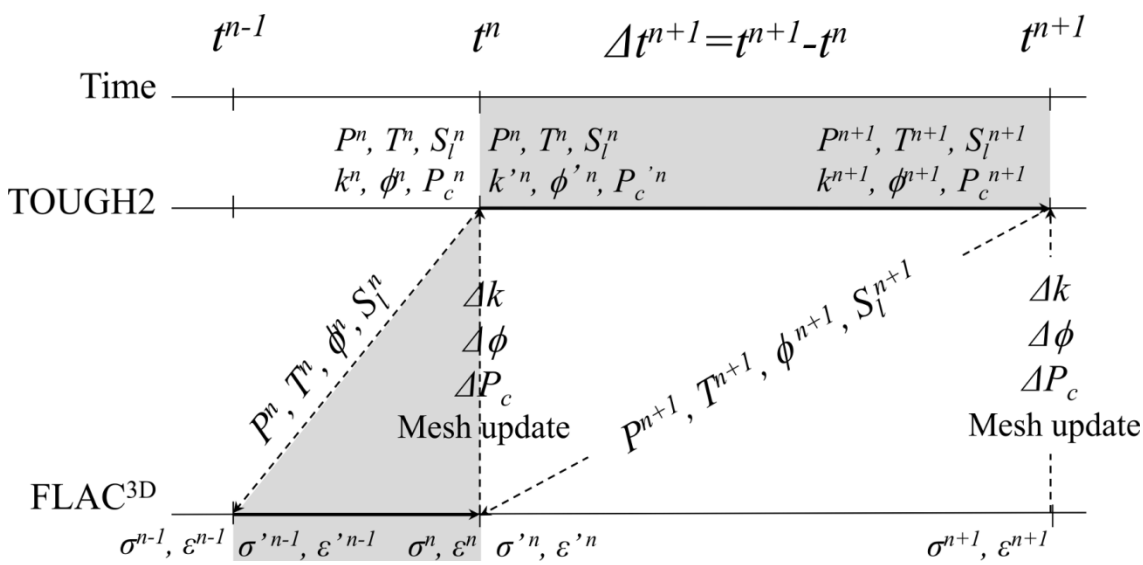

Figure 2-1. Explicit sequential THM analysis scheme (adapted from (Rutqvist et al., 2002)). The highlighted zones correspond to the time step between time t^n and t^{n+1}.

Once all the updates are made, FLAC^{3D} runs in creep and large strain modes from time t^{n-1} to time t^n. A new equilibrium mechanical state is obtained at time t^n (stresses σ^n and strains ε^n in Figure 2-1). Recall that during the mechanical calculation, the flow data (P^n, T^n, S_l^n, and ϕ^n) remain constant. In FLAC^{3D} the new static equilibrium is established internally through a dynamic-solution approach, solving the equation of motion in which the inertial terms are used as numerical means to reach the equilibrium state of the system under consideration. The established new static equilibrium brings about a new strain tensor and a new effective stress tensor (i.e., a new mechanical state).

From geomechanics to flow, geometrical changes are first accounted for. The geometrical data updated in TOUGH2 are: volume of the elements, distances of the centroids of two connected elements to their common interface, common interface area, and cosine of the angle between the gravitational acceleration vector and the line between the centroids of two connected elements. Also, as explained before, in the first Newton-Raphson iteration, the accumulation terms in the balance equations are updated to account for possible volume changes.

Additionally, the new mechanical state obtained at t^n is used through several coupling functions to compute mechanically induced changes in permeability and capillary pressure (Δk and ΔP_c in Figure 2-1). The coupling functions depend on each material (and the phenomena it goes through) and should be based on specific laboratory and theoretical results; they have been presented previously for the natural salt and the crushed salt (Rutqvist et al. 2013), and only the improvements will be discussed here. The mechanically modified flow properties (k'^n, ϕ'^n and $P_c'^n$ in Figure 2-1) are used to solve the residual equations of the flow problem. Within a time step, the Newton-Raphson iteration process is continued until the residuals are reduced below a preset convergence tolerance. At the end of the current time step (time t^{n+1} in Figure 2-1), a new set of primary thermodynamic variables (P^{n+1}, T^{n+1} and S_l^{n+1} in Figure 2-1) and new flow properties (k^{n+1}, ϕ^{n+1} and P_c^{n+1} in the figure) are obtained.

Another improvement incorporated into TOUGH-FLAC during FY2014 consists in the use of a Voronoi discretization in the flow subproblem, even when the mesh deforms over time due to the creep and the large strains associated with the mechanical behavior of saliniferous materials. Since the resolution method used in TOUGH2 is based on the Voronoi partition (Pruess et al. 2011), more accurate solutions will be obtained when the discretization of the flow subproblem conforms to this technique. If the domain under study deforms over time, the partition used in the flow subproblem should still comply with the resolution method of the code. Bearing this in mind, we use the software library Voro++ (Rycroft, 2009) to ensure that the mesh used in TOUGH2 conforms to the principles of the Voronoi tessellation. This is an innovation with respect to previous studies using TOUGH-FLAC.

As the mesh deforms in the geomechanics subproblem, Voro++ is executed to compute the corresponding Voronoi tessellation. This operation is performed every time the mesh deforms with respect to strains a preset value, typically 2–5 % (Benz 2007). In the current approach, the centroids of the deformed geomechanical mesh are transferred to Voro++, which computes the corresponding Voronoi discretization. Geometrical data of the new Voronoi mesh (volumes, common interface area between two adjacent grid blocks, etc.) are then transferred to TOUGH2.

Figure 2-2 shows a detail of two grids (flow and geomechanics) used in some of the THM simulations performed during FY2013 (initial mesh and deformed mesh after 20 years). As can be seen, the flow subproblem uses Voronoi cells, both in the initial and the deformed configurations. In addition, it can be seen in the figure that the grid blocks at the boundary between two different domains (waste package, backfill, and host rock) are slim and have the same thickness. This way, Voro++ will conserve the volume of each domain even when the mesh deforms (the generators of the Voronoi mesh are the centroids of the mesh used in FLAC^{3D}).

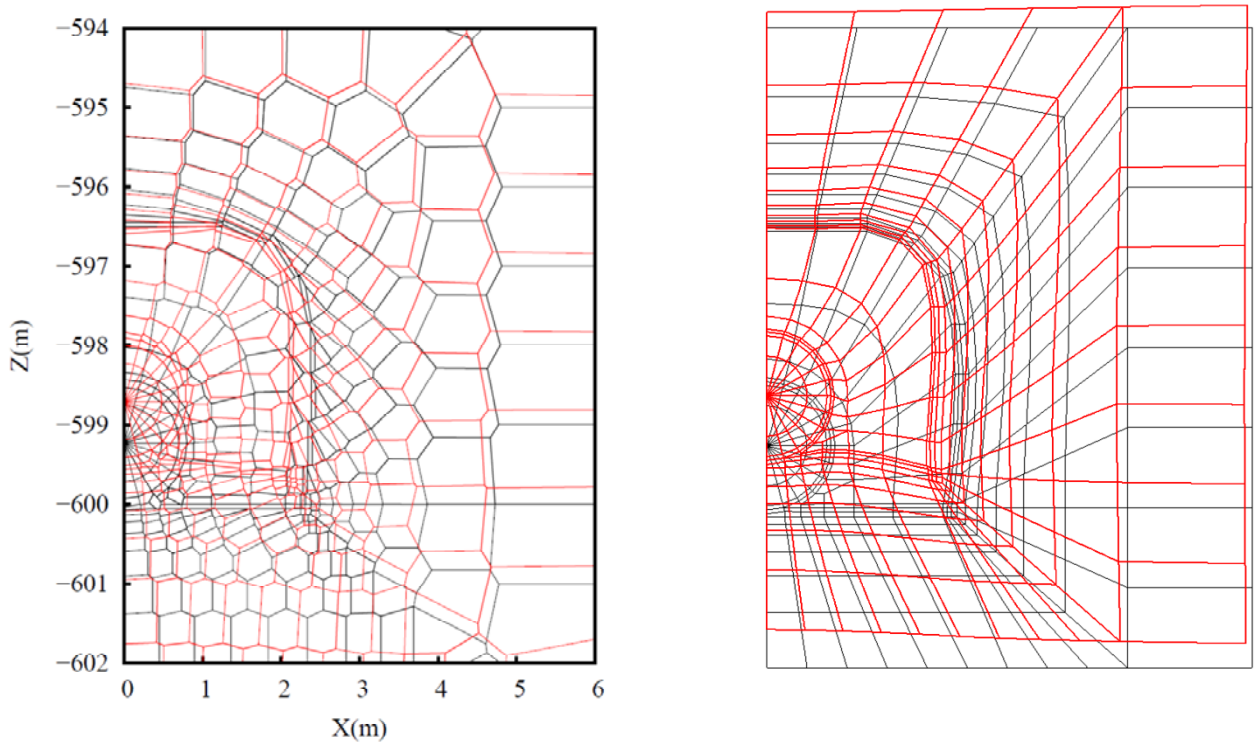

Figure 2-2. Mesh update in large strain mode. Example of initial and deformed discretizations in the (left) flow sub-problem and (right) geomechanics sub-problem.

Finally, in order to reduce the simulation times (a 2D THM simulation of one backfilled drift, run to 100,000 years, takes between 3–5 weeks on a PC [mesh discretized into about 1000 grid blocks]), it was decided to perform the coupling between TOUGH2 and FLAC^{3D} every two time steps after 10,000 years. Indeed, the most relevant coupled processes take place within the first 1000 years, as will be shown in Section 3. Performing the coupling less often when relevant processes are attenuated lets us decrease the time needed to compute one simulation and conduct more simulations to explore the effect of different parameters on the long-term predictions. We recall that FLAC^{3D} only runs on Windows-based OS, and that only two FLAC^{3D} simulations are allowed simultaneously on a PC for license reasons.

2.2 Pore pressure definitions in geomechanics

Different pore pressure concepts are available to use in geomechanics when several fluid phases occupy the pores:

- Maximum pore pressure (gas pressure in TOUGH2);
- Saturation-weighted average fluid pressure, and
- Equivalent pore pressure (Coussy, 2004). The equivalent pore pressure is defined as

$$P_{eq} = \sum_{i=1}^{NPH} P_i S_i + U \tag{2.5}$$

where P_i is phase pressure, S_i is phase saturation, U is the interfacial energy per unit of pore volume, and NPH is the number of phases present (Coussy 2004). Neglecting the temperature dependence of capillary forces, the interfacial energy can be determined from the capillary curve according to

$$U(S_w) = \int_{S_w}^{1} P_{cap}(S)dS \tag{2.6}$$

where $P_{cap}<0$ is the capillary pressure. According to Coussy (2004), the equivalent pore pressure should be used in multiphase flow problems when capillary forces are non-negligible, which is the case with natural salt and the reconsolidated crushed salt, due to their very low porosity (ϕ<1-2 %). In addition, this pressure is the proper definition of multiphase pore pressure, because it renders a formulation that is dissipative (Kim et al. 2013).

In order to investigate the sensitivity of the THM predictions to the pore pressure used in geomechanics, we have conducted simulations using the three different concepts, but we have retained the equivalent pore pressure as our reference pore pressure (i.e., this is the pore pressure used in the base-case scenario presented in Section 3). The main differences between the three concepts arise when capillary effects are important, i.e., when liquid saturation and porosity are low. In the generic salt repository considered in this research, the host rock adjacent to the drift contour will be the most sensitive zone to the pore pressure used, particularly during the first years, when liquid saturation drops in this area. The backfill THM evolution may also be sensitive to the pore-pressure concept if the saturation is low by the end of the reconsolidation process; nonetheless, our simulation results show that saturation in the backfill approaches 1 when porosity approaches the characteristic porosity of the natural salt (see Section 3 for a description of the results).

Overall, the higher the pore pressure used in geomechanics, the higher the damage to the barriers, which leads to a higher porosity increase, higher permeability increase, and also an increase in coupling effects (through the Biot coefficient, which is damage-dependent, as will be explained below). Since salt damage is reversible, once the pore pressure drops, all these effects are reversed. However, in other situations, damage may not be reversed, and hence the choice of the pore pressure used in geomechanics may have a significant impact on the numerical predictions. We note that our results show that the use of the maximum pore pressure in geomechanics leads to the most conservative predictions.

2.3 Improvements in the modeling of THM processes in natural salt

Currently, we model the behavior of the natural salt using the *Lux/Wolters* constitutive model, developed at Clausthal University of Technology (TUC). This model has been under development and improvement since the 1980s (Hou 2003; Hou and Lux 2000, 1999, 1998; Hou

et al. 1998; Lux 1984; Wolters et al. 2012). Based on continuum damage mechanics, it has been established using a series of laboratory investigations designed to study, from a macroscopic viewpoint, the mechanisms involved in the short- and long-term responses of rock salt. This model has been validated against field- and laboratory-scale data (Hou 2003) and has been implemented as a plug-in (user-defined model) in FLAC^{3D}.

The *Lux/Wolters* model was detailed previously (Rutqvist et al., 2013; Wolters et al., 2012). The total strain rate tensor, $\dot{\varepsilon}_{ij}$, is composed of the superposition of four strain-rate tensors issued from different mechanisms: elastic (ε^{e}_{ij}), viscoplastic (ε^{vp}_{ij}), damage-induced (ε^{d}_{ij}) and healing processes (ε^{h}_{ij}). The total strain rate tensor reads

$$\dot{\varepsilon}_{ij} = \dot{\varepsilon}^{e}_{ij} + \dot{\varepsilon}^{vp}_{ij} + \dot{\varepsilon}^{d}_{ij} + \dot{\varepsilon}^{h}_{ij} \tag{2.7}$$

Each of these components has been detailed previously (Rutqvist et al. 2013). They all take a damage-induced reduction of the load-bearing cross-sectional area into account, in accordance with a previous study (Kachanov 1986). We recall that the damage-strain-rate tensor comes into play if there is an excess of either tensile or shear stresses beyond a failure (or dilatancy) boundary. In practice, the tensile strength is often set to zero. Shear strength is a function of the minimum principal stress and the Lode angle. The damage strain rate tensor has a non-zero volumetric component (i.e., damage causes a nonelastic volume change, also referred to as dilatancy). In turn, healing reduces dilatancy and damage, but cannot occur while damage (shear or tensile yielding) is taking place. Moreover, some damage is necessary before healing can actually start. According to laboratory observations, in the *Lux/Wolters* model, the recovery of damage is faster at the beginning of the healing process (due to a rapid volume contraction), while in a second stage, slower mechanisms such as re-crystallisation or diffusion dominate, (Hou 2003). In total, the *Lux/Wolters* constitutive model needs 34 parameters (Lerche 2012). However, the number of parameters used in a simulation may be reduced depending on the phenomena under investigation.

During FY2014, we have introduced some improvements to the *Lux/Wolters* model, as provided by Prof. Lux's team, with whom we collaborate closely. The main improvement concerns the damage dependence of the Biot coefficient (recall that the Biot coefficient controls the strength of the coupling effects between flow and geomechanics). In the undisturbed state, the Biot coefficient of rock salt is very close to zero (Hou 2002), but increases as damage takes place. From the interpretation of laboratory-scale results, the evolution of the Biot coefficient is described by

$$\alpha_{salt} = \max\left(\frac{D}{D_{\alpha}},\ 1 - \exp\left(\frac{\sigma_v\, m\, D}{D - D_{\alpha}}\right)\right) \tag{2.8}$$

where D [-] is a damage parameter (Hou, 2002; Wolters et al., 2012), D_{α}=0.1 [-] is a constant, σ_v [MPa] is von Mises equivalent stress and m<0 [MPa^{-1}] is a parameter that enhances Maxwell viscosity. Note that healing can restore the initial Biot coefficient.

Finally, we highlight that the simulation results presented in this report include healing processes. (We received a new version of the *Lux/Wolters* model during the last part of FY2013, but could not provide long-term results using this new version in last year's report [Rutqvist et al. 2013]. With this new version, the modeling of dilatancy and healing can be now performed much more accurately.)

2.4 Improvements on the modeling of THM processes in crushed salt

In last year's report, we presented the *cwipp* model available in FLAC^{3D} to model the reconsolidation process of granular salt. This model is based on previous studies on crushed salt compaction (Callahan and DeVries 1991; Sjaardema and Krieg 1987) and on the *wipp* model for natural salt, also implemented in FLAC^{3D} (Itasca 2011).

The main characteristic of the *cwipp* model is that it allows modeling volumetric strain changes associated with creep processes (classically, viscoplasticity occurs at constant volume). The total strain rate tensor, $\dot{\varepsilon}_{ij}$, comprises a nonlinear elastic component, a viscous compaction component and a viscous shear contribution. The latter is adapted from the *wipp* model and is purely deviatoric. The total strain rate tensor reads

$$\dot{\varepsilon}_{ij} = \dot{\varepsilon}_{ij}^{e} + \dot{\varepsilon}_{ij}^{vc} + \dot{\varepsilon}_{ij}^{vs} \tag{2.9}$$

where superscripts *e*, *vc* and *vs* stand for elastic, viscous compaction, and viscous shear, respectively. As reconsolidation occurs, density increases towards that of the natural salt. In the *cwipp* model, density is a monotonic function. The nonlinear compaction density rate is derived from experimental results (Callahan and DeVries 1991; Sjaardema and Krieg 1987). The viscous compaction term in the model accounts for the density evolution during compaction. This term is only active if the mean effective stress is compressive and if the monotonic density has not yet reached the intact salt density (i.e., there is no further compaction beyond the intact salt density). During compaction, the elastic properties (shear, *G,* and bulk, *K,* moduli) increase as the monotonic density increases according to a nonlinear empirical expression of the form

$$a = a_{salt} \exp\left(a_1 \left[\rho - \rho_{salt}\right]\right) \tag{2.10}$$

where $a=\{K,G\}$. Variables ρ and ρ_{salt} stand for the drained densities of the crushed salt and the natural salt, respectively. Parameter a_1 [kg^{-1}m^3] is obtained from the condition that the moduli take their initial value at the initial value of density. When $\rho=\rho_{salt}$, the elastic moduli are those of the natural salt, $K=K_{salt}$ and $G=G_{salt}$. In total, the *cwipp* model is characterized by 17 parameters.

During FY2014, we have worked on an improved version of the *cwipp* model. Indeed, in this model, density is monotonic, and therefore it is not allowed to increase even if the mean compressive stress increases. To avoid this limitation, we have developed a modified version in which density honors the volumetric strain evolution, but we have respected the other features of the original *cwipp* model.

As the bulk modulus increases towards that of the intact salt, the Biot coefficient decreases from almost 1 to the Biot coefficient of the host rock; therefore, the poromechanical effects within the backfill will be more important before substantial compaction occurs The Biot coefficient is calculated using

$$\alpha_{crushed\ salt} = 1 - \frac{K}{K_s} \tag{2.11}$$

where K is the drained bulk modulus, and K_s is the bulk modulus of the solid material.

It is important to highlight that the long-term mechanical responses predicted by the *cwipp* and the *Lux/Wolters* models are similar: due to the creep over time, the stresses tend toward the isotropic state and therefore the deviatoric components of both models tend to zero. For the crushed salt, the compaction component vanishes after full reconsolidation, and for the natural salt, damage and healing counteract each other. Consequently, only the elastic components prevail (see Equations (2.7) and (2.9)). Given that after reconsolidation the elastic moduli of the crushed salt are equal to those of the natural salt, the modeled long-term response of the two materials is similar.

3. MODELING OF THM PROCESSES IN THE LONG TERM FOR A GENERIC SALT-BASED REPOSITORY

In this section, we first describe the generic salt repository for high-level nuclear waste that we have investigated. This repository is based on the in-drift emplacement concept (DOE/CBFO, 2012), and we have assumed that the drifts are backfilled with granular salt (i.e., crushed salt) after the waste packages are emplaced. In such a scenario, the crushed salt backfill gets progressively compacted as the natural salt creeps. Once the reconsolidation process is over, it is expected that the backfill will provide an engineered barrier (Bechthold et al. 2004; Wieczorek et al. 2012), thereby contributing to the natural barrier supplied by the host rock (geological barrier). In this context, the main goal of our simulations is to evaluate the long-term integrity of these two barriers. The analysis of the results will also let us evaluate possible improvements needed in the updated TOUGH-FLAC simulator.

After a description of the model, THM properties, and initial and boundary conditions, we present the results of our base-case scenario. This scenario is characterized by the use of the equivalent pore pressure in the geomechanics subproblem, and by the assumption that the host rock is fully saturated with brine. Then, in order to evaluate the importance of coupled THM processes in the long-term predictions, we compare THM and TH simulation results. The importance of accounting for capillary forces is also discussed. Finally, we investigate the sensitivity of the coupled simulation results to the initial saturation within the natural salt.

3.1 Model description

In our generic salt repository, the waste packages are parallel to the drift axis. The model extends 1200 m in the vertical direction (Z axis) and starts at the ground surface (Z=0). The repository is located in the middle of a 400 m thick salt layer, at a depth of 600 m. Two 400 m thick sandstone

layers confine the salt seam. The drifts are 4.5 m wide and 3.5 m high. Cylindrical metallic waste packages are 5.5 m long, have a diameter of 1.6 m, and are spaced 3 m along the drift axis.

Considering the expected drifts length, a plain-strain assumption is adequate, which reduces the 3D problem to two dimensions, so that only one element column is needed in the out-of-plane direction (*Y* axis). In addition, symmetry allows modeling just half of one drift. In the *X* direction, half the distance between drifts is considered, which corresponds to ~25 m. The model geometry is presented in Figure 3-1, with an enlarged view of the area near the drift. Model dimensions are similar to those presented in last year's report (Rutqvist et al. 2013). However, we now use a finer discretization in the drift area.

Along with the mechanical response, two-phase flow of water and air (by advection and diffusion) and heat flow (by conduction and convection) are modeled. TOUGH2 Equation Of State (EOS) module 4 is used (Pruess et al. 2011). This module provides a capability for vapor-pressure lowering, which allows a liquid phase to exist when the vapor partial pressure and the gas-phase pressure are lower than the saturation pressure (due to phase adsorption and capillary effects). Vapor pressure lowering is modeled via Kelvin's equation.

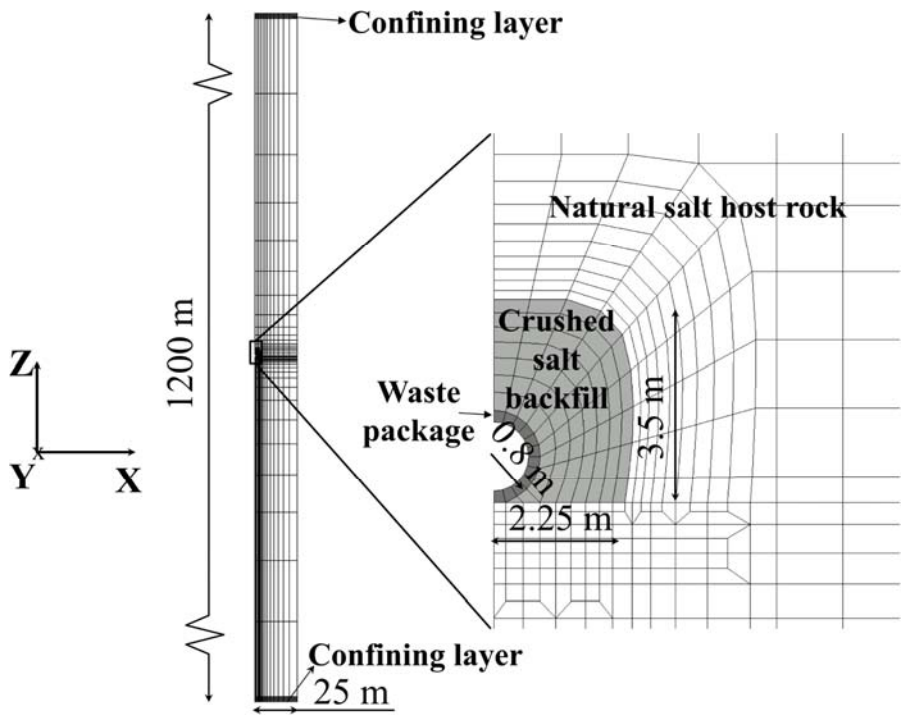

Figure 3-1. Geometry of the generic salt repository studied, with enlarged view of the drift area.

The heat released by each waste package is consistent with the expected nuclear waste characteristics in the U.S. Department of Energy Used Fuel Disposition Campaign (Carter et al. 2011). It is assumed that each waste package comprises ten pressurized water reactor (PWR) assemblies, and that the packages are emplaced underground after 20 years of interim storage. Under these conditions, and taking the size and distance between canisters into account, the average heat load per meter of drift is ~1000 W at the time of emplacement. The heat load evolution after emplacement is displayed in Figure 3-2. (Note that the time is reset when the waste packages are emplaced underground.)

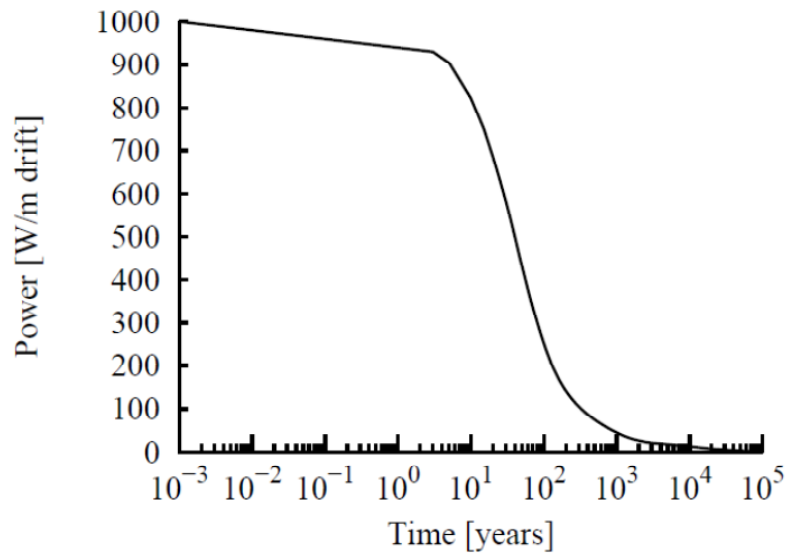

Figure 3-2. Heat load per meter of drift for a waste package containing 10 PWR assemblies, assuming underground emplacement 20 years after reactors shut-down (after Carter et al., 2011).

Error! Reference source not found. lists relevant parameters of the crushed salt, the host rock and the confining layers. Some capillarity parameters of the van Genuchten function (van Genuchten 1980) have been adapted from previous research (Camphouse et al. 2012). Temperature and hysteresis effects on water retention are neglected.

From a mechanical viewpoint, the waste package and the confining layers are assumed to behave elastically. The *Lux/Wolters* model parameters used for the host rock have been obtained from the interpretation of experimental results (Lerche 2012). Regarding the *cwipp* model for the crushed salt, the values used have been retrieved from a report related to the German salt repository program (DBE 2011). They correspond to slightly wet crushed salt.

For the waste package, we assume ρ=7800 kg·m^{-3}, α=1, k=0 m^2 and ϕ=0.01%. Its pores are saturated with gas, and capillary effects are disregarded because no phase changes are expected. For this reason, the relative permeability functions do not have any influence on the simulation results. The elastic properties correspond to standard steel. Note that the compressibility and expansivity have been set to zero to block any change in porosity.

The evolution of the flow properties of the natural salt and the crushed salt has been described previously (Rutqvist et al. 2013; Blanco Martín et al. 2013; 2014a-c). We recall here that, for the natural salt, permeability increases if either thermomechanically or hydraulically induced damage occurs. Laboratory results have been used to formulate the permeability evolution for each of these two damage processes (Wolters et al. 2012). If healing occurs, the accompanying permeability decrease is calculated using the same formulations. In addition, the grain-specific heat of the natural salt increases linearly with temperature, and the thermal conductivity decreases nonlinearly with temperature (Bechthold et al. 1999). For the crushed salt, we account for well-known evolution of properties during compaction. These include a nonlinear decrease in permeability and a nonlinear increase in thermal conductivity and elastic parameters (Bechthold et al. 1999; 2004; Callahan and DeVries 1991). In addition, the Biot coefficient decreases (see Equation (2.11)) and capillary effects strengthened during compaction. We use a Leverett

function to scale capillary forces (Cinar et al. 2006). Finally, regarding the waste package and the confining layers, their properties are kept constant during the simulations: the waste package is only modeled to account for the heat release into the repository, and the confining layers are far from the drift, so they are hardly influenced by the THM processes occurring in the drift area.

Table 3.1. Mechanical and flow properties of the crushed salt, natural salt and sandstone layers.

Property [unit]	*Crushed salt*	*Rock salt*	*Sandstone layers*
Grain density, ρ [kg·m^{-3}]	2,200	2,200	2,600
K [MPa]	70	7,690	19,500
G [MPa]	150	16,650	37,900
α_{th} [K^{-1}]	$4\cdot10^{-5}$	$4\cdot10^{-5}$	10^{-5}
α [-]	1[a]	0.003 [b]	1
Relative permeability functions	Corey	Corey	Van Genuchten (liquid), Corey (gas)
Residual liquid saturation, S_{lr} [-]	0.05	0.05	0.02
Residual gas saturation, S_{gr} [-]	0	0	0.01
Van Genuchten's λ [-]	0.32	0.675	0.595
Van Genuchten's P_0 [MPa]	0.0005	14.7	14.7
Van Genuchten's P_{max} [MPa]	50	100	100
Van Genuchten's S_{lr} [-]	0.01	0.01	0.01

[a]: non-constant value; [b]: values are damage- and healing- dependent

The molecular diffusion coefficients (diffusion of water and air) depend on pressure and temperature (Vargaftik 1975; Walker et al. 1981). Moreover, tortuosity effects are accounted for using the nonlinear Millington-Quirk model (Millington and Quirk 1961). In previous simulations, tortuosity was assumed to be a linear function of saturation, and the diffusivities were assumed to be constant.

Initial flow parameters are listed in Table 3.2. The absolute permeability k is assumed isotropic for every material.

Table 3.2. Initial flow parameters of the crushed salt, natural salt and sandstone layers.

	Crushed salt	*Rock salt*	*Sandstone layers*
S_l [-]	0.02	1	1
ϕ [-]	30 %	0.2 %	12 %
k [m^2]	$3\cdot10^{-13}$	10^{-22}	10^{-17a}
λ [W·m^{-1}·K^{-1}]	0.9	4	1.8[a]
C [J·kg^{-1}·K^{-1}]	860	860	900[a]

[a]: constant values

A geothermal gradient of 0.025 K·m^{-1} is initially applied to the model. This corresponds to about 28ºC at the repository level, assuming a ground surface temperature of 10ºC. The initial mechanical condition is isotropic stress, equal to the lithostatic stress magnitude (overburden); this corresponds to about -14 MPa at Z=-600 m. The initial fluid pressure in the host rock and confining layers is hydrostatic. We assume that the water table is at the ground surface. Prior to the THM run, the excavation, subsequent emplacement of waste packages, and backfill are modeled in FLAC^{3D} to account for induced stress redistribution and possible changes in the pore pressure. The pore pressure obtained after the excavation is exported to TOUGH2, so that the initial conditions of the THM run are the same in the two codes. (The coupled THM simulation covers the post-closure phase of the repository, once the heat-generating waste packages are emplaced and the drifts are backfilled.) Note that the initial pore pressure within the backfill and the waste package is set to 0.1 MPa (atmospheric pressure). At this stage, and according to the fixed stress-split method to couple flow and geomechanics (Kim et al. 2011), the FLAC^{3D} capability to calculate pore pressure is deactivated (i.e., the pore pressure computed by TOUGH2 is used in both codes, see Figure 2-1).

In TOUGH2, Dirichlet boundary conditions are assigned to the top and bottom grid blocks, so that their thermodynamic state remains unchanged. Owing to symmetry, the lateral surfaces of the model are no-flow boundaries. In FLAC^{3D}, the horizontal displacement is blocked in planes X=0 and X=25 m, as well as the vertical displacement in plane Z=-1200 m. Gravitational effects are considered in both codes.

3.2 THM base-case scenario

As explained before, two features characterize the base-case scenario:

- The assumption that the host rock is fully saturated with brine at the beginning, and

- Use of the equivalent pore pressure in the geomechanics subproblem. We believe that this is the correct definition of pore pressure when capillarity effects are important (Coussy 2004).

Figure 3-3 displays the temperature evolution at different positions in the repository over the simulated 100,000 years of post-closure phase. The waste-package surface temperature peaks slightly above 200°C after one year. Note that the nearby crushed salt and host rock also show an initial temperature peak. This local peak results from the low thermal conductivity of the backfill before significant compaction takes place (see Table 3.2). After 25 years, a temperature peak of about 160ºC is obtained in the drift area. The temperature 25 m away from the drift peaks at about 108ºC after 80 years, reflecting progressive heat propagation through the natural salt. As compared to other potential host rocks such as clay or granite, and for a given heat load, the peak temperature in a salt-based repository is lower, owing to a higher thermal conductivity. A comparatively low peak temperature is a desirable performance indicator for a high-level nuclear waste repository.

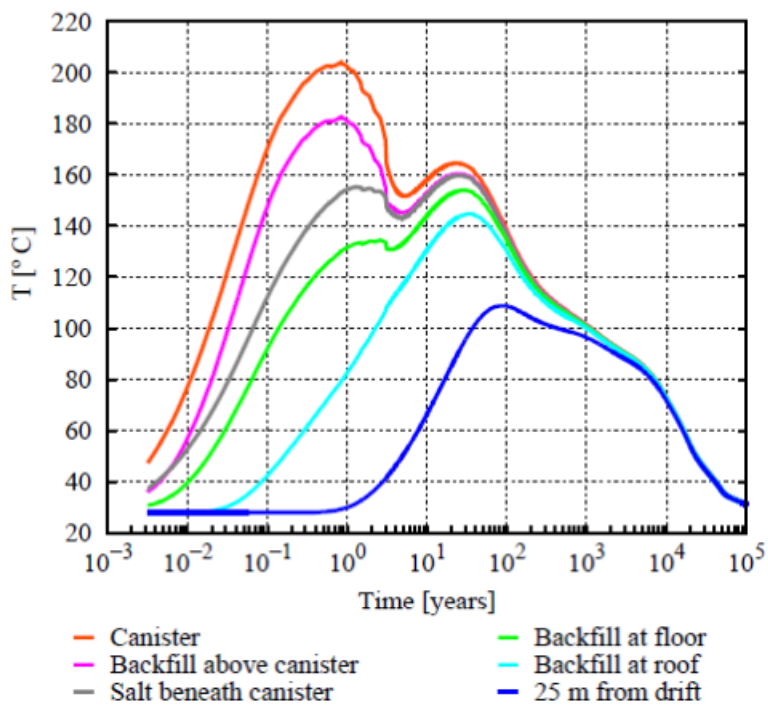

Figure 3-3. THM base case scenario: evolution of temperature at several locations in the repository.

During the excavation phase, simulated before the THM run, a damaged zone develops in the host rock adjacent to the drift contour, due to the high deviatoric stresses in this zone. The thickness of the EDZ is about 1.4 m at the drift floor and 1 m at the sidewalls and roof. Shear damage spreads all around the drift, but tensile damage occurs mostly in the corner area, due to the shape of the drift (see the enlarged view in Figure 3-1). After 4 years, shear dilatancy peaks at 0.71 %, and tensile dilatancy reaches 1.38% (but remains localized in the corner). As a consequence of damage, the permeability increases several orders of magnitude in the EDZ. Porosity also increases, but remains very low (ϕ_{max}<1 %). Moreover, the Biot coefficient

increases according to Eq. (2.8) up to 0.44 in the most damaged areas, thereby intensifying the poromechanical effects.

As the salt creeps under the effect of temperature and deviatoric stresses, the reconsolidation of the crushed salt starts (Figure 3.4). Our results suggest that the reconsolidation process is not uniform in space, due mainly to the shape of the drift and the position of the heat source: greater compaction occurs in the roof and floor areas, and lesser compaction in the sidewalls. These results agree with previous numerical investigations (Stone et al. 2010). Overall, the backfill reconsolidation process takes between 6 and 20 years to complete. This predicted time for reconsolidation is on the same order of magnitude as experimental data (Bechthold et al. 2004; Callahan and DeVries 1991), although some differences exist due to the creep parameters selected for the natural salt (the parameters in Lerche (2012) do not cover the range of very low deviatoric stresses). We note that when the crushed salt is reconsolidated, its porosity has reached the characteristic value of the undisturbed salt; therefore, the new formulation implemented in TOUGH-FLAC to compute porosity changes successfully allows for modeling mechanical compaction. Note that the geomechanical component dominates over the pressure- and temperature-related components in the computation of porosity changes. As the crushed salt reconsolidates, its permeability reduces by up to nine orders of magnitude, and its thermal conductivity increases from 1 to about 4-5 W/m/ ºC. At the same time, the elastic moduli increase towards those of the natural salt (two-orders-of-magnitude increase, cf. Equation (2.10)); as a result, the Biot coefficient decreases towards the characteristic value of the undisturbed natural salt (~0.003) according to Equation (2.11). Note also that capillary forces become stronger as porosity and permeability decrease. An engineered barrier system is progressively created during the reconsolidation process.

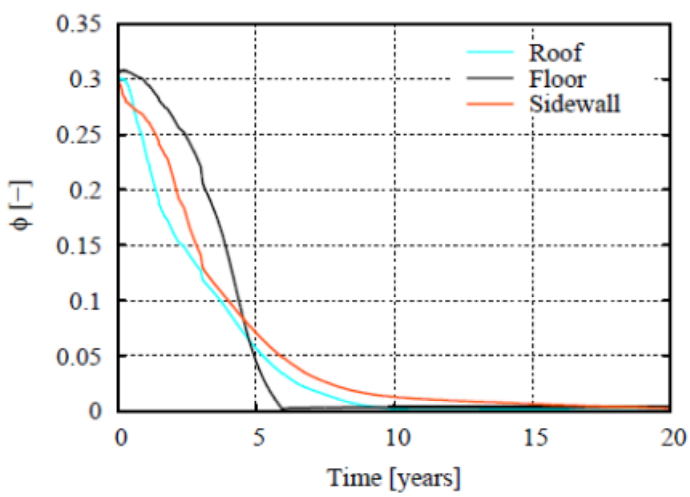

Figure 3-4. THM base case scenario: evolution of porosity within the crushed salt during the first 20 years.

As the crushed salt strengthens, an internal support is provided at the drift walls, which helps decrease the deviatoric stresses. The stress state in the drift area progressively evolves towards isotropic (thus, away from the dilatancy boundary). The occurrence of healing is closely related to the backfill compaction, which confirms the strong two-way interaction between the host rock and the backfill THM evolution. After about 6 years, healing has significantly reduced damage and dilatancy, and, after 7 years, dilatancy has decreased to its initial value. Host-rock tightness is restored to initial conditions after about 7 years. The three images in Figure 3-5 compare the

extension of the EDZ at three moments: after excavation, after 4 years, and after 7 years. While the damaged area increases during the first years, it decreases until vanishing once healing starts.

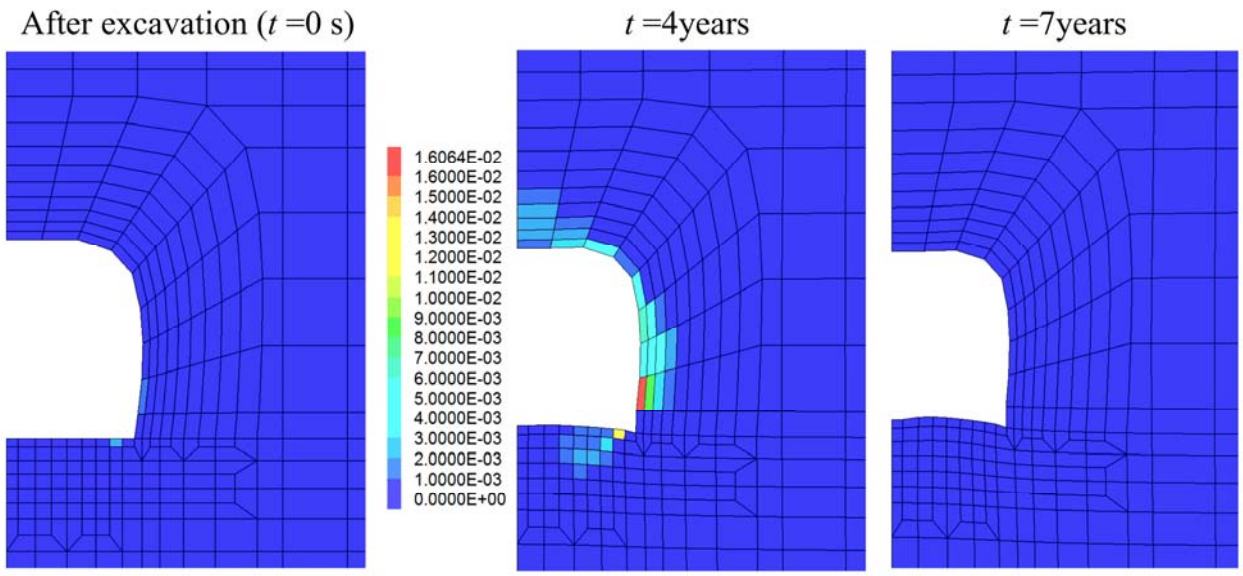

Figure 3-5. THM base case scenario: extension of EDZ at three different moments. For *t*=0 s, *k*=10^{-20} m^2; *t*=4 years, *k*=10^{-18} m^2 and *t*=7 years, *k*=10^{-22} m^2.

As temperature increases overall after about 5 years, the pore pressure increases, too, and exceeds the hydrostatic value. In the natural host rock salt, the very low permeability, saturated conditions, and high thermal expansion coefficient of the pore fluid relative to the host rock are key factors for this thermal pressurization. Concerning the crushed salt backfill, the compaction-induced volume reduction facilitates resaturation and therefore, a significant pore-pressure increase. Figure 3-6 shows the evolution of pore pressure (equivalent pore pressure as defined in Equations (2.5) and (2.6)) and liquid saturation at five different positions in the repository: three locations in the host rock and two in the crushed salt. Note that, depending on capillary forces, the equivalent pore pressure may be negative. As the backfill liquid saturation increases steeply just before 10 years, the pore pressure increases in a similar fashion. As can be observed in the left-hand side plot, as the backfill saturation increases, the pore pressure is the same at the five locations monitored. The equivalent pore pressure peaks at around 25 MPa.

Analysis of the results shows that hydraulically induced damage starts after 6 years at a location 8 m away from the drift along the *X* axis. Hydraulically induced damage does not start in the drift area because the pore pressure is smaller in this zone, due to the partial desaturation of the near-field host rock prior to the crushed salt reconsolidation (see Figure 3-6). After 10–20 years, the pressure is uniform in the backfill, and near-field host rock and pressure-driven fluid infiltration occurs. Owing to this phenomenon, a permeability increase of two orders of magnitude is estimated (Rutqvist et al. 2013; Wolters et al. 2012). The area that may undergo infiltration extends at the repository-level along the *X* and *Z* axis as pressure increases (thermal pressurization). Since rock salt damage is reversible, after about 700 years, the initial tightness of the host rock is restored. Note that the reconsolidated backfill may also undergo hydraulically induced damage if the pore pressure locally exceeds the minimum principal stress.

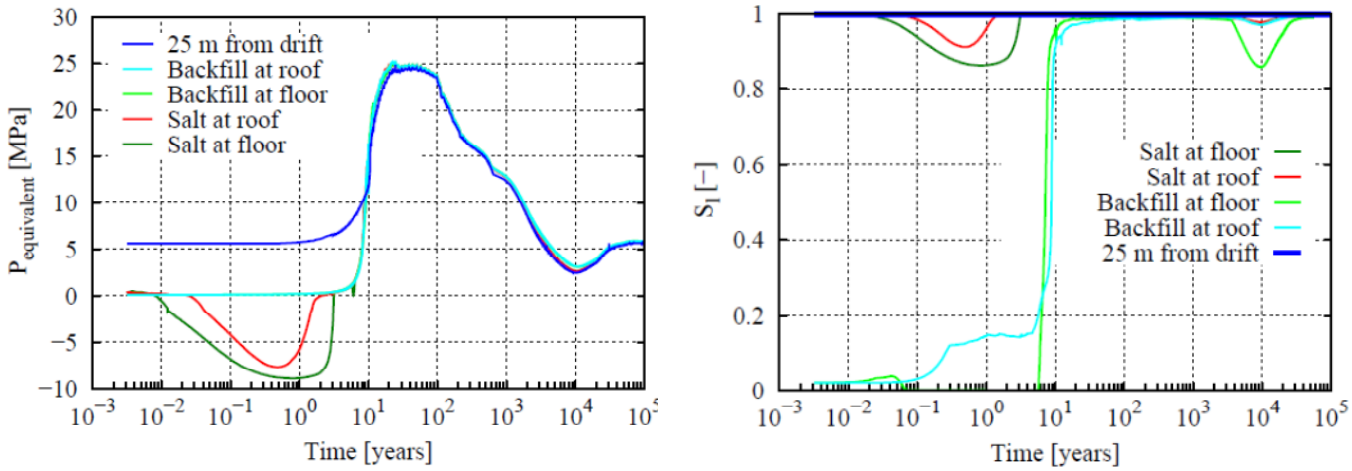

Figure 3-6. THM base case scenario: evolution of (left) equivalent pore pressure and (right) liquid saturation at several locations in the repository.

After 100 years, pressure decreases progressively following the temperature evolution. The pressure and saturation drop that occurs around 10,000 years is due to a thermal depressurization at the repository level (compare simultaneous temperature and pressure drops in Figure 3-3 and Figure 3-6). After 100,000 years, once the heat load released by the waste packages tends to zero, the initial temperature and (hydrostatic) pore pressure are restored.

3.3 Comparison of TH and THM results

A thermal-hydraulic simulation (without the mechanical component) has been conducted to determine how relevant the coupling to mechanical processes is for the long-term evaluation of natural salt and crushed salt barriers.

Figure 3-7 displays the temperature evolution at the same locations as in Figure 3-3. The temperature at the waste package peaks at 267ºC after 10 years. As the figure shows, only one temperature peak is obtained. Indeed, if the mechanical effect is not accounted for, the backfill porosity hardly changes, and therefore the thermal conductivity of this material remains low (see Table 3.2). The low thermal conductivity of the crushed salt explains the higher temperatures; the nearly constant value of this property explains that only one temperature peak is obtained. As in the THM case, the temperature 25 m away from the drift peaks is ~108ºC after 80 years.

In Figure 3-8, the evolution of pore pressure and liquid saturation is given at the same locations as in Figure 3-6. If the mechanical component is neglected, the far-field pressure peaks above 37 MPa after 27 years. This pressure is significantly higher than the one obtained in the THM run, P_{max}≈25 MPa. In the TH run, no damage is accounted for, and as a result, the permeability of the natural salt remains constant at its initial very low value, which explains the higher pressures reached. (The higher temperatures in the TH case also influence this higher pressure obtained.) In the drift area, the pore pressure remains low: in the backfill, P<1 MPa and in the host rock, P<1-2 MPa. Note that since the crushed salt porosity barely changes, k=10^{-13} m^2, which is a very high permeability value in the context of a nuclear waste repository. Also, the very low permeability of the host rock and its strong capillary forces delay the flow towards the drift. In the long term, the TH simulation captures the pressure decrease below the hydrostatic

level after 10,000 years. The hydrostatic pressure is not recovered in the area under investigation after 100,000 years.

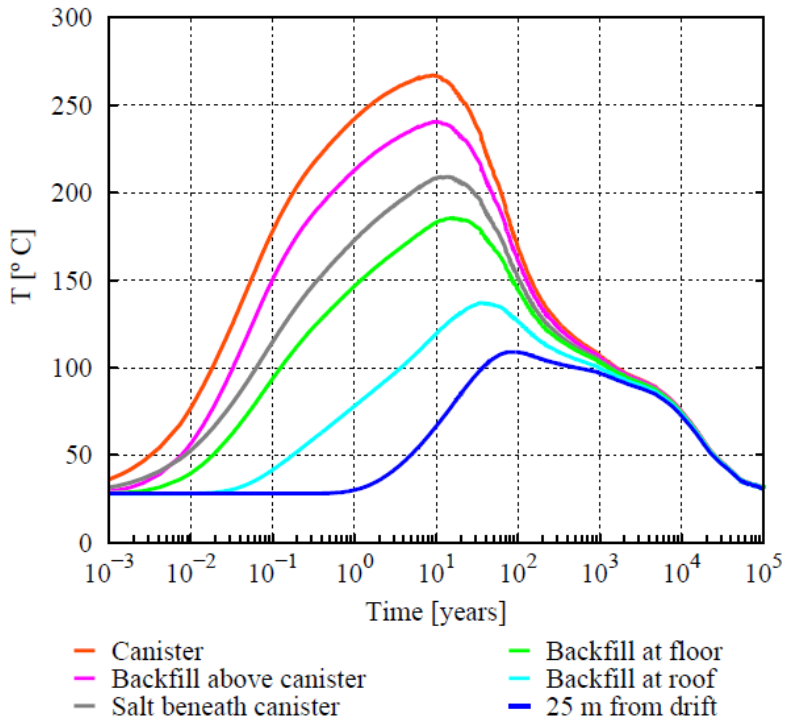

Figure 3-7. TH-only scenario: evolution of temperature at the locations displayed in Figure 3-3.

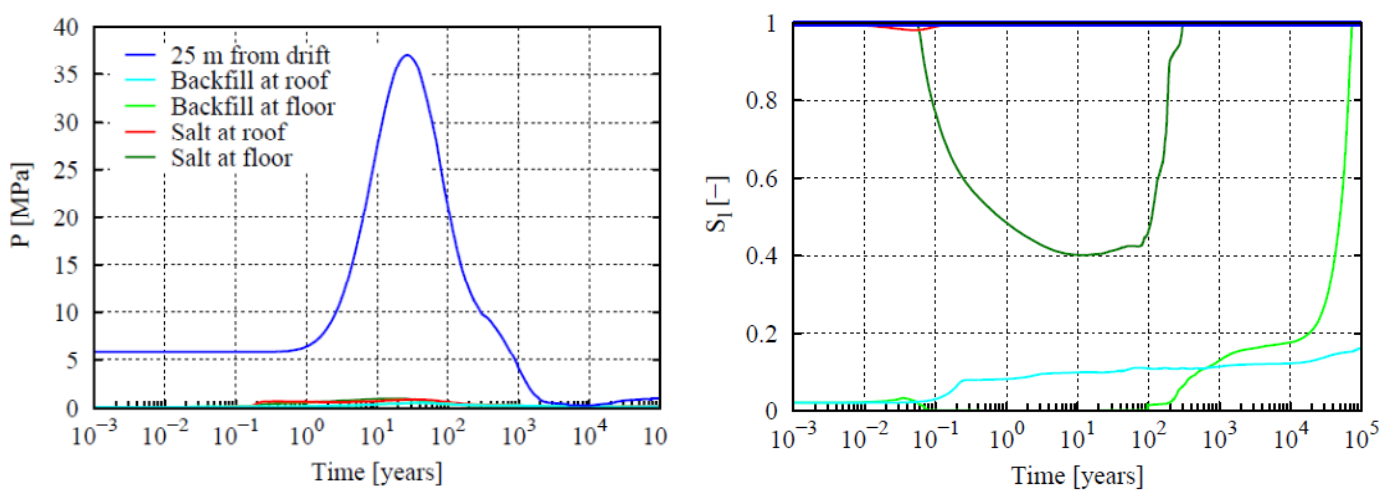

Figure 3-8. TH-only scenario: evolution of (left) pressure (maximum pore pressure) and (right) liquid saturation at the five locations displayed in Figure 3-6.

As compared to the right-hand side plot in Figure 3-6, the liquid saturation evolution displayed in Figure 3-8 (right-hand side plot) is also quite different: in the host rock around the drift, the lowest value is reached after 10 years (temperature peaks at that time), and the subsequent

resaturation takes longer, due mainly to the higher temperatures and the lower permeability of the host rock in this case. In the backfill, resaturation is not complete after 100,000 years. The liquid phase in the crushed salt progressively flows by gravity towards the drift floor, so that after 100,000 years, only the crushed salt in the floor area is saturated (note that capillary forces within the unconsolidated crushed salt are weak, because porosity is 30%).

From these results, it can be concluded that TH simulations cannot capture key aspects such as backfill resaturation, or temperature and pore-pressure evolution. Furthermore, backfill-barrier development cannot be evaluated without accounting for the mechanical effects. Additionally, a realistic analysis of the natural salt barrier cannot be conducted if damage and healing processes, which have been observed in the field and in the laboratory, are disregarded. Therefore, we conclude that coupled THM simulations are needed.

3.4 Importance of capillary forces

When capillary forces are disregarded, the gas and liquid pressures are identical and equal to the equivalent pore pressure, defined in Equations (2.5) and(2.6).

As compared to the base-case scenario, the most important differences when capillary effects are neglected are found in non-fully-saturated areas (backfill and host rock adjacent to the drift contour; see the right-hand side plot in Figure 3-6). Given that for $S_l<1$, the pore pressure is higher if capillary forces are not accounted for (cf. Section 2.1.1), there is more damage and dilatancy in the EDZ (same extension, but shear dilatancy reaches 1.4 % and tensile dilatancy at the drift corner gets to 2.6 %). As with the base-case scenario, the EDZ is sealed after 7 years, and the backfill is reconsolidated after about 20 years.

Figure 3-9 displays the pore-pressure and liquid-saturation evolution at the same locations as in Figure 3-6 (an extra location, right above the waste package, has been added to the saturation plot). When temperature peaks at 1 year, liquid saturation at the drift contour is reduced significantly, in particular at the floor, where the liquid phase disappears. As temperature increases after 5 years, pressure starts increasing everywhere, too, quite steeply just before 10 years as the backfill resaturates (pore volume reduction). The pressure peaks at 25 MPa and hydraulically induced damage develops similarly to the base case scenario. On the other hand, in the long term, the saturation profile in the backfill is quite different (see the right-hand side plot in Figure 3-9): the lack of capillary forces promotes gravity-dictated mass flow. As a result, only the crushed salt close to the drift roof is not saturated after 100,000 years (in the base-case scenario, the saturation is lower in the sidewalls because porosity is slightly higher in this zone, and therefore the capillary forces are lower). As a result of the gravity-dictated flow, the liquid saturation in the crushed salt above the waste package increases significantly after about 30,000 years. Note that the host rock above the drift is not completely saturated, owing to the downward flow ($S_l\approx0.8$ over 14 m from the drift roof along the Z axis).

To conclude, if capillary effects are disregarded, more damage and dilatancy are predicted in the partially desaturated EDZ, due to a higher pore pressure used in geomechanics when $S_l<1$. In the long-term, the saturation profile in the drift area is dictated by gravity, as opposed to the more realistic capillary-dictated profile obtained when water-retention curves are accounted for.

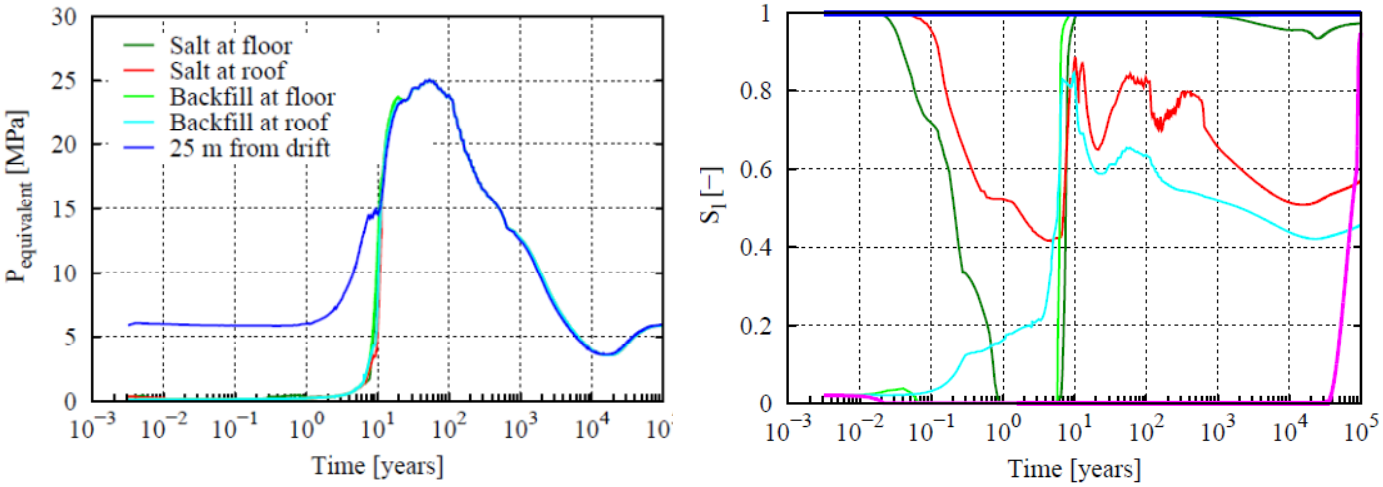

Figure 3-9. THM predictions without capillary pressure. Evolution of (left) equivalent pore pressure and (right) liquid saturation at the locations shown in Figure 3-6 (the crushed salt element right above the waste package has been added to the saturation plot).

3.5 Sensitivity of the THM predictions to the initial saturation of the host rock

A THM simulation in which the host rock has an initial saturation of 0.5 has been performed. Intercrystalline brine has been observed in some salt samples (Desbois et al. 2012) and justifies the assumption of initial fully saturated conditions in the host rock. However, it is considered important to analyze the effects of a possible lower initial saturation on the long-term predictions.

The temperature evolution obtained is similar to that of the base-case scenario, displayed in Figure 3-3. In the first years, damage and dilatancy develop as well, although after 4 years the values are lower than in the base case, mainly because the pore pressure is lower in the current scenario (cf. Equations (2.5) and (2.6)). The crushed salt reconsolidation process and barrier development occur in a similar way, with the majority of crushed salt elements reaching the final porosity within 20 years. After 7 years, the EDZ is sealed, and the initial tightness of the host rock is restored.

The evolution of pore pressure and liquid saturation is displayed in Figure 3-10, at the same locations as in Figure 3-6. As expected, the first temperature peak brings about a decrease in liquid saturation in the drift area. Owing to a bigger pressure in this zone, there is fluid flow towards the far field, where capillary forces are important (the initial saturation of the host rock is 0.5). This outward flow is a slow process, extending over thousands of years, due to the low permeability of the host rock.

As the backfill compacts, its liquid saturation increases. The equivalent pore pressure also increases in the drift area—see the left-hand side plot in Figure 3-10. This overpressure is dissipated progressively through the outwards flow. Overall, the equivalent pore pressure peaks at about 17 MPa. Note that in the crushed salt, the equivalent pore pressure may exceed this value if porosity is slightly higher than 0.2 % (recall Equations (2.5) and (2.6)), and that capillary forces are lower for higher porosities). The peak pressure obtained is lower than the one in the

base-case scenario. Additionally, as the figure shows, the far-field pressure and saturation barely change. In the host rock near the drift, the liquid saturation gets back to 0.5 by the end of the simulated time. In the crushed salt, the liquid saturation increase triggered by the pore volume reduction is overcome in the long term by the outwards flow (for the light green curve, the sudden increase in liquid saturation after about 100 years is related to a delayed compaction of that grid block). Due to this progressive flow towards the far field, the backfill is not resaturated at the end of the simulated time, as shown in the right-hand side plot in Figure 3-10.

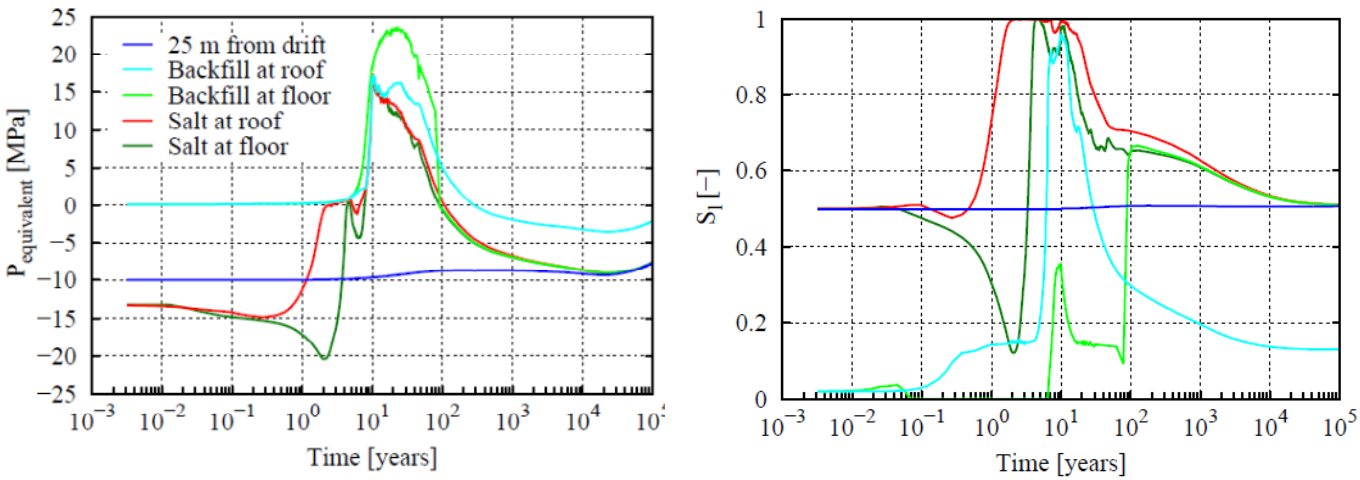

Figure 3-10. THM predictions with 50 % initial saturation in the host rock. Evolution of (left) equivalent pore pressure and (right) liquid saturation at the locations shown in Figure 3-6.

Owing to the lower pore pressure predicted in this scenario as compared to the base case, hydraulically induced damage only occurs in the drift area, between 9 and 20 years. After 20 years, the sealing capacity of the host rock is fully restored.

From these results, it can be concluded that the impact of damage processes on the sealing capacity of the host rock decreases as the initial saturation decreases; nevertheless, even when the host rock is initially fully saturated, the damage-induced secondary permeability is very low, $k_{max}^{secondary} \leq 10^{-18}$ m^2 (value still characteristic of an impervious material; see Bérest et al. (2005) or Cosenza (1996)). The engineered barrier provided by the backfill is also less subjected to hydraulically induced damage if the initial saturation of the host rock is low.

4. INTERNATIONAL BENCHMARK EXERCISES

During FY2014, we have continued our beneficial collaboration with Clausthal University of Technology (TUC). This collaboration started in late 2012 and has led to the following benefits to the UFD Campaign:

- Use of the *Lux/Wolters* constitutive model (Wolters et al. 2012; Rutqvist et al. 2012; 2013) in the TOUGH-FLAC simulator. As discussed in Section 2 and in Rutqvist et al. (2013), this model includes state-of-the-art knowledge (mechanical, hydraulic and thermal) about the behavior of rock salt;
- Comparison of the numerical predictions obtained using the two simulators developed by the two institutions: TOUGH-FLAC (LBNL) and FLAC-TOUGH (TUC). This has led to an international benchmark between LBNL and TUC, comprising two different exercises, which will be described in this section;

- Improvements in the numerical schemes and procedures used by LBNL and TUC. These have helped reduce the computational cost of the simulations, for instance by optimizing the transfer of information between the two software programs (TOUGH2 and FLAC^{3D}), by preserving the data that need to be saved throughout a simulation, and by determining which phenomena are relevant for a particular application. This leads to a reduction in the number of processes that need to be modeled.

In this section, we present the benchmark exercises performed during FY2014 between LBNL and TUC. The first exercise, already finished, focused on a comparison of the numerical predictions obtained by TOUGH-FLAC and FLAC-TOUGH when the same scenario is modeled using the two simulators. The main goal of this first exercise was to get a satisfactory agreement between the numerical results obtained, concerning the different processes occurring in the rock mass as well as in the backfill material. Because the goal was mainly numerical, a comprehensive validation based on measurement data of the physical processes was not addressed. This first benchmark is described in Section 4.1. It consists of a 2D model of an emplacement drift backfilled with crushed salt, and includes heat and gas generation from the high-level waste.

The second exercise started recently (late June 2014) and focuses on the 3D modeling of the TSDE (*Thermal Simulation for Drift Emplacement*) test conducted in the Asse Mine between 1990 and 1999. In this case, we aim not only to achieve a satisfactory agreement between the numerical predictions offered by TOUGH-FLAC and FLAC-TOUGH, but we also intend to compare numerical results with measurement data (temperature, stress changes, drift convergence and crushed salt porosity) to analyze the capabilities of the constitutive models and numerical approaches used to reproduce relevant processes. This will let us evaluate in particular some processes that are difficult to study at the laboratory scale, because they occur at very low deviatoric stresses, needing extremely slow strain rates to be investigated. Some model parameters will likely be recalculated from the comparison between numerical predictions and experimental data. To do this in an optimal way, combining mechanical, hydraulic and thermal data, one possibility would be to use iTOUGH2 (Finsterle 2007) in the upcoming months, provided that the computational cost is reasonable. For now, we are modeling the TSDE experiment using the two aforementioned simulators and the parameters used in the 2D case investigated in the first benchmark exercise. iTOUGH2 is a software developed at LBNL for parameter estimation, sensitivity analysis, and uncertainty propagation analysis. Its main utility is the automatic calibration of TOUGH2 models against observed data (i.e., determination of model parameters that best fit the observed system response). However, calibration of THM models is also possible through the PEST protocol (Doherty 2008), that we may use once the forward modeling of the TSDE experiment is complete. The current status of the second benchmark exercise is described in section 4.2.

Finally, we note that the plan of participating in an international benchmark exercise involving other U.S. and German research teams has not materialized, since LBNL is presently not a member in this benchmark project. The purpose of LBNL participation would be to extend that benchmark project from pure TM modeling exercises to full coupled THM problems, involving brine migration.

4.1 First benchmark exercise: 2D model of emplacement drift for HLW, backfilled with crushed salt

The principal objectives of the first benchmark exercise carried out are to model the same scenario using different numerical schemes and to compare and analyze the results obtained, so that the capabilities of different approaches to model the long-term coupled THM response of a repository for high-level nuclear waste in rock salt can be investigated. In addition, it is acknowledged that the comparison of numerical results issued from different approaches and institutions increases confidence in and reliability of the long-term predictions, and enhances acceptance of the conclusions (Hampel et al. 2013). In the current case, we have focused on the backfill evolution (in particular, reconsolidation process) of processes that could affect the integrity of the host-rock natural barrier at different temporal and spatial scales (i.e., temperature changes, damage, dilatancy, and healing/sealing), and on the effect of gas generation from the waste packages on barrier integrity. For this, we have used the updated version of TOUGH-FLAC presented in this report (LBNL) and an updated version of the FLAC-TOUGH simulator, developed by TUC (Lux et al. 2014). As their names suggest, both simulators use TOUGH2 for the flow subproblem (Pruess et al. 2011), and FLAC^{3D} to solve the geomechanics subproblem (Itasca 2011). In addition, they both offer the capability of using a Voronoi discretization in the flow subproblem, even when the mesh deforms over time due to the creep and the large strains associated with the mechanical behavior of saliniferous materials (Blanco Martín et al. 2014b; 2014d).

The FLAC-TOUGH simulator has been implemented based on two different sequential methods (Lux et al. 2014; Blanco Martín et al. 2014d). In the first approach, the sequential undrained split method is used (Kim 2010). Accordingly, FLAC^{3D} is the master code and sequentially (e.g., after a given number of iteration steps) calls TOUGH2 as a slave code. The geomechanical deformations and the resulting changes in stress, pore volume, and pore pressure are computed first by FLAC^{3D} in each iteration step of the mechanical simulation part, while fluid masses and temperature are kept constant for each element. Afterwards, the multiphase mass and heat flows are computed by TOUGH2. The coupling scheme based on the undrained split method is quite computationally cost intensive, because the necessary FISH-functions in FLAC^{3D} used for updating pore pressures are not parallelized, and called at every FLAC^{3D} iteration step. In the second approach, to reduce the amount of FISH-function calls, the FLAC-TOUGH simulator is implemented in a way such that the pore pressure is kept constant during the mechanical simulation part, and updated with the overall deformation increment occurring between two consecutive calls to TOUGH2, at the end of the mechanical simulation part. Therefore, this second approach may be seen as a mixture of the undrained-split and the drained-split methods (Kim 2010). The numerical results shown hereafter have been obtained using this faster second coupling-scheme approach.

4.1.1 Benchmark description

The scenario investigated within the framework of the first benchmark exercise is similar to the one presented in Section 3 of this report, analyzed with TOUGH-FLAC. It consists of a two-dimensional model of one emplacement drift, the waste packages being parallel to the drift axis. Crushed salt is used as backfill material (initial porosity of 30%), and we model the phases of excavation, waste emplacement, backfilling, and 100,000 years of post-closure.

As compared to the scenario described in Section 3, in the first benchmark exercise we have included gas generation (and not only heat generation) from the waste packages, so that its influence on the long-term evolution of the natural salt and backfill barriers can be evaluated. This gas generation could be caused by corrosion and biodegradation processes. The gas-generation rate used here has been determined assuming a corrosion rate of 1 μm/y. From the chemical reaction describing corrosion, $3\ Fe + 4\ H_2O \rightarrow Fe_3O_4 + 4\ H_2$, the amount of H_2 released per meter of drift and per unit of time has been calculated. Note that the corrosion rate assumed in this study is an average value of available corrosion data for steel nuclear waste packages (Suter 2003).

Figure 4-1 shows an overall view of the model and an enlarged view of the drift area. We note that the current discretization is different from the one shown in Figure 3-1, particularly in the near field. In the present case, not only similar grid blocks are defined at the boundary between two different domains, but also the partition in the near-field host rock is different, oriented parallel to the *X* and *Z* axes as much as possible. This way, the effect of the mesh structure on the results and on the contour profiles can be evaluated. Furthermore, here we use a Voronoi discretization in the flow subproblem (we note that the update of the flow mesh using Voro++ has been implemented into TOUGH-FLAC in the context of our collaboration with TUC). The heat load used in the benchmark exercise is the same as the one displayed in Figure 3-2.

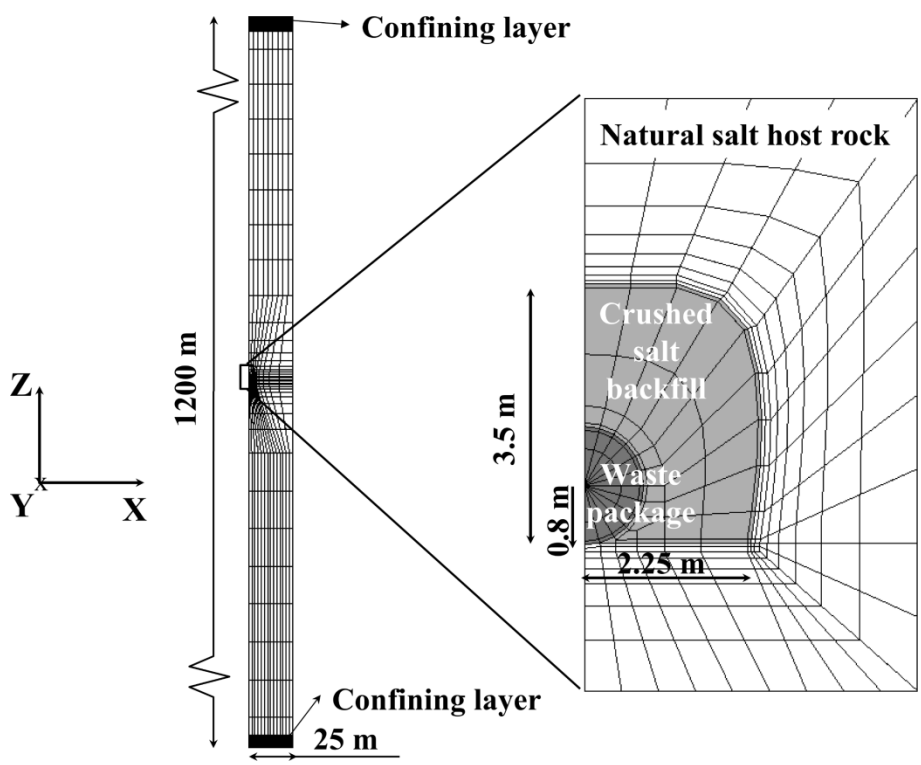

Figure 4-1. Geometry of the generic salt repository studied in the first benchmark exercise, with enlarged view of the drift area.

Table 4.1 lists the initial flow parameters of the crushed salt, the natural host rock salt, and the confining layers. We note that, as compared to the base-case scenario presented in Section 3,

here we assume that the undisturbed permeability of the natural salt is 0 m^2, and that the initial saturation of the host rock is 50%.

Table 4.1. Initial flow parameters of the crushed salt, natural salt and confining sandstone layers considered in the first benchmark exercise.

	Crushed salt	*Rock salt*	*Sandstone layers*
S_l [-]	0.02	**0.5**	1
ϕ [-]	30 %	0.2 %	12 %
k [m^2]	$3 \cdot 10^{-13}$	**0**	10^{-17}[a]
λ [$W \cdot m^{-1} \cdot K^{-1}$]	0.9	4	1.8[a]
C [$J \cdot kg^{-1} \cdot K^{-1}$]	860	860	900[a]

[a]: constant values

It should be noted that, in this benchmark, we have not considered capillary effects because our priority has been to get a satisfactory agreement between the numerical predictions computed by the two simulators, trying to reduce the computational time needed to obtain comparable results. Consequently, the equivalent pore pressure used in geomechanics is equal to the gas pressure. Moreover, as explained before, because the main goal of the first benchmark is numerical, the analysis of the results presented hereafter does not include a comprehensive validation based on measurement data of the physical processes.

4.1.2 Comparison and analysis of the results

Figure 4-2 displays the evolution of temperature over time at four locations in the repository. As the figure shows, the predictions offered by TOUGH-FLAC and FLAC-TOUGH are very similar. The temperature at the waste package peaks slightly above 180°C after about 1 year. The nearby crushed salt and natural host rock salt also show an initial temperature peak; as in the scenario discussed in Section 3, this local peak is due to the relatively low thermal conductivity of the crushed salt before significant compaction occurs. After about 20 years, the crushed salt is reconsolidated and the temperature evolution is uniform. In the near field, the temperature peaks at 162°C after 25 years. Twenty-five meters far from the drift, the temperature reaches 100°C before 100 years (progressive heat propagation through the host rock). From then on, temperature decreases progressively, and after 100,000 years, the initial temperature is restored.

The evolution of dilatancy (i.e., nonelastic volumetric strain) at the drift contour during the first years of the post-closure phase is displayed in Figure 4.3. We note that the drift is backfilled since the beginning of this phase. As the figure shows, the predictions provided by the two simulators are very similar. In the first years, dilatancy increases and peaks at about 2.1 % after 4 years. The excavation damaged zone (EDZ) extends about 1.5 m below the drift floor and 1 m

beyond the roof and sidewalls. Due to the dilatancy increase, the secondary porosity of the host rock reaches 2.3 % at the drift sidewall (still very low value). In addition, the Biot coefficient of the natural salt also increases (Equation (2.8)), thereby increasing the strength of the coupling between flow and geomechanics. A maximum value of 0.66 is predicted at the sidewall by the two simulators. In turn, the secondary permeability increases several orders of magnitude (thermomechanically induced damage).

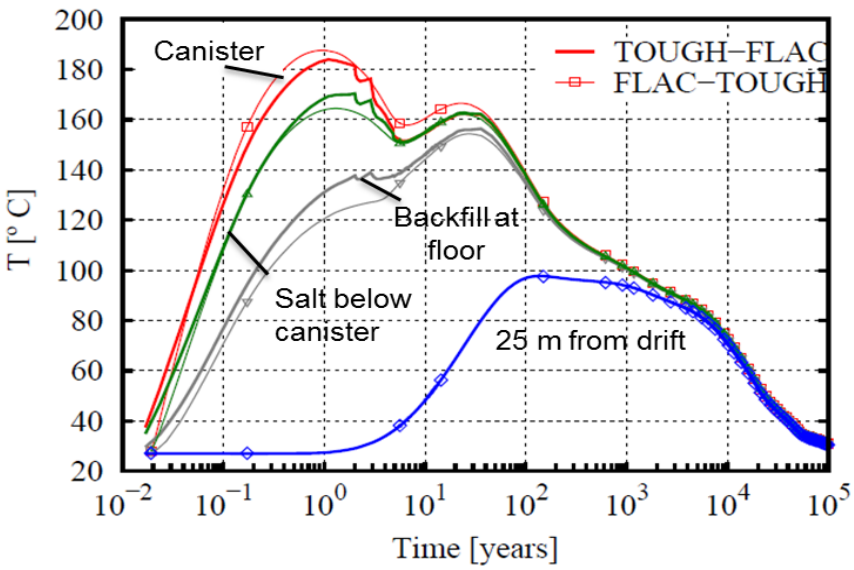

Figure 4-2. First benchmark exercise: evolution of temperature. Solid lines correspond to TOUGH-FLAC; lines with points correspond to FLAC-TOUGH.

Creep and dilatant behavior of the host rock trigger the progressive compaction of the crushed salt. As in the case described in Section 3, as compaction moves forward, the crushed salt strengthens (cf. Eq. (2.10)), and an internal support is progressively developed in the rock salt at the drift contour. Healing mechanisms are activated, and dilatancy and damage decrease. As the last columns of pictures in Figure 4.3 show, the EDZ is sealed after about 7 years. Again, this time for EDZ sealing is a good performance indicator of a nuclear waste repository. The initial tightness of the host rock is restored, and the stress state progressively evolves to the initial isotropic state. The evolution of porosity within the crushed salt during the first 20 years of post-closure phase is displayed in Figure 4-4. The predictions obtained by the two simulators are very similar. As in Section 3, most of the crushed salt has reached the final porosity (0.2%) within the first 20 years, which is comparable to previous numerical investigations (Stone et al. 2010). During reconsolidation, the flow and mechanical properties of the crushed salt evolve towards those of the natural salt, cf. Section 2 and Blanco Martín et al. (2014a; 2014c), and Rutqvist et al., (2013). Again, we highlight that the time-dependent evolution of the host rock and the crushed salt is extremely related: the natural host rock salt triggers the crushed salt reconsolidation, and this reconsolidation favors the onset of healing processes and the restoration of the initial natural salt barrier.

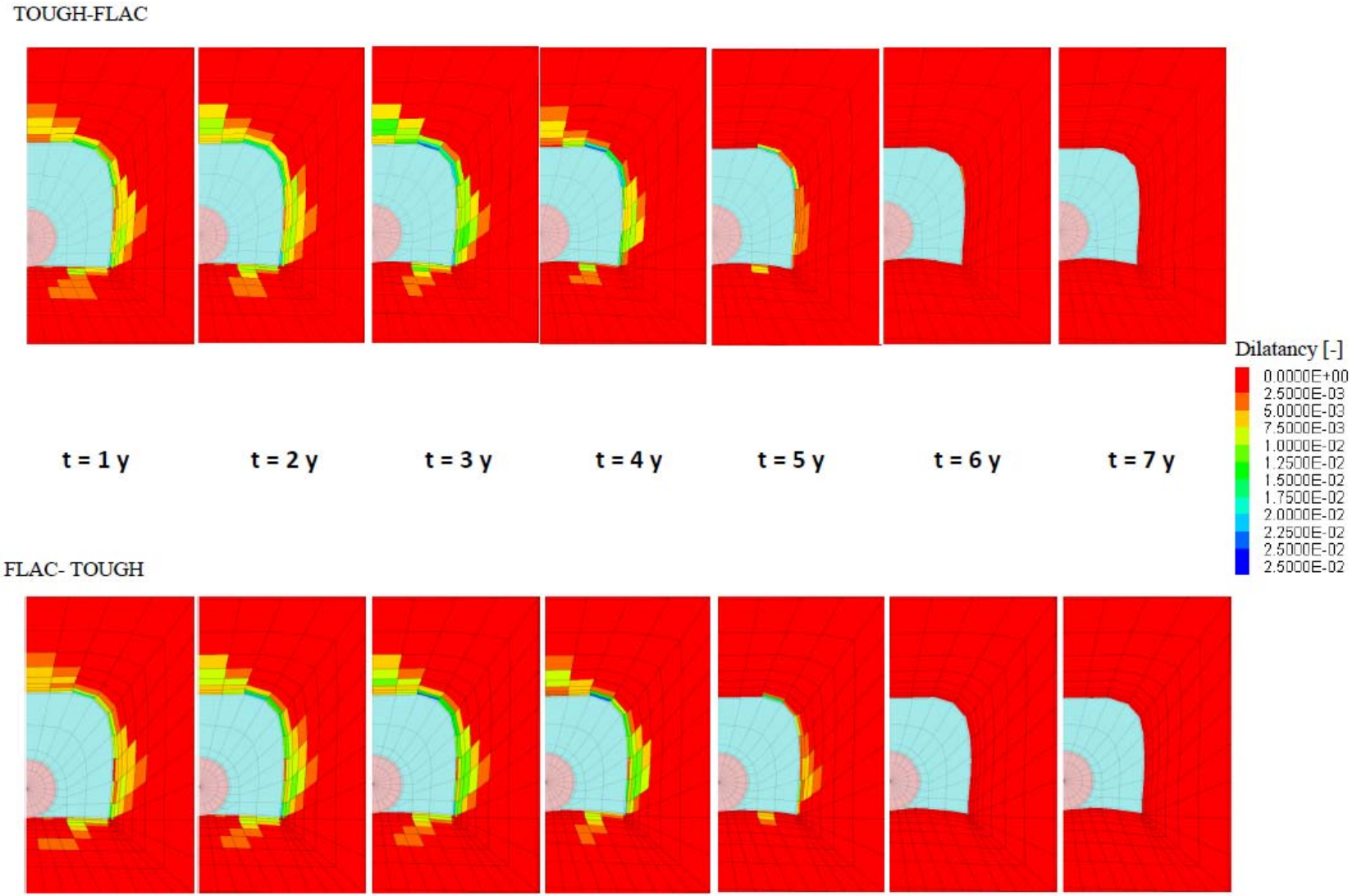

Figure 4-3. First benchmark exercise: evolution of dilatancy at the drift contour during the first years of post-closure phase, as obtained by TOUGH-FLAC (top) and FLAC-TOUGH (bottom).

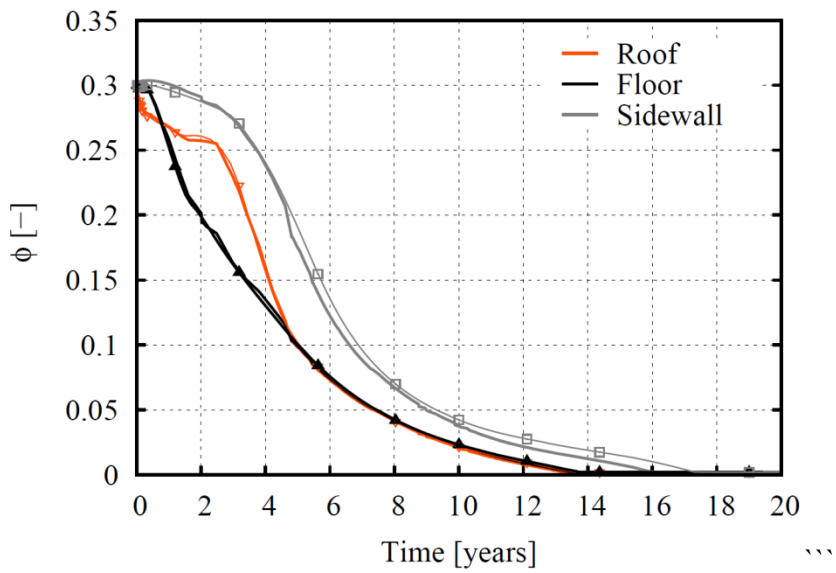

Figure 4-4. First benchmark exercise: evolution of porosity within the backfill during the first 20 years of post-closure phase. Solid lines correspond to TOUGH-FLAC; lines with points correspond to FLAC-TOUGH.

The evolution of pore pressure in the drift area is displayed in the left-hand side plot of Figure 4-5. A location in the host rock, 25 m away from the drift, is also displayed. In the drift area, a strong increase is predicted by the two simulators between 6 and 20 years as porosity becomes very low (see Figure 4-4). In the crushed salt, the pore pressure peaks at about 19 MPa as the porosity tends to 0.2 %. Shortly after (about 45 years), the pore pressure stabilizes at 13.7 MPa, which is the value of the minimum principal stress in the drift area. Indeed, infiltration takes places if $\Delta P_{Fl} = \sigma_3 + P \geq 0$, where P is the pore pressure and σ_3 is the minimum principal stress (Blanco Martín et al. 2014a-d; Rutqvist et al. 2013; Wolters et al. 2012). If P exceeds locally σ_3, a secondary permeability develops in the host rock (hydraulically induced damage). The factors that can make the pore pressure increase are the gas generation, the thermal expansion of the fluids, and the effect of crushed salt compaction. However, after 45 years, gas generation is the main factor, although its effect is very small due to the low generation rate used. Because of the local secondary permeability, and the fact that gas is very compressible, the pore pressure remains nearly stable. As Figure 4-5 left shows, 25 m far from the drift, the pore pressure starts increasing after 10,000 years, and gets to 13.7 MPa as the infiltration front propagates through the rock. (Note, however, that the infiltration front remains within the rock salt layer [more details are given below]).

The evolution of liquid saturation at the same locations is displayed in the right-hand side graph of Figure 4-5. Overall, the results of the two simulators are in good agreement. As expected, in the crushed salt and rock salt at the drift contour, the liquid saturation increases steeply as reconsolidation takes place. In the crushed salt, the reduction of the pore volume explains the saturation increase. As for the natural salt, water is squeezed from the crushed salt during compaction. Note that in the first years, liquid saturation decreases in the natural salt at the drift contour due to the temperature increase (vaporization—this also happened in the scenario discussed in Section 3). In the long term, the liquid saturation in the drift area decreases, and

liquid water accumulates below the drift, since it flows by gravity. (Below the drift, some secondary permeability develops due to damage, so that $k > 0\ m^2$.) On the other hand, 25 m far from the drift, the saturation barely changes over time.

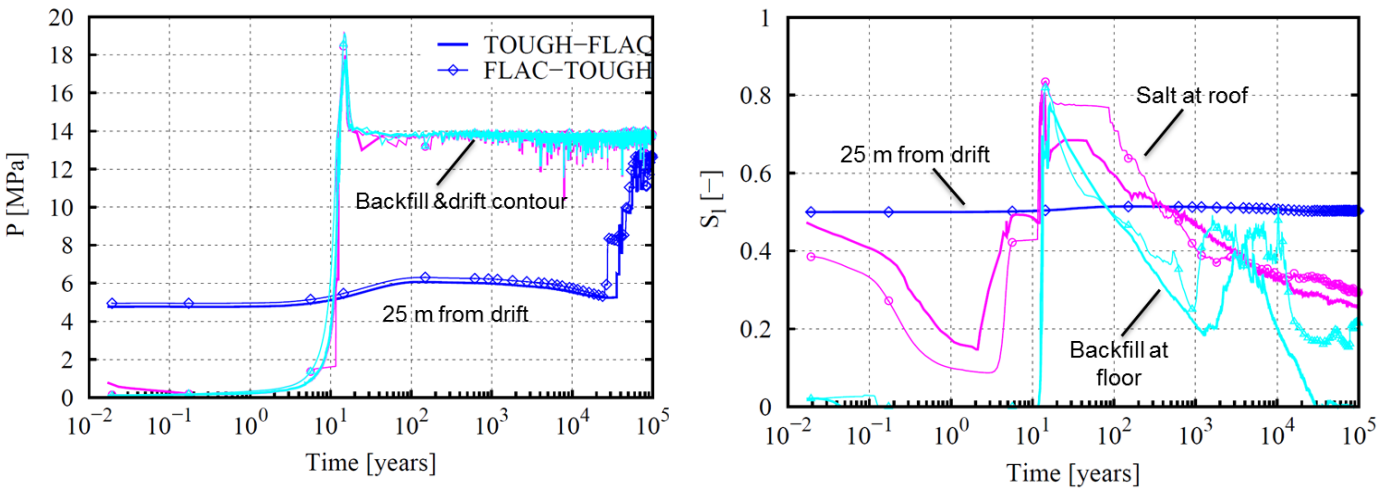

Figure 4-5. First benchmark exercise: evolution of (left) pore pressure and (right) liquid saturation. Solid lines correspond to TOUGH-FLAC; lines with points correspond to FLAC-TOUGH.

The evolution of ΔP_{Fl} predicted by the two simulators is compared in Figure 4.6. The initial condition at the repository level is $\Delta P_{Fl} \approx$ -8 MPa. Over time, because the pore pressure increases due to the gas generation, the thermal expansion of the fluids, and the crushed salt compaction, ΔP_{Fl} increases and may become positive, allowing some infiltration. The zone in which infiltration could take place extends 67 m above the drift (the gas moves upwards), which is smaller than the rock salt thickness above the drift (200 m).

Overall, from Figure 4-2 to Figure 4-6, it can be concluded that the results obtained by TOUGH-FLAC and FLAC-TOUGH are quite comparable, both in terms of the evolution of the natural salt barrier and the consolidation of the crushed salt backfill. Key aspects of the THM evolution of these two materials can be captured with the simulators used. Moreover, for the reference situation investigated, the integrity of the geological barrier (host rock) can be demonstrated due to the fact that the spatial extension of the infiltrated zone is limited within the tight salt rock mass, and does not reach the confining layer. The satisfactory comparison of the results obtained helps increase confidence in and reliability on the numerical predictions. From the work performed, we conclude that TOUGH-FLAC and FLAC-TOUGH are suitable to model the long-term coupled thermal-hydraulic-mechanical response of a generic salt repository for high-level nuclear waste.

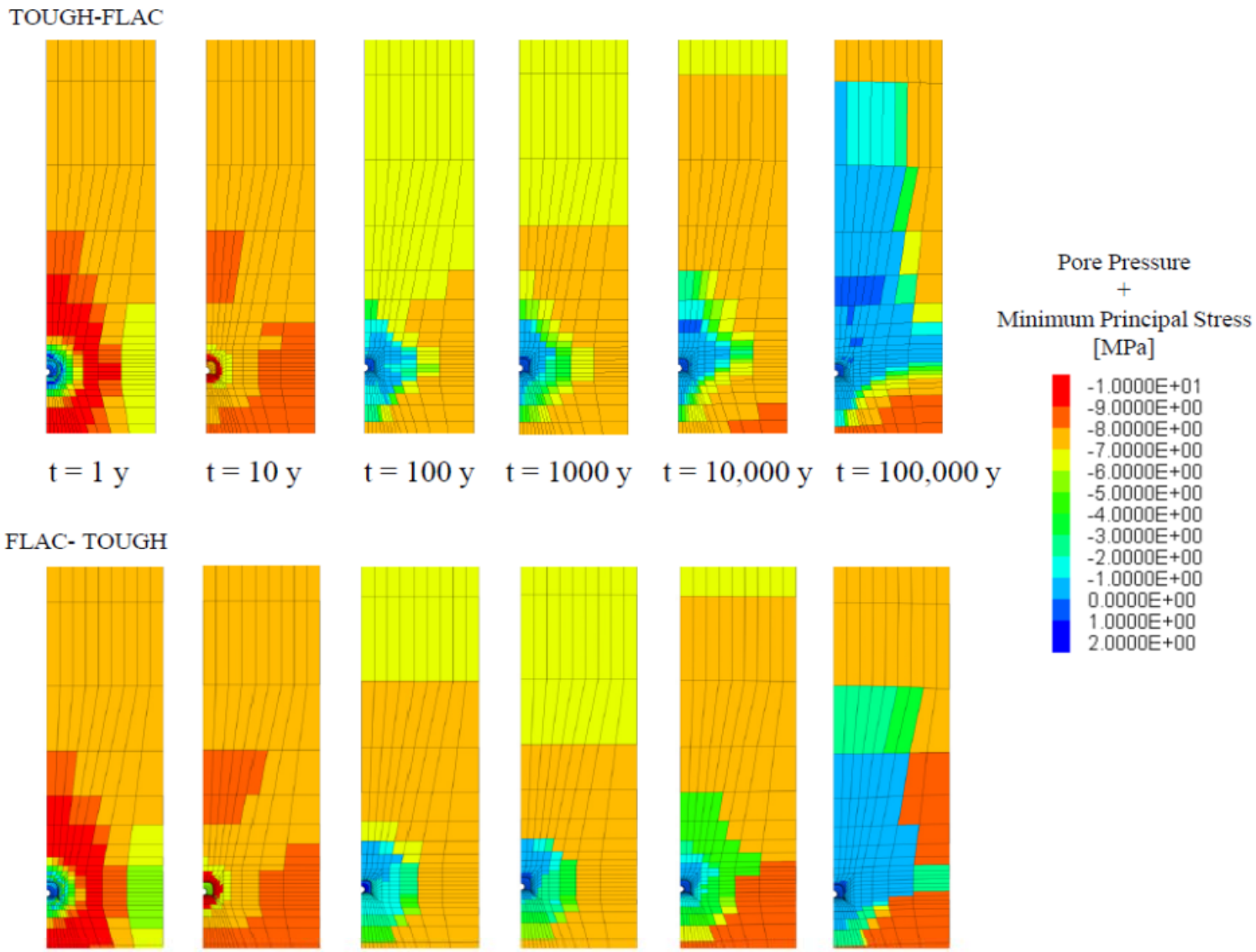

Figure 4-6. First benchmark exercise: evolution of $\Delta P_{Fl}=\sigma_3+P$ predicted by TOUGH-FLAC (top) and FLAC-TOUGH (bottom).

4.2 Second benchmark exercise: 3D modeling of the TSDE experiment and recalculation of model parameters

In the second benchmark exercise currently being performed, we are modeling the TSDE (*Thermal Simulation for Drift Emplacement*) experiment, conducted in the Asse Salt Mine in Germany from September 1990 to February 1999 (Bechthold et al. 1999). During this unique test, conducted to simulate reference repository conditions for spent nuclear fuel, a significant amount of data was measured in 20 monitoring cross sections: temperature, stress changes, displacement, convergence and porosity of crushed salt, among others. These data could be used to validate the large-scale applicability of models developed from laboratory data, and also to calibrate some model parameters whose identification is difficult at the laboratory scale.

The TSDE experiment was conducted in two parallel drifts, drilled for the purposes of this test, at a depth of 800 m in the Asse Salt Mine. These drifts are both about 76 m long and lie 10 m apart. In each of the drifts, three electrical heaters were emplaced, each of them releasing a constant power of 6.4 kW. The heaters were placed in the central part of the drifts, at a constant distance of 3 m. Each heater is 5.5 m long; see Bechthold et al. (1999) for a detailed description of the test. The heaters were emplaced 1.4 years after the excavation of the drifts, parallel to the drifts' axis. The open space was subsequently backfilled with crushed salt, with an initial porosity of 35%. Figure 4-7 shows a view of the two drifts, including the position of the electrical heaters and also the monitoring sections.

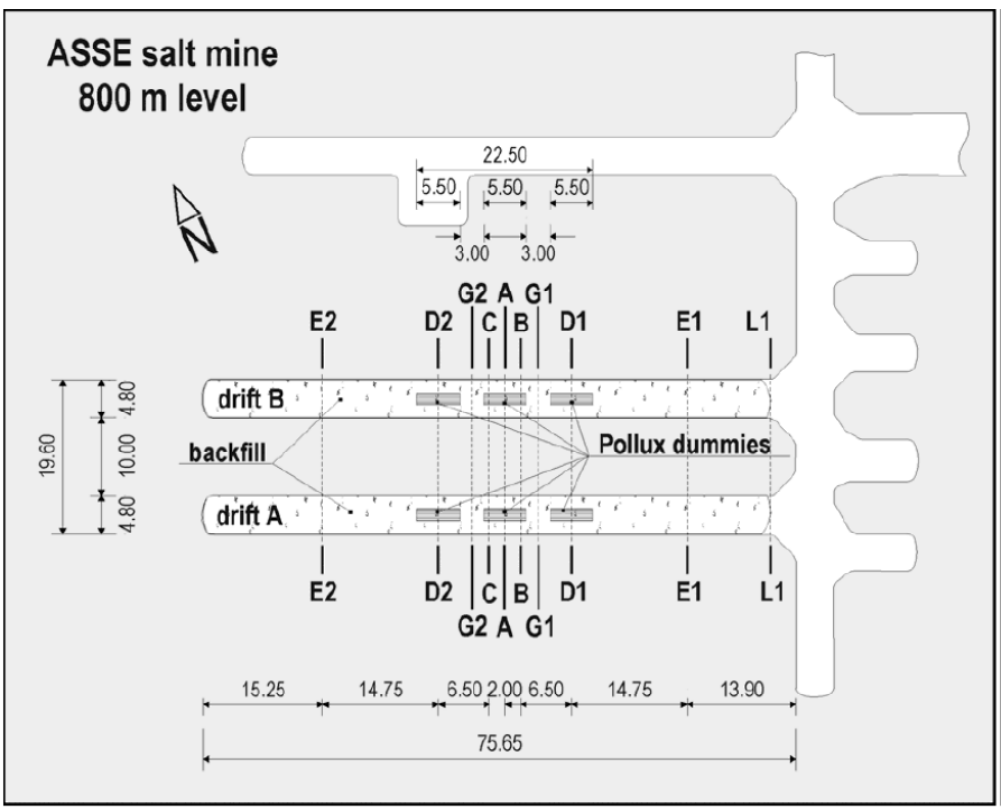

Figure 4-7. Schematic view of the two drift tests used in the TSDE experiment (800 m level of the Asse salt mine). From (Bechthold et al., 1999).

LBNL is currently modeling this experiment using TOUGH-FLAC. The open drift phase (1.4 years) has already been successfully modeled. In parallel, TUC is modeling the TSDE experiment using FLAC-TOUGH (the open drift phase is also finished). Once the simulations are over, we intend to compare the numerical results between them and also with the experimental data available through the BAMBUS project (Bechthold et al. 1999). Figure 4-8 shows several views of the three-dimensional model. For symmetry reasons, we only model half of one drift (i.e., 1.5 heaters). The geometry is discretized into about 86,000 grid blocks, and we use a Voronoi mesh in the flow subproblem, updated every time the geomechanics mesh deforms relative to strains more than 1%. Since the simulations are not finished yet, we do not present here any results obtained so far; the full analysis and comparison with experimental data will be presented in next year's report.

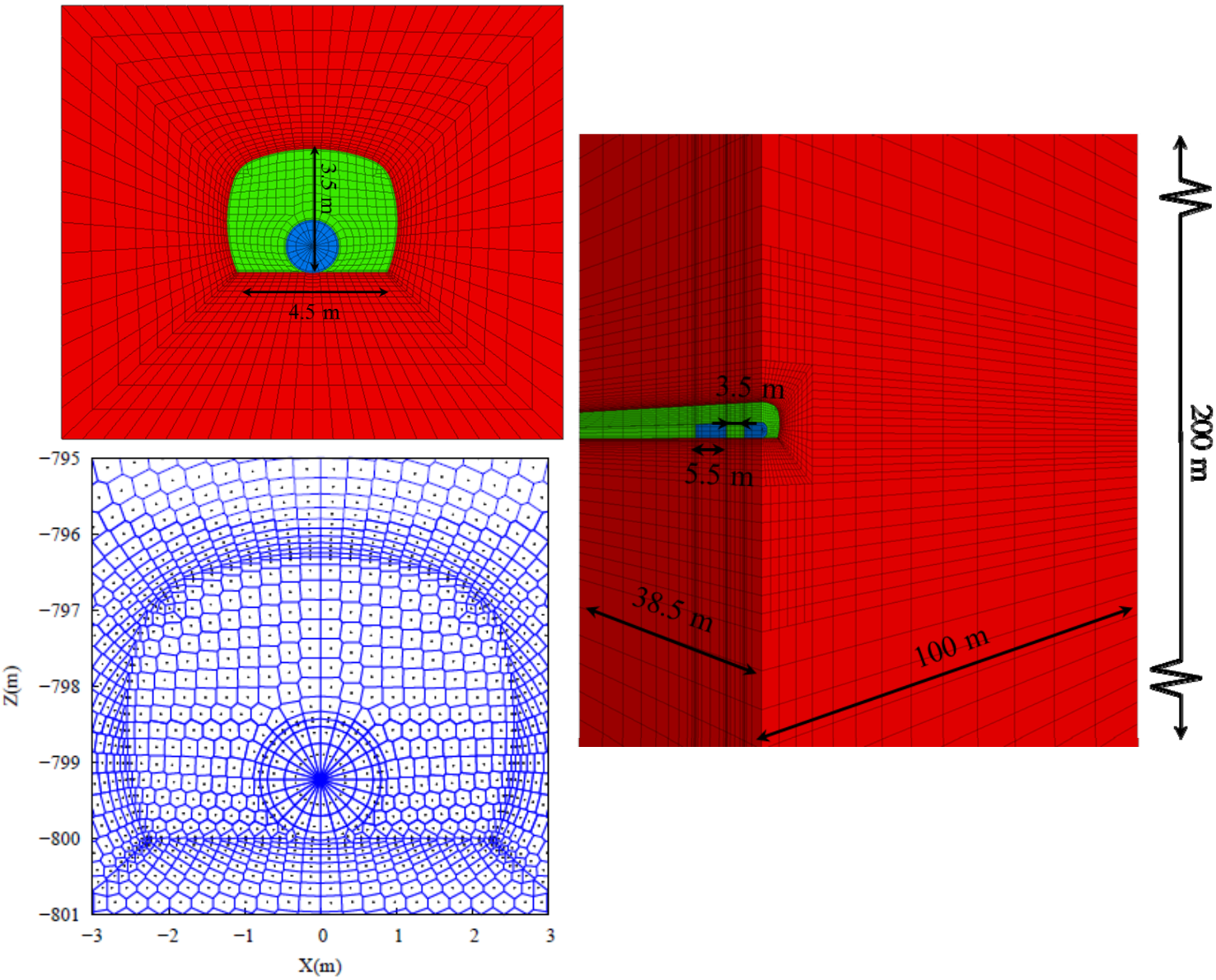

Figure 4-8. Views of the 3D mesh used in the modeling of the TSDE experiment (flow and geomechanics discretization).

We note that, because of the size of the model and the complexity of the phenomena investigated (rock salt damage and healing, crushed salt compaction, effect of temperature, etc.), the simulations are expected to last several weeks. Depending on the computational cost, we will decide whether inverse modeling (to calibrate the parameters over which some uncertainty exists) is a viable solution in this case. Otherwise, we may perform certain forward cases to try to "manually" calibrate the most uncertain parameters.

5. CONSTITUTIVE RELATIONSHIPS FOR BRINE MIGRATION

In this section, we discuss the development of a conceptual model for simulating the flow and transport of brine in salt formations. In particular, we present a dual-continuum approach for modeling brine migration. In this approach, we conceptualize the interconnected pore space of salt formations as one continuum. The second continuum consists of the salt grains which, partially comprise of brine inclusions. While single-continuum models of brine migration in salt have been recently developed (Olivella et al. 1994; Kuhlman and Malama 2013), the dual-continuum description, to the best of our knowledge, has not been developed in the past. Given the strong thermal gradients that are expected to exist in salt formations hosting high-level radioactive waste repositories, the applicability of a single-continuum approach, based on the assumption of equilibrium between the pore fluid and surrounding solids, is questionable. A dual-continuum approach, in which the pore fluid and solids are treated as two separate but interacting continua occupying the same physical space, one can resolve the strong gradients at the fluid-solid interface more efficiently.

We begin by discussing the need for understanding brine migration under thermal gradients. We then review some of the historical work that has been done in the context of modeling brine migration in salt formations. Most of these earlier modeling efforts were restricted to understanding brine migration in single salt crystal; however, a continuum description of brine flow has also emerged more recently (Olivella et al. 1994). In the next section, we present the necessity for a dual-continuum approach for understanding brine migration in salt formations. We then develop the differential mass and energy conservation equations for brine migration in salt formations for an arbitrary representative control volume, which is large enough to permit a continuum description of flow and transport. This is followed by development of mathematical expressions for advective and diffusive fluxes, both under pressure and thermal gradients. We also develop mathematical equations for obtaining the mass and energy exchange terms between the two continua. We conclude by discussing how we intend to implement the above modeling scheme into a general-purpose flow and transport simulator such as TOUGH2. This initial model building effort was restricted to only flow and transport modeling without consideration of mechanical effects. In the next step, mechanical effects including movement of the grain boundaries will be addressed.

5.1 Background

In future nuclear waste repositories groundwater is considered to be the main agent for corrosion of waste packages, solubilization of the waste forms, and transport of the wastes to the accessible environment. Natural salt deposits have low permeability and are thus excellent candidates for hosting heat-emanating wastes (e.g., used nuclear fuels). However, they will still contain a

certain amount of water, either deposited with the salt or emplaced during some secondary process. This water may be present in intercrystalline pore space, intracrystalline inclusions, and hydrated or hydrous minerals. The significance of the presence of brine in salt rock is that, under a temperature, pressure, and/or chemical potential gradient, such water has been shown to migrate. The brine volumes can move either up or down a gradient, depending upon its occurrence. . Therefore, despite the basic impermeability of salt rock, brine may still reach the waste packages and compromise their performance under repository-induced conditions (Kelly 1985).

In the past, brine-migration research for nuclear waste disposal has focused primarily on brine-inclusion migration caused by thermal gradients (e.g., Anthony and Cline 1971; Jenks and Claiborne 1981; Roedder and Chou 1982; Yagnik 1983; Olander 1984). These previous investigations show that when a temperature gradient is applied to an all-liquid inclusion, migration is driven by solubility differences. Because the solubility of salt increases with temperature, salt will dissolve at the interface closest to the heat source (the "hot" face), diffuse through the brine as a result of solution composition and temperature gradients, and precipitate at the interface furthest from the heat source (the “cold” face). This is brought about because the thermal conductivity of the salt is higher than that of the brine, which produces a higher temperature gradient within the liquid than the applied gradient to the solid (Yagnik 1983). Thus, the inclusions tend to migrate toward the heat source. A number of mathematical expressions have been developed (Anthony and Cline 1971; Jenks and Claiborne 1981; Yagnik 1983; Olander 1984) for estimating the brine-inclusion-migration velocities up a thermal gradient.

The impact of the presence of a gas phase within the brine inclusions has also been investigated, and has been found to have a profound effect on brine migration (Olander 1984). In gas-liquid brine inclusions, the increase in vapor pressure of water over brine with increase in temperature seems to be the primary factor controlling inclusion behavior. Water evaporates at the hot side of the gas bubble, then is transported to the cold side and condenses (Anthony and Cline 1972; Olander, 1984). The condensed water in turn flows back to the hot side, carrying dissolved salt from the cold face of the inclusion to the hot face. This backflow effect overwhelms any solubility-driven salt flux if the gas volume fraction is >0.1. Thus, the gas-liquid inclusions tend to migrate away from the heat source, and expressions have been developed to estimate the velocities of gas-liquid inclusions away from a heat source. Note that these mathematical expressions for estimating brine-inclusion migration velocity are strictly applicable to single salt crystals only.

In addition to the above research focusing on brine migration at the scale of single crystals, Olivella et al. (1994) presented the macroscopic governing equations (continuum scale) for nonisothermal multiphase flow of brine and gas through porous deformable salt rock media. Their balance equations included species (i.e., salt, water, and air) mass balance, equilibrium of stresses and energy balance. The balance of salt allowed the establishment of the equation for porosity evolution due to solid skeleton deformation, dissolution/precipitation of salt and migration of brine inclusions. The mechanical problem was formulated through the equation of stress equilibrium. Finally, the balance of internal energy was established assuming thermal equilibrium between phases. Olivella et al. (1994) used these mathematical formulations to

develop a numerical finite element model called CODE-BRIGHT (Coupled DEformation, BRine, Gas and Heat Transport).

5.2 Recent Observations and Advances

While past research focused primarily on brine-inclusion migration under thermal gradients, temperature gradient is not the only driving force for brine migration (which includes both intercrystalline and intracrystalline or inclusion migration). For example, the behavior of intercrystalline brine under a temperature gradient is mostly unknown, even though it has been postulated that its migration is likely to be governed more by pressure gradients than thermal gradients. Moreover, temperature is not the only thermodynamic condition that alters solubility (which, as discussed in Section 5.1, is the primary driving force for intracrystalline brine migration); pressure and chemical potential also play a role and can also lead to analogous migration behavior (Urai et al. 2008). Finally, the migration of an aqueous phase in salt rock by dissolution-diffusion-precipitation affects not only fluid inclusions but also grain-boundary brine as well. When fluid inclusions and grain boundaries migrate, they can also collide, leading to interactions between these different brine configurations in salt rock. Complex relationships have been observed regarding the ability of such collisions to result in, for example, incorporation of the fluid-inclusion brine into the grain-boundary brine, or alternatively that the fluid inclusion passes through the grain boundary essentially unaffected (Schenk and Urai 2005).

In most of the past research, it has been routinely assumed that the fluid inclusions migrated (under thermal gradient) and "collided" with stationary grain boundaries, where small inclusions were stopped at the grain boundary while larger inclusions released fluid into the grain boundaries. There exists also some research work on grain-boundary migration under natural conditions, which focused on migration caused by pressure-solution, dislocation energy density, and grain-boundary surface curvature. In this case, grain boundaries are migrating whereas fluid inclusions are stationary. More recent work on grain-boundary collisions with fluid inclusions, on the other hand, have shown a variety of behaviors, including (1) incorporating inclusion fluid into grain boundary; (2) causing a temporary bulge in the grain boundary that is subsequently cut off and left behind as a fluid inclusion; (3) passing through the grain boundary unaffected. These different modes of interaction were observed to depend on the rate of grain-boundary migration, thickness of the grain boundary, and size and shape of the inclusion (Schenk and Urai 2005). After grain-boundary migration ceases, there is also a tendency of grain-boundary water to break up into isolated inclusions (Desbois et al. 2010). Note that while fluid inclusion migration speed under a temperature gradient increases with inclusion size up to 1 cubic millimeter in volume (Roedder and Belkin 1980), grain-boundary migration speed, driven by pressure or dislocation density gradients, peaks at a thickness between 10 and 100 nm (Urai et al., 1986).

Recently, Caponruscio et al. (2013) examined brine inclusion migration in single salt crystals and salt aggregates as a function of thermal gradients. They found that at temperatures larger than 160 °C all inclusions became two-phase inclusions. In such two-phase inclusions, they observed brine to migrate up the thermal gradient, while the gas migrated down the thermal gradient. Furthermore, they found that brine inclusion migration velocity depended on the magnitude of the thermal gradient within the inclusion, the temperature of the hot face of the inclusion, the size of the inclusion, and the chemical composition of the brine. Even though these

experimental observations are strictly valid for inclusion migration within a single salt crystal, they are nonetheless important results for building a reliable conceptual model of brine migration at the continuum scale, and we intend to utilize these latest experimental observations while developing our conceptual model. Finally, while some results (both experimental and theoretical) are available for brine migration in salt crystals, very little information seems to be available at present linking the thermally-driven fluid inclusion migration process with the pressure-dislocation-driven grain-boundary migration process and the different forms of grain-boundary interactions with fluid inclusions. Filling this knowledge gap is one of the primary objectives of the modeling effort proposed herein.

5.3 Modeling Approach

Based on the above discussion, it is clear that the development of constitutive models for brine migration first requires an understanding of the behavior of brine migration through interconnected intergranular (i.e., intercrystalline) pore spaces, migration of brine in isolated fluid inclusions (i.e., intracrystalline brine inclusions), interactions between these two configurations of brine, the impacts of mechanical deformation and temperature gradient, and the ways in which clays and other constituents of salt rock contribute to brine migration. At present, this understanding is mostly limited, if not completely absent, even though some advances have been made recently (Olivella et al. 1994; Kuhlman and Malama 2013). The conceptual models currently available in the literature for describing brine migration in salt rock are single-continuum models, which make the tacit assumption that the fluids in the inter- and intracrystalline pore space are in physical and chemical equilibrium with one another. Given the differences in driving forces controlling flow and transport in the inter- and intracrystalline pore spaces, and also because of the differences in temporal scales associated with each of these pore spaces, such an assumption of equilibrium between these two spaces is questionable. Even though the resulting mathematics (and subsequent computer coding) is considerably more complicated, we believe that a dual-continuum description is needed to properly understand brine migration in salt rocks under expected repository-induced conditions.

Central to our dual-continuum postulation is the assertion that a salt rock, which contains both interconnected intercrystalline pore spaces and intracrystalline brine inclusions, can be separated into two distinct continua (Figure 5-1). In this dual-continuum model, one continuum represents the connected intercrystalline pore space (where flow and transport is mostly controlled by pressure gradients, and molecular and thermal diffusion) and the other represents the intracrystalline inclusions (where the primary transport mechanism is temperature-driven solubility changes). Because both media are treated as separate systems, flow and transport processes are described by two sets of conservation equations (one set each for each of the two continua), which are coupled through suitably defined exchange terms. In essence, our proposed modeling approach is similar to the classical dual-continuum approaches used for modeling flow and transport in fractured rock systems (Warren and Root 1963; Gerke and van Genuchten 1993), where one continuum represents the fracture system with large fluid conductivities, and the other represents the rock matrix with large storage capacity.

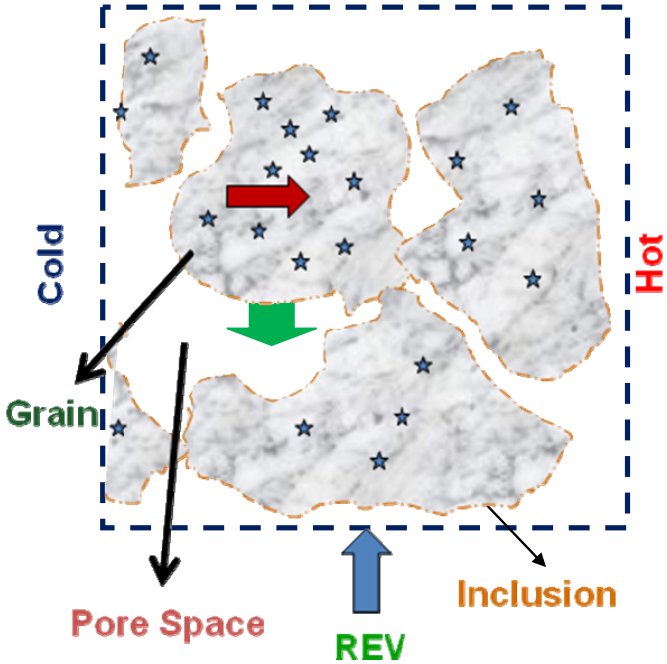

Figure 5-1. Schematic diagram showing the interconnected pore space and the intracystalline inclusions within an representative elementary volume (REV) in a dual-continuum conceptualization of salt formations. Figure also shows the various fluxes and inter-continuum exchanges

Apart from a dual-continuum approach, a rethinking is also needed with regards to modeling fluid flow through the connected intercrystalline pore spaces of salt rock. Brine movement through the interconnected pore space may be described in terms of traditional Darcy-flow equations, where pressure and gravitational potentials drive fluid flow. However, because salt rock has extremely low permeability, the possibility of non-Darcy flow also needs to be investigated. Non-Darcy flow has been reported in low-permeability clay rock, and recent investigations have found that flow behavior in nanotubes exhibits non-Darcy behavior (Liu and Birkholzer, 2012). This suggests that flow through the extremely narrow intercrystalline pore spaces in salt rock may also be subject to non-Darcy flow mechanisms. Additional factors that drive brine flow include the Soret effect, where brine flux is driven by the temperature gradient, as well as osmotic couplings caused by chemical potential gradients. Inter and intragranular brine may also be found in association with a noncondensable gas phase and may require consideration of two-phase flow.

5.4 Governing Equations

When brine flows through the interconnected pore space of a salt rock formation, which we conceptualize as analogous to its flow in a simple porous medium, the main flow mechanisms are advection and diffusion. The dissolved salt in the pore fluid, as it flows through the pore space by advection or diffusion, may enter the intracryastalline continuum through solute exchange governed by thermal and chemical potential gradients, and can undergo precipitation

and/or dissolution at the solid-fluid boundaries depending on solubility conditions, which are again controlled by temperature and pressure. Assuming single-phase flow conditions only, i.e., ignoring the presence of any vapor- or gas-phase flow, the transport of salt in the dissolved phase in the connected pore space can be described by the following equation at the continuum scale (i.e., at the scale of a representative elementary volume, REV, over which an average value of the variables can be defined):

$$\begin{aligned}&\frac{\partial}{\partial t}\left(\varphi_p \rho_l S_{pl} X_{pls}\right)= \\ &-\nabla\cdot\left(\varphi_p \mathbf{q_{pa}} \rho_l X_{pls}\right)-\nabla\cdot\left(\varphi_p \mathbf{q_{pds}} \rho_l\right)+\varphi_p \rho_l R_p\left(X_{sol}-X_{pls}\right)+\Gamma_s+X_{pls}M_p\end{aligned} \tag{5.1}$$

where φ_p is the porosity of the intercrystalline pore space, ρ_l is the density of the liquid (i.e., brine) phase [kg m^{-3}], S_{pl} and X_{pls} are the liquid saturation and mass fraction of salt in the liquid phase of the same space, and X_{sol} is the equilibrium solubility of salt in water expressed in terms of mass fraction. $\mathbf{q_{pa}}$ [m s^{-1}] and $\mathbf{q_{pds}}$ [m s^{-1}] in the first and second term on the right-hand side of Equation (5.1) are, respectively, the advective and diffusive fluxes of salt in the interconnected pore space. While the fourth term on the right-hand side of Equation (5.1) represents an exchange of salt mass between the two continua per unit salt rock volume (we discuss this term later), the third term simply specifies a rate law for exchange of salt mass between the liquid and solid phases in the interconnected pore space. The exchange of salt between the solid and liquid phases is postulated to be governed by an "effective" rate law constant, R_p. The last term on the right-hand side of Equation 1 is a generation term (sink or source) for brine.

A water mass balance in the intercrystalline pore space can be similarly written as

$$\frac{\partial}{\partial t}\left(\varphi_p \rho_l S_{pl} X_{plw}\right)=-\nabla\cdot\left(\varphi_p \mathbf{q_{pa}} \rho_l X_{plw}\right)-\nabla\cdot\left(\varphi_p \mathbf{q_{pdw}} \rho_l\right)+\Gamma_w+X_{plw}M_p \tag{5.2}$$

where the subscript '*w*' has been added to the variables and parameters to denote water. Within the interconnected pore space, mass balance of solid salt yields the following equation:

$$\frac{\partial}{\partial t}\left(\varphi_p S_{ps} \rho_s\right)=-\phi_p \rho_l R_p\left(X_{sol}-X_{pls}\right) \tag{5.3}$$

where ρ_s [kg m^{-3}] is the density of solid salt. In writing Equation (5.2), we have made the tacit assumption that solid salt is immobile, and is therefore not included in the intercontinuum mass-exchange processes. It is also assumed that the solid phase consists of pure salt (note the absence of any mass fraction terms). For the intracrystalline pore space, conservation of salt mass in the brine phase takes the form

$$\begin{aligned}\frac{\partial}{\partial t}\left[\left(1-\varphi_p\right)\left\{\varphi_{inc} \rho_l S_{inc,l} X_{inc,ls}\right\}\right]&=-\nabla\cdot\left[\left(1-\phi_p\right)\varphi_{inc} \mathbf{q_{inc,a}} \rho_l X_{inc,ls}\right]-\nabla\cdot\left[\left(1-\varphi_p\right)\varphi_{inc} \rho_l \mathbf{q_{inc,ds}}\right] \\ &+\left(1-\varphi_p\right)\phi_{inc} \rho_l R_{inc}\left(X_{sol}-X_{inc,ls}\right)-\Gamma_s\end{aligned}$$

(5.4)

where the subscript "inc" has been used to denote the intracrystalline or inclusion continuum; otherwise, the symbols have similar meanings to those introduced in Equations (5.1) and (5.2). The corresponding water balance can be written as

$$\frac{\partial}{\partial t}\left[\left(1-\varphi_p\right)\varphi_{inc}\rho_l S_{inc,l} X_{inc,lw}\right] = -\nabla\cdot\left[\left(1-\varphi_p\right)\varphi_{inc}\mathbf{q}_{\mathbf{inc},a}\rho_l X_{inc,lw}\right] - \nabla\cdot\left[\left(1-\varphi_p\right)\varphi_{inc}\rho_l \mathbf{q}_{\mathbf{inc,dw}}\right] - \Gamma_w \quad (5.5)$$

Conservation of solid salt in the intracrystalline solid takes the following form, which is similar to Equation (5.3),

$$\frac{\partial}{\partial t}\left[\left(1-\varphi_p\right)\left(1-\varphi_{inc}\right)S_{inc,s}\rho_s\right] = -\left(1-\varphi_p\right)\varphi_{inc}\rho_l R_{inc}\left(X_{sol} - X_{inc,ls}\right) \quad (5.6)$$

Note that, in this initial stage of model building, we assumed that the solid phase is immobile. This restriction can be relaxed by adding a solid velocity term in Equation (5.6). The mass-balance equations (Equations (5.1) through (5.6)) need to closed with the following equations

$$S_l + S_s = 1 \quad (5.7)$$

$$X_{pls} + X_{plw} = 1 \quad (5.8)$$

$$S_{inc,l} + S_{inc,s} = 1 \quad (5.9)$$

$$X_{inc,ls} + X_{inc,lw} = 1 \quad (5.10)$$

Equations (5.1) through (5.10) completely describe the mass-transport processes in salt rock for single-phase flow, and can be solved for the ten unknowns φ_p, φ_{inc}, S_{pl}, S_{ps}, X_{pls}, X_{plw}, $S_{inc,l}$, $S_{inc,s}$, $X_{inc,ls}$ and $X_{inc,lw}$, provided we can formulate suitable mathematical descriptions for the different fluxes and mass exchange terms, i.e., the constitutive relationships (see Section 5.5).

Before developing expressions for the fluxes and mass-exchange terms, however, we must first develop the energy-balance equations for the two continua. For the interconnected pore space, energy balance yields an equation of the following form:

$$\begin{aligned}&\frac{\partial}{\partial t}\left[\varphi_p S_{ps}\rho_s C_s T_p + \varphi_p S_{pl}\rho_l\left(X_{pls}u_s + X_{plw}u_w\right)\right] = \\ &-\nabla\cdot\left[-\lambda\nabla T_p + \varphi_p S_{pl}\rho_l\left\{\left(X_{pls}h_{pls} + X_{plw}h_{plw}\right)\mathbf{q}_{\mathbf{pa}} + h_{pls}\mathbf{q}_{\mathbf{pds}} + h_{plw}\mathbf{q}_{\mathbf{pdw}}\right\}\right] + G_p + \Lambda_E\end{aligned} \quad (5.11)$$

In Equation (5.11), T_p is the temperature in the continuum of the interconnected pore space, λ is the (effective) thermal conductivity of the brine system in the same continuum, G_p represents an energy generation (sink or source) term per unit volume of the rock, and Λ_E is the energy

exchange term between the two continua. Furthermore, C, u and h are the specific heat capacity, specific internal energy, and specific enthalpy (with subscript s representing salt and w representing water) of the brine system, both of which depend on temperature of the continuum, T_p.

Energy transport in the solid phase of the intracrystalline continuum (i.e., the grains) can be simplified to the form

$$\frac{\partial}{\partial t}\left[\left(1-\varphi_p\right)\left(1-\varphi_{inc}\right)S_{inc,s}\rho_s C_s T_s\right] = \lambda_s \nabla^2 T_s + G_s + E_s \tag{5.12}$$

where the symbols have their usual meanings with subscript 's' denoting solid salt. In Equation (5.12), G_s is the internal energy generation term (sink or source) within the grains, and E_s is the energy exchange term with the fluid inclusions. Finally, the energy transport in the inclusions within the intracrystalline continuum can be expressed as

$$\frac{\partial}{\partial t}\left[\left(1-\varphi_p\right)\varphi_{inc}S_{inc,l}\rho_l\left(X_{inc,ls}u_s + X_{inc,lw}u_w\right)\right] = -\nabla\cdot\begin{bmatrix} -\lambda_{inc}\nabla T_{inc} \\ +\left(1-\varphi_p\right)\varphi_{inc}S_{inc,l}\rho_l\left(X_{inc,ls}h_s + X_{inc,w}h_w\right)\mathbf{q_{inc,a}} + \\ \left(1-\varphi_p\right)\varphi_{inc}S_{inc,l}\rho_l h_{inc,ls}\mathbf{q_{inc,ds}} + \\ \left(1-\varphi_p\right)\varphi_{inc}S_{inc,l}\rho_l h_{inc,lw}\mathbf{q_{inc,dw}} \end{bmatrix} \tag{5.13}$$

$$-\Lambda_E$$

Note that in writing Equation (5.13), we have denoted the temperature of the inclusions as T_{inc}, which is different from the temperature of the grains $\left(T_s\right)$. Because of the vastly different thermal conductivities of brine and solid salt, it is expected that the temperature gradients within the brine of the inclusions and those in the grains are going to be different, resulting in different patterns of temperature evolution in the two. Past experimental works have confirmed the existence of two different temperature fields within the intracystalline pore space. Note that, in writing Equation (5.11) and (5.13), we have ignored the impact of heat of dissolution and recrystallization.

5.5 Fluxes and Inter-Continuum Exchange Terms

Darcy's law is commonly used to relate the flow rate of a fluid in a porous medium and the applied pressure gradient. Thus, for the interconnected pore space continuum (or the intercrystallline continuum), we can write the advective flux of brine as (Kuhlman and Malama, 2013)

$$\mathbf{q_{ap}} = -\frac{\mathbf{K}}{\mu}\nabla\left[P_p + \rho_l g z\right] - \sigma_p \nabla T_p \tag{5.14}$$

where $\mathbf{q_{ap}}$ is the advective [m s^{-1}], $\mathbf{K}$ is the permeability tensor [m^2], μ is the viscosity of brine, P_p is pressure, g is acceleration due to gravity, and z is the vertical coordinate. While the first term on the right-hand side of Equation (5.14) represents the contribution of pressure gradient

(and gravity) to the advective flux in the interconnect connected pore continuum, the second term is the contribution of thermal gradient (i.e., Soret effect) to the advective flux, where σ_p is the Soret coefficient (the subscript *p* has been added because Equation (5.14) is valid for the pore continuum).

As discussed in Sections (5.1) and (5.2), there are concerns regarding the applicability of Darcy's law for brine flow in salt formations. This is primarily because salt formations have extremely low permeabilities. For such low-permeability porous media, the linear relationship between advective flux and pressure (or hydraulic) gradient often breaks down. Hansbo (1960) was the first to report that, in low-permeability porous formations such as clay, the linear relationship between flux and hydraulic gradient, as postulated by Darcy's law, is strictly applicable if the hydraulic gradient is above a critical value, below which the relationship is highly nonlinear. Hansbo (1960) explained this behavior by positing that a certain hydraulic gradient was required to overcome the maximum binding energy of mobile pore water. This postulation has been later confirmed by many experimental observations (e.g., Miller and Law 1963; Klausner and Craft 1966; Antia 2008; Cui et al. 2008; Alabi et al. 2009). After reviewing several set of experimental data sets relating flux and hydraulic gradients, Liu and Birkholzer (2012) suggested a relationship for fluxes and hydraulic gradients in clay formations with very low permeabilities. Based on their formulations, Equation (5.14) can be written as

$$\mathbf{q_{ap}} = -\frac{\mathbf{K}}{\mu}\nabla\left[P + \rho_l g z - C_{ND}\right] - \sigma_p \nabla T_p \tag{5.15}$$

where C_{ND} is a correction factor to the flux term resulting from non-Darcy (ND) effects. Liu and Birkholzer (2012) suggest the following equation for this correction term:

$$C_{ND} = \frac{1}{\gamma\left(\frac{1}{\alpha}\right)}\left[\gamma\left\{\frac{1}{\alpha}, \left(\frac{j}{J^*}\right)^{\alpha}\right\}\right] \tag{5.16}$$

where γ refers to the Gamma functions

$$\gamma(\alpha) = \int_0^{\infty} t^{\alpha-1} e^{-t} dt \tag{5.17a}$$

$$\gamma(\alpha, \chi) = \int_0^{\chi} t^{\alpha-1} e^{-t} dt \tag{5.17b}$$

In Equation (5.16), j is the magnitude of hydraulic gradient, and J^* is defined as follows:

$$J^* = \frac{J\alpha}{\gamma\left(\frac{1}{\alpha}\right)} \tag{5.18}$$

where J is a threshold gradient. If the applied gradient is below this threshold value, water becomes immobile. The parameter α depends on the nature of the clay, and its value for different kinds of clay can be found in Liu and Birkhozer (2012). While these non-Darcy effects have been developed for clay materials, we believe they can be used for modeling advective fluxes in low-permeability salt formations, though some modifications may be needed.

A large volume of literature exists on the migration velocities of brine inclusions within salt crystals, a review of which can be found in Kelly (1985). Because we are developing a continuum description for flow and transport of brine, these expressions for migration of brine inclusions in single salt crystals are not directly relevant, because we need to obtain an expression for flux in an "average" sense. We thus follow the formulations of Olivella et al. (1994), and write the following expressions for advective transport in the intracrystalline continuum:

$$\mathbf{q_{inc,a}} = -\sigma_{inc} \nabla T_{inc} \tag{5.19}$$

Note that, in writing Equation (5.19), we have assumed that the only mechanism for advective transport within the intracrystalline continuum is the movement of inclusions under a thermal gradient (i.e., Soret effect). In other words, we have neglected advection under pressure gradient within that continuum, which is a reasonable approximation because the intracrystalline pore space consists of isolated inclusions.

For the different diffusive flux terms, we simply assume that Fick's law of diffusion is valid. Thus, for the diffusive flux of salt in the interconnected pore space, we have

$$\mathbf{q_{pds}} = -D_s^l \nabla X_{pls} \tag{5.20}$$

where D_s^l is the diffusion coefficient of salt in the liquid phase (i.e. brine). The diffusive flux of water in the same pore space is written as

$$\mathbf{q_{pdw}} = -D_w^l \nabla X_{plw} \tag{5.21}$$

where D_w^l is the diffusion coefficient of water in brine. Similarly, the diffusive fluxes within the intracrystalline continuum can be expressed as

$$\mathbf{q_{inc,ds}} = -D_s^l \nabla X_{inc,ls} \tag{5.22}$$

and

$$\mathbf{q_{inc,dw}} = -D_s^l \nabla X_{inc,lw} \tag{5.23}$$

In addition to the advective and diffusive fluxes, we also need mathematical expressions for the exchange terms between the two continua. Two approaches are generally available for the representation of exchange terms (e.g., Bai et al. 1993; Birkholzer and Rouvé 1994), i.e., the quasi-steady state and the unsteady-state or transient approach. In the quasi-steady state approach, the intercontinuum exchange term is assumed to be proportional to the difference in the average values of the quantity of interest (e.g., flow potential or solute concentration) in the two continua. In the unsteady-state approach, on the other hand, the exchange term is proportional to the gradient of the quantity of interest evaluated at the interface of the two continua. It is obvious that the quasi-steady state approach is a special case of the unsteady-state approach, in which we can roughly approximate the gradient as a linear function over a small (but non-zero) distance around the interface location. The quasi-steady approach is thus most appropriate for situations in which the gradients of flow potential and concentrations are not very

steep at the interface of the two continua. Given the slow flow that is expected in the interconnected pore-space of the extremely low-permeability salt formations, it may be reasonable to assume that the quasi-steady state approach is adequate. Furthermore, to address inclusion migration behavior at the grain boundaries, we intend to adopt a probabilistic approach. In this approach, an inclusion after reaching the grain boundaries would drain into the inter-connected pore space continuum with a probability *p*. It may also simply bypass the pore space and migrate into the neighboring grains with a probability of 1-*p*.

The intercontinuum exchange term is best understood when presented in terms of the discretized form of the conservation equations. For example, the advective flux along the direction *ij* between two adjacent gridblocks *i* and *j* (see Figure 5-2) of the interconnected pore space can, in general, be written as (see Equation (5.14))

$$\begin{aligned} flow_{ij} &= A_{ij}\frac{k_{ij+1/2}}{\mu_{ij+1/2}\left(D_i+D_j\right)}\left(\psi_j-\psi_i\right)+A_{ij}\sigma_{p,ij+1/2}\left(\frac{T_j-T_i}{D_i+D_j}\right) \\ &= \frac{\omega_{ij}}{\mu_{ij+1/2}}\left(\psi_j-\psi_i\right)+\varepsilon_{ij}\left(T_j-T_i\right) \end{aligned} \tag{5.24}$$

where A_{ij} is the common interface area of gridblocks *i* and *j*, and D_i and D_j are the distances of the centers of gridblocks *i* and *j*, respectively, from the common interface. In Equation (5.24), we have defined the flow potential ψ_i in gridblock *i* as

$$\psi_i = P + \rho_{l,ij+1/2} g z_i - C_{ND,i} \tag{5.25}$$

In Equations (5.24) and (5.25) (and hereafter), the subscript *ij*+1/2 is used to denote a proper averaging or weighting of fluid flow, component transport, or heat-transfer properties at the interface or along the connection between two blocks or nodes *i* and *j*. We can develop similar expressions for the diffusive flux terms and energy-transfer terms, but these are not repeated here for the sake of brevity.

The exchange term between two grid blocks belonging to different continua can be written with the same basic form defined in Equation (5.24); however, care must be taken in defining the effective surface areas (for exchange) and the effective distance over which this transfer takes place (i.e., the distance over which the quasi-steady state approximation is valid). In other words, we need different expressions for ω_{ij} and ε_{ij}, which are the parameters that actually control the intercontinuum exchange of mass and energy. In a general sense, these parameters can be expressed as

$$\eta_{p,inc} = \frac{A_{p,inc}\kappa_{p,inc}}{l_{p,inc}} \tag{5.26}$$

where $A_{p,inc}$ is the effective interface area between the two continuua of a particular grid block (which is different from its geometric area), $l_{p,inc}$ is the effective transfer distance, and $\kappa_{p,inc}$ is the relevant effective transport property (permeability, diffusivity, or Soret coefficient). For conventional fractured porous rock systems, expressions are available in the literature for estimating these parameters in different dimensions (Warren and Root 1963; Bai et al. 1993; Wu

and Pruess 1988; Wu et al. 2004; Wu and Qin 2009). We are evaluating these expressions for their applicability in salt formations, and suitable modifications will be made before they are incorporated in a numerical scheme.

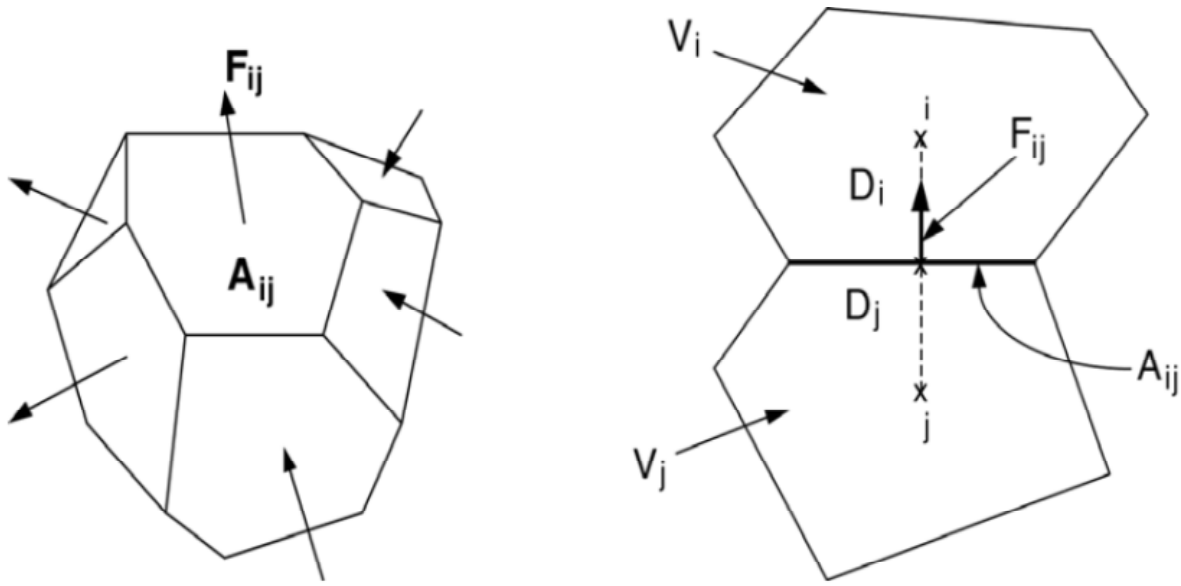

Figure 5-2. Space discretization and flow-term evaluation in the integral finite difference approach.

5.6 Numerical Formulation

The mathematical model presented above is well suited for implementation within the framework of the TOUGH2 numerical simulator. TOUGH2 (Pruess et al. 2011) is a general purpose software for simulating nonisothermal, multiphase flow and transport in porous and fractured formations. It uses an integral finite-difference scheme (Narasimhan and Witherspoon 1976) for spatial discretization, and a fully implicit scheme for spatial discretization. TOUGH2 provides options for modeling the pressure and temperature dependence of brine density and viscosity. It also provides some options to correlate the changes in permeability arising from porosity changes resulting from salt precipitation and dissolution. However, these relationships may have to be updated or newer correlations, which are specific for salt formations (e.g., Olivella et al. 2011), may have to be included. Newer subroutines will be added to simulate the migration of brine in the intracystalline continuum and the migration of brine under thermal gradient (i.e., Soret effect). We will also reevaluate the options available for modeling the dependence of salt diffusion coefficient on temperature and brine composition. Once the above are accomplished, we will extend these mathematical formulations to include the impact of mechanical deformations on brine migration in salt formations.

6. CONCLUSIONS

In FY2014, LBNL's work has been focused on continued testing, application, and improvement of the computational models and tools to simulate high-temperature coupled processes and their effect on brine accessibility and migration. LBNL has gained experience and made significant advancement in this research through collaboration with the research group led by Professor Lux at Clausthal University of Technology (TUC) in Germany. This includes improvements to the TOUGH-FLAC simulator related to constitutive models for both solid rock salt and crushed salt, as well as related to the use of a Voronoi discretization in the flow subproblem, even when the mesh deforms over time due to creep and large strains.

Based on the FY2014 model improvements, we have updated and completed our study of long term THM behavior of a generic repository, and this has also been summarized and submitted for publication in a journal (Blanco Martin 2014d). Overall, the generic repository simulation results suggest that the EDZ is healed within the first few years and that the backfill reconsolidates within the first two decades. Depending on the magnitude of the pore pressure relative to the minimum principal stress, damage-induced secondary permeability and fluid infiltration may occur at a larger temporal and spatial scale. Once damage processes are over, our predictions show that the initial tightness of the host rock is restored.

LBNL also conducted a benchmark simulation on the same scenario comparing the two simulators TOUGH-FLAC (LBNL) and FLAC-TOUGH (TUC), and achieved good agreement providing code-to-code verification and confidence in the simulation results achieved. The comparison of the results obtained from the two simulators is very satisfactory, both in terms of the evolution of the natural salt barrier and the consolidation of the crushed salt backfill. Another benchmark calculation has been initiated involving modeling of the TSDE (*Thermal Simulation for Drift Emplacement*) test conducted in the Asse Mine, Germany. The TSDE analysis will be a major modeling effort that will provide the opportunity to validate the TOUGH-FLAC simulator for drift closure and backfill compaction at a large 3D field setting.

Finally, LBNL developed a dual-continuum approach that accounts for brine migration through both interconnected intergranular (i.e., intercrystalline) pore spaces and isolated fluid inclusions (i.e., intracrystalline brine inclusions), considering both pressure and temperature gradients. The plan is to implement such an advanced brine-migration dual-continuum model into the TOUGH2 and TOUGH-FLAC simulators, and then validate the brine-migration model and its implementation against experimental data.

Thus, FY2014 accomplishments are summarized as follows:

- Improvements of the TOUGH-FLAC simulator, including the use of Voronoi discretization for a more accurate flow simulation under (large-strain) deforming numerical grid.
- Updates in the implement constitutive model for more accurate representation of damage and healing processes.
- Updated simulation on long-term THM evolution for a salt-based repository with methods and results summarized in a paper submitted to a journal.

- Completed code-to-code verification of TOUHG-FLAC and FLAC-TOUGH codes in collaboration with the Clausthal group achieving good agreement and confidence in respective simulators.
- Completed a 3D model setup of the TSDE experiment that will be used for model validation against field data.
- Developed a conceptual model for a dual-continuum approach for brine migration (involving both intercrystalline flow and intracrystalline brine inclusions).

To date, since the start of the work in FY2012 with adapting TOUGH-FLAC for salt related THMC modeling, the following successful model simulations have been conducted:

- Modeling of a brine infiltration laboratory experiment validating TOUGH-FLAC with the Lux/Wolter's constitutive model related to brine infiltration when pore pressure exceeds minimum compressible principal stress (FY2012).
- First TOUGH-FLAC modeling of long-term repository evolution without consideration of drift compaction (FY2012).
- Modeling of triaxial compression test to validate TOUGH-FLAC with Lux/Wolter's model regarding mechanical behavior under shear stress and strain (FY2013).
- Modeling of Terzaghi's 1D consolidation problems with comparison to analytic solution to verify TOUGH-FLAC hydraulic and mechanical pore-volume coupling under small and large strain (FY2013).
- Second TOUGH-FLAC modeling of long-term repository evolution using Lux/Wolter's constitutive model and crushed salt constitutive models with large-strain compaction of salt backfill (FY2013).
- Third TOUGH-FLAC modeling of long-term repository evolution using updated TOUGH-FLAC code with more accurate representation of flow though Voronoi mesh discretization and updated Lux/Wolter's model related to damage and healing (FY2014). This also involved code-to-code verification between LBNL's TOUGH-FLAC and Clausthal's FLAC-TOUGH simulators.

Thus, the work is progressed by gradually incorporating desired improvement into the simulator, conducting validation against experiments and to update the generic repository modeling to assess the relevance to the long term performance of the repository. The progress of LBNL's work related to modeling coupled processes in salt is very much in line with UFD goals to fill data needs and confirm advanced modeling approaches (by 2015), and to have a robust modeling and experimental basis for evaluation of multiple disposal system options (by 2020). In this context, we conclude that the TOUGH-FLAC combination can provide the necessary modeling tool for modeling coupled processes associated with nuclear waste disposal in salt formations, including high-temperature multiphase flow and transport processes, coupled with time-dependent geomechanical (creep) processes under large deformations. At the same time, we have gained access to both laboratory and field data that will be increasingly important for validation of the advanced numerical tools.

In FY2015, LBNL plans to continue the successful collaboration with the Clausthal group for further development, validation, and application of the TOUGH-FLAC simulator relevant to waste disposal in salt. Specific objectives of this research include:

- Continue salt-related model improvements and optimizing the TOUGH-FLAC simulator and conduct code-to-code verification with the fully coupled Code-Bright finite element code to investigate potential time-step limitations in the sequentially coupled TOUGH-FLAC solution.
- Conduct benchmarking and model validation against the Asse Mine TSDE experiment, with potential participation in the US-German benchmarking project.
- Extend modeling from THM to THMC processes considering salt precipitation and dissolution.
- Implement proposed dual-continuum model into TOUGH2 and test it for modeling thermally driven brine migration and investigate the roles of intercrystalline flow versus intracrystalline brine inclusions on the overall brine migration.
- Conduct coupled geomechanical model simulations to support the design of a proposed heater experiment in salt.

ACKNOWLEDGMENT

Funding for this work was provided by the Used Fuel Disposition Campaign, Office of Nuclear Energy, of the U.S. Department of Energy under Contract Number DE-AC02-05CH11231 with Lawrence Berkeley National Laboratory.

REFERENCES

Alabi, O.O., O.L. Popoola and J.A. Adegoke, 2009. Modification of fluid flow equation in saturated porous media, Global Journal of Pure and Applied Science, 15:395–400.

Anthony, T.R. and H.E. Cline, 1971. The thermal migration of liquid droplets through solids, Journal of Applied Physics, 42:3380–3387.

Anthony, T.R., and H.E. Cline, 1972. The thermomigration of biphase vapor-liquid droplets in solids, Acta Metallurgica, 20:247–255.

Antia, D.D.J., 2008. Oil polymerization and fluid expulsion from low temperature, low maturity, overpressured sediments. Journal of Petroleum Geololgy, 31:263–282.

Bai, M., D. Elsworth and J.-C. Roegiers, 1993. Multiporosity/multipermeability approach to the simulation of naturally fractured reservoirs, Water Resources Research, 29:1621-1633.

Bechthold, W., E. Smailos, S. Heusermann, W. Bollingerfehr, B. Bazargan Sabet, T. Rothfuchs, P. Kanlot, J. Grupa, S. Olivella, and F.D. Hansen, 1999. Backfilling and Sealing of Underground Repositories for Radioactive Waste in Salt (BAMBUS Project). Report EUR19124 EN: European Atomic Energy Community.

Bechthold W., E. Smailos, S. Heusermann, W. Bollingerfehr, B. Bazargan Sabet, T. Rothfuchs, P. Kanlot, J. Grupa, S. Olivella, and F.D. Hansen, 2004. Backfilling and Sealing of Underground Repositories for Radioactive Waste in Salt (BAMBUS II project). Report EUR 20621 EN: European Atomic Energy Community.

Benz T., 2007. Small-strain stiffness of soils and its numerical consequences. Ph.D. thesis: University of Stuttgart (Germany).

Bérest, P., B. Brouard and M. Karimi-Jafari, 2005. Deep salt caverns abandonment. In: Proceedings Post-Mining Symposium, Nancy, France, 12 pp.

Birkholzer, J.T. and G. Rouvé, 1994. Dual-continuum modeling of contaminant transport in fractured formations, In: Computational Methods in Water Resources X, A. Peters et al. (eds.), Kluwer Academic Publishers, Amsterdam, The Netherlands.

Blanco Martín L., J. Rutqvist, J.T. Birkholzer, and J.E. Houseworth, 2013. Thermal-Hydraulic-Mechanical Processes Modeling to Evaluate Salt-based Repositories in the Long-Term. American Rock Mechanics Association, ARMA 13-621, 47th US Rock Mechanics Symposium, San Francisco, California, June 23-26, 2013.

Blanco Martín L., J. Rutqvist, and J.T. Birkholzer, 2014a. Long-term analysis of thermal-hydraulic-mechanical processes in a generic salt repository for high-level nuclear waste. American Rock Mechanics Association, ARMA 14-7206, 48th US Rock Mechanics Symposium, Minneapolis, Minnesota, June 1-4, 2014.

Blanco Martín, L., J. Rutqvist, J.T. Birkholzer, R. Wolters, M. Rutenberg, J. Zhao and K.-H. Lux, 2014b. Comparison of two modeling procedures to evaluate thermal-hydraulic-mechanical processes in a generic salt repository for high-level nuclear waste. American Rock Mechanics Association, ARMA 14-7411, 48th US Rock Mechanics Symposium, Minneapolis, Minnesota, June 1-4, 2014.

Blanco Martín, L., J. Rutqvist and J.T. Birkholzer, 2014c. Long-term modelling of the thermal-hydraulic-mechanical response of a generic salt repository for high-level nuclear waste. Submitted to Engineering Geology.

Blanco Martín, L., R. Wolters, J. Rutqvist, K.-H. Lux and J.T. Birkholzer, 2014d. Comparison of two sequential simulators to investigate thermal-hydraulic-mechanical processes related to nuclear waste isolation in saliniferous formations. In preparation for Computers and Geosciences.

Callahan G., and K. DeVries, 1991. Analysis of Backfilled Transuranic Waste Storage Rooms, RE/SPEC, Inc., Report to Sandia National Laboratories SAND91-7052.

Camphouse C., C. Herrick, D. Kicker, and B. Thompson, 2012. Recommendations and Justifications of Parameters Values for the Run-of-Mine Salt Panel Closure System Design Modeled in the PCS-2012 PA. Final memo 5412, May, 2012.Carter J., A. Luptak, and J. Gastelum, 2011. Fuel cycle potential waste inventory for disposition. FCR&D-USED-2010-000031, Rev. 4. October, 2011.

Caporuscio, F.A., H. Boukhalfa, M.C. Cheshire, A.B. Jordan, and Ding, M., 2013. Brine migration experimental studies for salt repositories, LA-UR-13-27240, Los Alamos National Laboratory, Los Alamos, NM.

Cinar Y., G. Pusch, and V. Reitenbach, 2006. Petrophysical and Capillary Properties of Compacted Salt. Transport in Porous Media, 64, 199–228.

Cosenza, Ph., 1996. Sur les couplages entre comportement mécanique et processus de transfert de masse dans le sel gemme. Ph.D. dissertation, Université Paris 6, Paris, France, 184 pp.

Coussy O., 2004. Poromechanics, 1st edn. John Wiley and Sons, Chichester.

Cui, Y.J., A.M. Tang, C. Loiseau, P. Delage, 2008. Determining the unsaturated hydraulic conductivity of a compacted sand-bentonite mixture under constantvolume and free-swell conditions. Physics and Chemistry of the Earth, 33:S462–S471.

DBE, 2011. Numerische Untersuchungen zum Konvergenzverhalten eines Einzelhohlraumes. Report 22341011: DBE Technology GmbH (Germany).

Dean, R.H., X. Gai, C.M. Stone and S.E. Minkoff, 2006. A comparison of techniques for coupling porous flow and geomechanics. SPE Journal 11 (1), 132–140. doi: 10.2118/79709-PA.

Desbois, G., J.L. Urai, J. Schmatz, P. Zavada and H. de Bresser, 2012. The distribution of fluids in natural rock salt to understand deformation mechanisms. In: Bérest, P., Ghoreychi, M., Hadj-Hassen, F., Tijani, M. (Eds.), Proceedings 7th International Conference on the Mechanical Behaviour of Salt (SaltMech7), Paris, France, pp. 3-12.

Desbois, G., J.L. Urai and J.H.P de Bresser, 2010. Evidence of sealing and brine distribution at grain boundaries in natural fine-grained Halite (Qum Kuh salt fountain, Central Iran), implications for rheology of salt extrusions, Geophysical Research Abstracts Vol. 12, EGU2010-4336, EGU General Assembly 2010.

DOE/CBFO, 2012. A conceptual plan for sat defense disposal investigations for the disposal of DOE-EM managed wastes. Report DOE/CBFO-12-3485, Revision 0: DOE Carlsbad Field Office (USA).

Doherty, J., 2008. PEST: Model-Independent Parameter Estimation, Watermark Numerical Computing, Brisbane, Australia.

Felippa, C.A. and K.C. Park, 1980. Staggered transient analysis procedures for coupled mechanical systems: formulation. Computer Methods in Applied Mechanics and Engineering 24(1), 61–111. doi: 10.1016/0045-7825(80)90040-7.

Finsterle, S., 2007. iTOUGH2 User's Guide, Lawrence Berkeley National Laboratory report LBNL-40040.

Gerke, H.H., and M.T. van Genuchten, 1993. A dual-porosity model for simulating the preferential movement of water and solutes in structured porous media, Water Resources Research, 24: 1225-1236.

Hampel, A., J.G. Argüello, F.D. Hansen, R.M. Günther, K. Salzer, W. Minkley, K.-H. Lux, K. Herchen, U. Düsterloh, A. Pudewills, S. Yildirim, K. Staudtmeister, R. Rokahr, D. Zapf, A. Gährken, C. Missal and J. Stahlmann, 2013. Benchmark Calculations of the Thermo-Mechanical Behavior of Rock Salt – Results from a US-German Joint Project. American Rock Mechanics Association, ARMA 13-456, 47th US Rock Mechanics Symposium, San Francisco, California, June 23-26, 2013.

Hansbo, S., 1960. Consolidation of clay, with special reference to influence of vertical sand drains, In: Swedish Geotechnical Institute Proceedings, vol. 8., Stockholm, Sweden.

Hou Z., 2002. Geomechanische Planungskonzepte für untertägige Tragwerke mit besonderer Berücksichtigung von Gefügeschädigung, Verheilung und hydromechanischer Kopplung. Clausthal-Zellerfeld: Papierflieger, ISBN 3-89720-099-6.

Hou, Z., 2003. Mechanical and hydraulic behaviour of rock salt in the excavation disturbed zone around underground facilities. International Journal of Rock Mechanics and Mining Sciences 40, 725-738. doi:10.1016/S1365-1609(03)00064-9.

Hou, Z. and K.-H. Lux, 1998. Ein neues Stoffmodell für duktile Salzgesteine mit Einbeziehung von Gefügeschädigung und tertiärem Kriechen auf der Grundlage der Continuum-Damage-Mechanik. Geotechnik 21(3), 259–263.

Hou, Z., K.-H. Lux and U. Duesterloh, 1998. Bruchkriterium und Fließmodell für ductile Salzgesteine bei kurzzeitiger Beanspruchung. Glueckauf-Forschungshefte 59(2), 59–67.

Hou, Z. and K.-H. Lux, 1999. A constitutive model for rock salt including structural damages as well as practice-oriented applications. In: Proceedings of the Fifth Conference on the Mechanical Behaviour of Salt, Bucharest, Romania, pp. 151–169.

Hou, Z. and K.-H. Lux, 2000. Ein Schädigungsmodell mit Kriechbruchkriterium für duktile Salzgesteine auf der Grundlage der Continuum- Damage-Mechanik. Bauingenieur 75(13), 300–307.

Itasca, 2011. FLAC3D V5.0, Fast Lagrangian Analysis of Continua in 3 Dimensions, User's Guide. Itasca Consulting Group, Minneapolis, Minnesota, 438 pp.

Jenks, G.H., and H.C. Claiborne, 1981. Brine migration in salt and the its implications in the geologic disposal of nuclear waste, ORNL-5818, Oak Ridge National Laboratory, Oak Ridge, TN.

Kachanov L., 1986. Introduction to Continuum-Damage-Mechanics. Martinus Nijhoff.

Kim, J., 2010. Sequential Methods for Coupled Geomechanics and Multiphase Flow. Ph.D. Dissertation, Stanford University, Stanford, USA, 248 pp.

Kim J., H.A. Tchelepi, and R. Juanes, 2011. Stability and convergence of sequential methods for coupled flow and geomechanics: Fixed-stress and fixed-strain splits. Comput. Methods. Appl. Mech. Engrg. 200: 1591-1606.

Kim J., E. Sonnenthal, and J. Rutqvist, 2012. A modeling and sequential numerical algorithms of coupled fluid/heat flow and geomechanics for multiple porosity materials. International Journal of Numerical Methods in Engineering, 92, 425–456 (2012).

Kim, J., H.A. Tchelepi and R. Juanes, 2013. Rigorous Coupling of Geomechanics and Multiphase Flow with Strong Capillarity. SPE Journal 18(6), 1123-1139. doi:10.2118/141268-PA.

Kelly, W., 1985. Brine migration in salt, Topical Report 8505060429, Nuclear Regulatory Commission, Washington, DC.

Klausner, Y., and R. Craft, 1966. A capillary model for non-Darcy flow through porous media, Journal of Rheology, 10:603–613.

Kuhlman, K.L., and B. Malama, 2013. Brine flow in heated geologic salt, SAND2013-1944, Sandia National Laboratory, Albuquerque, NM.

Lerche S., 2012. Kriech- und Schädigungsprozesse im Salinargebirge bei mono- und multizyklischer Belastung. Ph.D. thesis: TU Clausthal (Germany).

Liu, H.-H., and J.T. Birkholzer, 2012. On the relationship between water flux and hydraulic gradient for unsaturated and saturated clay, Journal of Hydrology, 475:242–247.

Lux K., 1984. Gebirgsmechanischer Entwurf und Felderfahrung im Salzkavernenbau: Ein Beitrag zur Entwicklung von Prognosemodellen für den Hohlraumbau im duktilen Salzgebirge. Stuttgart: Ferdinand Enke Verlag.

Lux, K.-H., M. Rutenberg, R. Seeska and U. Düsterloh, 2014. Kopplung der Softwarecodes FLAC^{3D} und TOUGH2 in Verbindung mit in situ-, laborativen und numerischen Untersuchungen zum thermisch-hydraulisch-mechanisch gekoppelten Verhalten von Tongestein unter Endlagerbedingungen. Clausthal University of Technology (Germany). Final Report of BMWi-project 02E11041.

Miller, R.J., Low, P.F., 1963. Threshold gradient for water flow in clay systems, Soil Science Society of America Proceedings, 27:605–609.

Millington, R.J. and J.P. Quirk, 1961. Permeability of Porous Solids. Transactions of the Faraday Society 57, 1200-1207. doi: 10.1039/TF9615701200.

Narasimhan, T.N., and P.A. Witherspoon, 1976. An integrated finite difference method for analyzing fluid flow in porous media, Water Resources Research, 12:57 – 64

Nutt, M. (2011). Used Fuel Disposition Campaign Disposal Research and Development Roadmap (FCR&D-USED-2011-000065 REV0), U.S. DOE Used Fuel Disposition Campaign.

Olander, D.R., 1984. A study of thermal-gradient induced migration inclusions in salt: Final report, BMI/ONWI-538, Regents of the University of California, Oakland, CA.

Olivella, S., J. Carrera,, A Gens, E.E. Alonso, 1994. Nonisothermal multiphase flow of brine and gas through saline media, Transport in Porous Media, 15:271–293.

Olivella, S., S. Castagna, E.E. Alonso, and A. Lloret, 2011. Porosity variations in saline media induced by temperature gradients: Experimental evidences and modeling, Transport in Porous Media, 90:763-777.

Pruess K., C. Oldenburg, and G. Moridis, 2011, TOUGH2 User's Guide, Version 2, Lawrence Berkeley National Laboratory report LBNL-43134 (revised).

Roedder, E., and H.E. Belkin, 1980. Thermal gradient migration of fluid inclusions in single crystals of salt from the Waste Isolation Pilot Plant (WIPP), Scientific Basis for Nuclear Waste Management, Vol. 2 (1980) Edited by Clyde J.M. Northrup, Jr., Plenum Publishing Corporation, New York, NY.

Roedder, E., and L.M. Chou, 1982. A critique of "Brine migration in salt and its implications in the geologic disposal of nuclear waste," Oak Ridge National Laboratory Report 5818, by G.H. Jenks and H.C. Claiborne, USGS Open-File Report 82-1131.

Rutqvist J., 2011. Status of the TOUGH-FLAC simulator and recent applications related to coupled fluid flow and crustal deformations. Computational Geosciences, 37, 739–750.

Rutqvist, J. and C.-F. Tsang, 2003. TOUGH-FLAC: a numerical simulator for analysis of coupled thermal-hydrologic-mechanical processes in fractured and porous geological media under multi-phase flow conditions. In: Proceedings of the TOUGH Symposium 2003, Berkeley, CA, USA, 12 pp.

Rutqvist J., Y. S. Wu, C.- F. Tsang, and G. Bodvarsson, 2002. A Modeling Approach for Analysis of Coupled Multiphase Fluid Flow, Heat Transfer, and Deformation in Fractured Porous Rock, International Journal of Rock Mechanics and Mining Sciences, 39, 429–442.

Rutqvist J., L. Blanco Martín, and J. Houseworth, 2012. THM Coupled Process Modeling with TOUGHFLAC to Evaluate the Fate and Transport of Water in a Salt-Based Repository. Report FCRD-UFD-2012-000297.

Rutqvist J., L. Blanco Martín, J. Kim, and J.T. Birkholzer, 2013. Modeling Coupled THMC Processes and Brine Migration in Salt at High Temperatures. Report FCRD-UFD-2013-000262.

Rycroft, C.H., 2009. Voro++: a three-dimensional Voronoi cell library in C++. http://math.lbl.gov/voro++/

Schenk, O., and J.L. Urai, 2005. The migration of fluid-filled grain boundaries in recrystallizing synthetic bischofite: first results of in-situ high-pressure, high-temperature deformation experiments in transmitted light, Journal of Metamorphic Geology, 23:695-709.

Sjaardema G.D., and R.D. Krieg, 1987. A Constitutive Model for the Consolidation of WIPP Crushed Salt and Its Use in Analyses of Backfilled Shaft and Drift Configurations. Sandia National Laboratories, Albuquerque, NM, USA. Report SAND-87-1977.

Stone C., J. Holland, J. Bean, and J. Argüello, 2010. Coupled Thermal-Mechanical Analyses of a Generic Salt Repository for High-Level Waste. Proceedings of the 44th U.S. Rock Mechanics Symposium, Salt Lake City, Utah, USA, June 27-June 30, 2010: American Rock Mechanics Association ARMA, Paper No. 180.

Suter, D., 2003. Untersuchung der Gasbildungsmechanismen in einem Endlager für radioactive Abfälle und der damit verbundenen Auswirkungen auf die Führung des Nachweises der Endlagersicherheit. Bericht zur TA 1: Analyse der relevanten Gasbildungsmechanismen. Colenco Bericht 3161/03, Colenco Power Engineering AG, Baden, Schweiz.

Thomas, L.K., L.Y. Chin, R.G. Pierson and J.E. Sylte, 2003. Coupled geomechanics and reservoir simulation. SPE Journal 8(4), 350–358. doi: 10.2118/87339-PA.

Urai, J.L., W.D. Means and G.S. Lister, 1986. Dynamic recrystallization of minerals, mineral and rock deformation: Laboratory studies -The Paterson Volume, Geophysical Monograph 36, American Geophysical Union.

Urai, J.L., Z. Schléder, C.J. Spiers and P.A Kukla, 2008. Flow and Transport Properties of Salt Rocks, In: "Dynamics of Complex Intracontinental Basins", R. Littke, U. Bayer, D. Gajewski, and S. Nelskamp (Eds.), Springer-Verlag, Berlin Heidelberg, Germany.

van Genuchten MT, 1980. A closed-form equation for predicting the hydraulic conductivity of unsaturated soils. Soil Sci Soc Am J. 44, 892-898.

Vargaftik, N.B., 1975. Tables on the Thermophysical Properties of Liquids and Gases, 2nd edn. Hemisphere Publishing, New York, USA, 758 pp. doi: 10.1002/aic.690210636.

Vijalapura, P.K., J. Strain and S. Govindjee, 2005. Fractional step methods for index-1 differential-algebraic equations. Journal of Computational Physics 203, 305–320. doi: 10.1016/j.jcp.2004.08.015.

Walker, W.R., J.D. Sabey and D.R. Hampton, 1981. Studies of Heat Transfer and Water Migration in Soils. Department of Agricultural and Chemical Engineering, Colorado State University, Fort Collins, CO, USA. Final Report, 140 pp.

Wang, Y. (2011). Research & Development (R&D). Plan for Used Fuel Disposition Campaign (UFDC). Natural System Evaluation and Tool Development, U.S. DOE Used Fuel Disposition Campaign.

Wieczorek K., O. Czaikowski, C.L. Zhang, and D. Stührenberg. 2012. Recent Experimental and Modeling Results on Crushed Salt Consolidation. In Proceedings of the Third US/German Workshop on Salt Repository Research, Design and Operation, Albuquerque, 8-10 October 2012.

Warren, J.E., and P.J. Root, 1963. The behavior of naturally fractured reservoirs, Society of Petroleum Engineers Journal, Trans. AIME, 228: 245-255.

Wolters R., K.-H. Lux, and U. Düsterloh, 2012. Evaluation of Rock Salt Barriers with Respect to Tightness: Influence of Thermomechanical Damage, Fluid Infiltration and Sealing/Healing. SaltMech7 (p. 10). Paris: Balkema, Rotterdam.

Wu, Y.-S., and K. Pruess, 1988. A multiple-porosity method for simulation of naturally fractured petroleum reservoirs, SPE Reservoir Engineering, 3:327-336.

Wu, Y.-S., and G. Qin, 2009. A generalized numerical approach for modeling multiphase flow and transport in fractured porous media, Communications in Computational Physics, 6:85-108.

Wu, Y.-S., Liu, H.-H., and Bodvarsson, G.S. (2004), A triple-continuum approach for modeling flow and transport processes in fractured rock, Journal of Contaminant Hydrology, 73:145-179.

Yagnik, S. K., 1983. Interfacial stability of migrating brine inclusions in alkali halide single crystals supporting a temperature gradient, Journal of Crystal Growth, 62:612-626.